Daniel Júlio Freire Monsanto Marques

Licenciado em Ciências da Engenharia Electrotécnica e de Computadores

Implementação de códigos LDPC em OFDM e SC-FDE

Dissertação apresentada para obtenção do Grau de Mestre em Engenharia Electrotécnica e de Computadores, pela Universidade Nova de Lisboa, Faculdade de Ciências e Tecnologia.

Orientador : Doutor Paulo Montezuma de Carvalho, Prof. Auxiliar da FCT-UNL

Júri:

Presidente: Dr.ª Maria Helena Silva Fino, Professora Auxiliar da FCT-UNL

Vogais: Dr. Rui Morgado Dinis, Prof. Associado com Agregação da FCT-UNL

Dr. Paulo Montezuma de Carvalho, Prof. Auxiliar da FCT-UNL

Setembro, 2014

FACULDADE DE CIÊNCIAS E TECNOLOGIA
UNIVERSIDADE NOVA DE LISBOA

Implementação de códigos LDPC em OFDM e SC-FDE

To my beloved mother and father.

Agradecimentos

Em primeiro lugar quero expressar a minha profunda gratidão ao Prof. Dr. Paulo Montezuma de Carvalho e Prof. Dr. Rui Dinis, por todo o conhecimento que me conseguiram transmitir ao longo destes anos. Com uma enorme boa disposição, disponibilidade, paciência e sabedoria, foram preponderantes para a conclusão de Mestrado.

Reitero também o meu agradecimento à Prof.ª Dr.ª Helena Fino, que sempre esteve disponível com enorme simpatia para me ajudar com os meus problemas académicos.

Também quero fazer destaque àqueles que considero como família. Sempre me deram força da melhor forma que sabiam, sempre suportaram as minhas lamúrias em tempos complicados e nunca duvidaram das minhas capacidades. Espero agora poder dar-vos um pouco desta minha alegria como forma de gratidão.

Quero realçar também a importância de uma pessoa em especial nos últimos tempos, que me deu uma força enorme para finalmente concluir esta dissertação. A essa pessoa, Alice, agradeço toda a inspiração e carinho que me dá todos os dias.

Por último mas não menos importante, quero agradecer às pessoas que me viram crescer. Susana e Ulisses, obrigado por serem os melhores irmãos que podia ter. Obrigado por me ajudarem a ser a pessoa que sou hoje. E finalmente aos meus dois ídolos mais importantes: os meus pais Júlio e Maria. Por todos os sacrifícios que fizeram por mim e amor que me dão, devo-lhes tudo. Serão sempre a pedra basilar na minha vida.

Acknowledgements

First of all, I want to express my deepest gratitude to Prof. Dr. Paulo Montezuma de Carvalho and Prof. Dr. Rui Dinis, for all the knowledge given to me throughout these years, always accessible patient and kind, were crucial for my Master's degree conclusion.

Also, I am thankful to Prof. Dr. Helena Fino, that always helped me with my academic issues with an enormous sympathy.

I wish to extend my warmest gratitude to those which I consider as family. With all the encouragement, endless support in rough times. I hope I can reward sharing my joy of my accomplishment.

A special thought goes to my dearest person, who gave me strength to conclude this dissertation. To this person, Alice, I thank her for all the inspiration and affection she gives me everyday.

Last but not least, I want to thank those who watch my first steps and grow old. Susana and Ulisses, my sister and brother, the best I could ever had. And to the most important idols in my life: my parents. For all the sacrifices they have done and all the love they give me, I owe them everything. You will always be the cornerstone of my life.

Resumo

Os desenvolvimentos dos sistemas de comunicação sem fios apontam para transmissões de alta velocidade e alta qualidade de serviço com um uso eficiente de energia. Eficiência espectral pode ser obtida por modulações multinível, enquanto que melhorias na eficiência de potência podem ser proporcionadas pelo uso de códigos corretores de erros. Os códigos Low-Density Parity-Check (LDPC), devido ao seu desempenho próximo do limite de Shannon e baixa complexidade na implementação e descodificação são apropriados para futuros sistemas de comunicações sem fios. Por outro lado, o uso de modulações multinível acarreta limitações na amplificação. Contudo, uma amplificação eficiente pode ser assegurada por estruturas de transmissão onde as modulações multinível são decompostas em sub-modulações com envolvente constante que podem ser amplificadas por amplificadores não lineares a operar na zona de saturação. Neste tipo de estruturas surgem desvios de fase e ganho, produzindo distorções na constelação resultante da soma de todos os sinais amplificados. O trabalho foca-se no uso dos códigos LDPC em esquemas multiportadora e monoportadora, com especial ênfase na performance de uma equalização iterativa implementada no domínio da frequência por um Iterative Block-Decision Feedback Equalizer (IB-DFE). São analisados aspectos como o impacto do número de iterações no processo de descodificação dentro das iterações do processo de equalização. Os códigos LDPC também serão utilizados para compensar os desvios de fase em recetores iterativos para sistemas baseados em transmissores com vários ramos de amplificação. É feito um estudo sobre o modo como estes códigos podem aumentar a tolerância a erros de fase que incluí uma análise da complexidade e um algoritmo para estimação dos desequilíbrios de fase.

Palavras-chave: LDPC, descodificação iterativa, desequilíbrios de fase, recetores iterativos, eficiência energética.

Abstract

Further wireless communication systems point towards high bit rates transmissions, very high quality of service together with efficient use of energy. Spectral efficiency can be achieved by multilevel modulations while improvements on optimizing power consumption can be allowed by the use of powerful error control codes. Low-Density Parity-Check (LDPC) codes due to their performance near Shannon limit, low implementation complexity and low decoding complexity are well suited for further wireless communications. On the other hand, the use of multilevel modulations imposes problems on power amplification. Nevertheless, an efficient amplification can be assured by transmission structures where multilevel modulations are decomposed in terms of constant envelope sub-modulations that can be amplified by a Nonlinear (NL) amplifier operating in saturation zone. A problem that arises with these structures is the negative impact on performance of phase and gain imbalances that can cause distortions on the constellation resulting from the sum of all amplified signals.

The focus of the present work is on the use of LDPC codes with Multi-Carrier (MC) and Single-Carrier (SC) block transmission techniques, where special emphasis is given to the influence of LDPC codes on the performance of iterative equalization process implemented by an Iterative Block-Decision Feedback Equalizer (IB-DFE). LDPC codes are also employed in transmission systems based on multi-branch amplification stages to compensate phase imbalances at the receiver. A study about how LDPC can increase the tolerance against phase imbalances is also presented, as well as a new algorithm to estimate these phase imbalances at the receiver.

Keywords: LDPC, low decoding complexity, multilevel modulations, multi-branch amplification structures, Phase imbalances, Iterative Receivers, power efficiency.

Contents

List Of Acronyms

ADC Analog-to-Digital Converter

ARQ Automatic Repeat Request

AWGN Additive White Gaussian Noise

BER Bit Error Rate

BEC Binary Erasure Channel

BSC Binary Symmetric Channel

BP Belief Propagation

CP Cyclic Prefix

CIR Channel Impulsive Response

CPM Continuous Phase Modulation

DAC Digital-to-Analog Converter

DFT Discrete Fourier Transform

DFE Decision Feedback Equalizer

DVB Digital Video Broadcasting

DVB-S2 Digital Video Broadcasting - Satellite - Second Generation

FDE Frequency-Domain Equalization

FDM Frequency Division Multiplexing

FEC Forward Error Correction

FFT Fast Fourier Transform

IB-DFE Iterative Block-Decision Feedback Equalizer

IDFT Inverse Discrete Fourier Transform

IFFT Inverse Fast Fourier Transform

IBI Inter-Block Interference

ICI Inter-Carrier Interference

IRA Irregular Repeat-Accumulate

ISI Inter-Symbol Interference

LDPC Low-Density Parity-Check

LLR Log-Likelihood Ratios

LTE Long Term Evolution

MC Multi-Carrier

MFB Matched Filter Bound

ML Maximum-Likelihood

MMSE Minimum Mean Square Error

MRC Maximal-Ratio Combining

MS Min-Sum

MSE Mean Square Error

MSK Minimum Shift Keying

NL Nonlinear

OFDM Orthogonal Frequency-Division Multiplexing

OOFDM Optical Orthogonal Frequency-Division Multiplexing

PAPR Peak to Average Power Ratio

PCCC Parallel Concatenated Convolutional Codes

PMEPR Peak-to-Mean Envelope Power Ratio

PDP Power Delay Profile

PSD Power Spectrum Density

PSK Phase Shift Keying

QAM Quadrature Amplitude Modulation

QPSK Quadrature Phase-Shift Keying

QoS Quality of Service

RA Repeat-Accumulate

SC Single Carrier

SCCC Serial Concatenated Convolutional Codes

SC-FDE Single Carrier with Frequency Domain Equalization

SINR Signal to Interference-plus-Noise Ratio

SNR Signal to Noise Ratio

SISO Soft-Input, Soft-Output

SP Sum-Product

TCM Trellis Coded Modulations

ZF Zero-Forcing

List of Figures

Chapter 1

Introduction

1.1 Motivation and Scope

Further trends on wireless communication systems point towards high bit rates transmissions, very high quality of service together with efficient use of energy. To increase power and spectral efficiencies, powerful error control codes can be applied together with multilevel modulations. Besides that, the spectral efficiency achieved by multilevel modulations should remain almost unaffected when error control codes are adopted which can be attained by high code rates. Low-Density Parity-Check (LDPC) codes [1] are well suited for further wireless communication systems due to its performance near Shannon limit and low implementation complexity. Also, low latencies can be achieved through low decoding complexity when compared with turbo-codes with similar performance. Moreover, they are specially suited to assure the quality of service requirements of Long Term Evolution (LTE) where it is needed to approach 1 Gbps on downlink.

On the other hand, the use of multilevel modulations imposes problems on power efficiency and consequently on battery usage in mobile devices. For efficient amplification of multilevel modulations, multi-branch amplification structures were proposed in [2], where multilevel modulations are decomposed in terms of constant envelope sub-modulations. Due to the constant envelope, power amplification's efficiency can improve significantly since each amplification branch can employ a non-linear amplifier operating in saturation zone. However, this structure imposes that the M amplifiers must take well defined phase values to avoid imbalances that can cause distortions in the constellation that results from

the sum of all amplified signals.

Time dispersive channels and their frequency selectivity over the signals' bandwidths comprise other problems associated to wireless transmission in mobile communications. Block transmission techniques such as Orthogonal Frequency-Division Multiplexing (OFDM) and Single Carrier with Frequency Domain Equalization (SC-FDE) with a appropriate Cyclic Prefix (CP) (i.e., with a size that deals with the maximum channel delay) and employing FDE techniques, have shown to be suitable for high data rate transmission over highly dispersive channels [3] [4]. Multi-Carrier (MC) modulation systems employing frequency-domain equalization are an alternative to SC modulation systems. OFDM has become very popular in several standards of mobile communications systems operating in severely frequency-selective fading radio channels. For channels with severe delay spread, OFDM employs frequency domain equalization which is computationally less complex than the corresponding time domain equalization. The reason for that lies on the fact that equalization is performed on a data block at each time, and the operations on this block involve only a Discrete Fourier Transform (DFT) implemented by an efficient Fast Fourier Transform (FFT) [5] operation plus a simple channel inversion operation.

On the other hand, Single Carrier (SC) modulations with non-linear equalizers implemented in the frequency-domain employing FFTs, are a good alternative to MC, due to better performances than the corresponding OFDM, while offering low complexity of implementation.

LDPC codes have been employed with success as alternative to turbo and convolutional codes in several standards such as Digital Video Broadcasting - Satellite - Second Generation (DVB-S2) and LTE. Large codeword sizes are found to approach the channel capacity and have lower decoding complexity [6]. LDPC codes were applied to OFDM systems without iterations between the LDPC's decoder block and another functional block [7][8]. Iteration between LDPC decoder and soft demodulator has been proposed for LDPC coded OFDM systems [9][10]. Iteration between LDPC decoder and channel estimator has been proposed for LDPC coded OFDM systems [11].

In [12] an equalizer algorithm for the cellular relay system, which uses a Decision Feedback Equalizer (DFE) combined with a LDPC code to achieve better Quality of Service (QoS)

was considered. In [13] SC signals were combined with powerful LDPC codes and iterative frequency-domain equalization based on the Iterative Block-Decision Feedback Equalizer (IB-DFE) concept to minimize distortion of multipath time dispersive channels.

1.2 Objectives

The focus of this work is on the use of LDPC codes in MC and SC systems. Special emphasis is given to the influence of LDPC codes on the performance of a special designed iterative equalization process implemented by an IB-DFE that interacts with the soft decisions of LDPC decoder. For both systems two types of channels are considered: Additive White Gaussian Noise (AWGN) and time-dispersive channels. Aspects as the impact of the iterations in the LDPC soft-decision decoding process in the convergence of the equalizing process are analysed. The simulation results show that, for SC systems, the performance improvements can be achieved without increasing the system complexity since the number of iterations in the equalizer can be significantly reduced due to the presence of LDPC codes.

It is also analyzed how LDPC codes can be employed to compensate phase imbalances and increase the tolerance against these imbalances in transmission systems based on multi-branch amplification stages. Performance results allow to conclude that even very simple LDPC codes increase significantly the tolerance margin for hardware implementation without compromising system's performance. Moreover, this higher tolerance comes associated to a better power efficiency due to coding gain introduced by LDPC codes. Although, the compensation of phase imbalances may be achieved by LPDC codes, a better approach is to compensate those imbalances and use LDPC codes to improve the system's energy efficiency. Having in mind these considerations, a method to correct phase imbalances at the receiver that estimates the values of phase imbalances with good accuracy and reduces their impact on system's performance to a negligible effect is proposed.

1.3 Outline

This thesis is organized as follows:

After this introductory chapter, Chapter 2 presents the basic principles of block codes. It starts with the characterization of linear block codes, followed by the study of LDPC codes. LDPC's characterization includes aspects such as construction and representation methods and trade-offs regarding implementation's complexity. Several decoding processes are characterized in section 2.3.4. Finally, LDPC applications are presented at the end of the chapter.

Chapter 3 focuses on the characterization of SC and MC modulations. OFDM modulations and SC-FDE modulations with linear and nonlinear equalizers at the receiver are described, including transmitter and receiver's characterization as well as the analytical representation in time and frequency domains. The analysis also addresses IB-DFE receivers with emphasis to the characterization of IB-DFE "turbo like" equalizer employing in the feedback loop the "soft decisions" from the LDPC's Soft-Input, Soft-Output (SISO) block. The impact of code's block length and number of iterations on the asymptotic performance of IB-DFE schemes are investigated. For comparison purposes, some performance results for MC systems are also presented and discussed.

Chapter 4 introduces the study of techniques for compensation of phase imbalances. Two approaches are adopted: the first one employs simple and powerful error correcting codes, such as LDPC codes used to increase the system's robustness. We propose a receiver that combines a SISO block with a modulator that tries to compensate phase imbalances' effects in constellation symbols to achieve better estimates of the symbols in the feedback loop. The higher tolerance against phase imbalances shown by simulation results confirms the assumption that we can improve robustness of these systems at cost of a slight increase on complexity. In the second one, the receiver is designed to compensate these phase rotations using an iterative estimate process of the phase imbalances that practically cancels the impact of phase imbalances due to the good accuracy of the estimates.

Lastly, chapter 5 presents the final conclusions and remarks of this thesis, as well as some future work perspectives.

Chapter 2

Error-Correcting Codes

In further wireless communications systems very high bit rates will be necessarily associated to high quality of service requirements. Despite these requirements, the available bandwidth and transmission power are limited resources. To overcome these limitations, modulations with high spectral efficiency should be used and power efficiency must be increased. Several techniques are available to improve power efficiency, such as the use of power efficient modulations, the resort to better amplification stages and finally the use of error correcting codes. However, two problems may arise with error correcting codes: one is the eventual reduction on spectral efficiency and the other is related with the complexity of encoding and decoding processes. Therefore, an excellent performance due to implementing error correcting codes with low complexity at the decoder, will be crucial to assure low latency. Another key aspect is related with the spectral efficiency that should not be heavily sacrificed. Having in mind these requirements, LPDC codes due to their low complexity and performance similar to turbo codes, seem to be a good option for error correction technique in block transmission systems. Thus in sections 2.1 and 2.2 the reasons behind the usage of error correcting codes and the generic properties of block codes are presented. In section 2.3 the characterization of LDPC codes is made, which includes the construction methods, decoding process and key characteristics associated to the performance of such codes. To conclude this chapter, the applications of LDPC codes and their role in the present work are presented in section 2.4.

2.1 Shannon Limit

Claude Shannon established a theorem about channel capacity [14]. Such theorem states that it is possible to calculate the maximum data transmission rate without error or with low bit error rate for a given channel with a specific bandwidth, interference power and noise. According to Shannon's theorem, when the transmitted signal y and the noise n are uncorrelated, the channel capacity C is given by the difference of the signal and noise entropies

$$C = H(y) - H(n), \tag{2.1}$$

where $H(y)$ and $H(n)$ are the signal and noise entropies, respectively. For an AWGN channel, the entropy of the transmitted signal y with power P and the noise's entropy with power N are

$$H(y) = W \cdot log_2\,[2\pi e(P+N)], \tag{2.2}$$

and

$$H(n) = W \cdot log_2\,[2\pi eN], \tag{2.3}$$

respectively. Replacing (2.2) and (2.3) in (2.1) results

$$C = W \cdot log_2\left(\frac{P+N}{N}\right) = W \cdot log_2\left(1+\frac{P}{N}\right) \qquad [bit/s], \tag{2.4}$$

where $\frac{P}{N}$ represents the Signal to Noise Ratio (SNR).

From (2.4) it is obvious that the channel capacity can be raised by increasing bandwidth or signal power. Increases in bandwidth are difficult since it is a limited resource. On the other hand, due to limitations on battery usage and radiated power, increases in power should be avoided. Nevertheless, it is possible to increase the system's power efficiency without any increment in the transmitted power or changes on SNR through the introduction of error correcting codes. Several techniques can be adopted to implement error correcting codes, such as block codes, convolutional codes or Trellis Coded Modulations (TCM) when the system's spectral efficiency must remain unchanged.

2.2 Error-Control Coding

In wireless communication systems, reliability and efficiency of data transmission are the main requirements for the conception of error-control coding. Error detection and correction capabilities can be assured by adding extra bits for information redundancy. When redundancy is enough it is possible to rectify the wrong bits and unveil the correct information. The simplest way to do error control is to carry out error detection only, using an Automatic Repeat Request (ARQ) strategy, where the receiver requests the retransmission of the data block whenever an error is detected. Another possibility, when the error code has ability to correct errors, is Forward Error Correction (FEC) where the receiver tries to correct the incorrect bits. This strategy can also be adopted when retransmissions are impossible or when it is intended to keep low the delay associated to the retransmission. Obviously, both strategies can be employed together in a ARQ/FEC scheme, where the receiver asks for a retransmission every time that the correction capacity is exceeded. Usually, in wireless systems low latency and delays are required to sustain high bit rates. Therefore, powerful error correcting codes should be employed to achieve the QoS imposed by the supported services without many retransmissions.

The simplest error-control code is the repetition code which consists on repeating the message bit n times. The drawback is a reduction on spectral efficiency that is proportional to the repetition factor n. Let us consider the following example of a repetition code with $(n, 1)$, where $k = 1$ denotes the number of information bits.

Example 1. *If a message bit $m = 0$ was to be transmitted and a repetition code $(n, 1)$ is used for error-control, the codeword is $\mathbf{c} = \begin{bmatrix} 0 & 0 & .. & 0 \end{bmatrix}$ with size n. And for a message $m = 1$, $\mathbf{c} = \begin{bmatrix} 1 & 1 & .. & 1 \end{bmatrix}$.*

Therefore, the Hamming distance between the two possible codewords is n (the Hamming distance between two codewords agrees with the number of different bits). The minimum Hamming distance between codewords is directly related with its detection and correction capabilities. For the maximum number of errors achievable of detection l_{max} obeys the following rule

$$l_{max} = d_{min} - 1. \tag{2.5}$$

For correction the maximum size of the error t_{max} should be

$$t_{max} = (d_{min} - 1)/2. \tag{2.6}$$

Considering that the error bit probability is given by, $Pe = \alpha$, for the n-bit codeword, the probability of having i errors will be

$$Pe(i, n) = \binom{n}{i} \alpha^i (1 - \alpha)^{n-i} \tag{2.7}$$

$$Pe(i, n) \approx \binom{n}{i} \alpha^i \qquad \alpha << 1 \tag{2.8}$$

Therefore, with this codes, the error probability will be lower. However, the high impact of repetition codes on spectral efficiency makes them a bad option for wireless transmission systems and communication systems in general. Hence, more efficient coding techniques should be adopted, such as parity-check codes[1] that are characterized in next section.

2.2.1 Parity-Check equations

Parity-check codes are built by adding extra bits to the message bits, called check-bits. The purpose of check bits is to make the parity even or odd, in every codeword. Those check bits can be added before or after the set of message bits. For instance, let us consider a message $\mathbf{m} = \begin{bmatrix} m_1 & m_2 & m_3 & m_4 & m_5 \end{bmatrix}$ containing 5 bits of information plus one check bit p_1 at the end. The resulting codeword is

$$\mathbf{c} = \begin{bmatrix} m_1 & m_2 & m_3 & m_4 & m_5 & p_1 \end{bmatrix} = \begin{bmatrix} c_1 & c_2 & c_3 & c_4 & c_5 & c_6 \end{bmatrix}. \tag{2.9}$$

Therefore, every valid codeword must verify the parity-check equation given by

$$c_1 \oplus c_2 \oplus c_3 \oplus c_4 \oplus c_5 \oplus c_6 = 0, \tag{2.10}$$

where $\oplus$ denotes a Modulo-2 addition. Clearly, if $\mathbf{c}$ is a valid codeword there is no error, otherwise we have at least one error. If the parity is set to be even, this code is only

[1] it should be pointed that repetition codes are a particular case of parity check codes

able to detect odd errors. To detect even errors, more check bits should be added to the original set of bits, i. e. we need to increase the redundancy of the code. And to make the error detection more reliable it is necessary to have more parity-check equations. The set of parity-check equations can be written in a matrix format H, where each row of parity-check matrix H is a parity-check equation.

2.2.2 Linear Block codes

Both repetition codes and parity-check codes are special cases of block codes. Such type of error-control is based on adding extra bits not related to whatsoever with message bits. The encoding process can be described by an $k \times n$ generator matrix $\mathbf{G}$, where n are the number of bits in the codeword and k represents the number of information bits. Thus, any codeword $\mathbf{c}$ can be found based on the message word $\mathbf{m}$, by a simple matrix multiplication

$$\mathbf{c} = \mathbf{m}G. \tag{2.11}$$

Obviously, for a $(n, 1)$ repetition code, the generator matrix $\mathbf{G}$ is a matrix of ones with size $n \times 1$. Let us consider now a $(3, 2)$ code with the following coding table:

m	c
00	000
01	101
10	110
11	011

Table 2.1: Encoding table

The corresponding 2×3 generator matrix $\mathbf{G}$ is given by

$$\mathbf{G} = \begin{bmatrix} g_{11} & g_{12} & g_{13} \\ g_{21} & g_{22} & g_{23} \end{bmatrix} = \begin{bmatrix} g_1 \\ g_2 \end{bmatrix}, \tag{2.12}$$

where $g_1 = \begin{bmatrix} g_{11} & g_{12} & g_{13} \end{bmatrix}$ and $g_2 = \begin{bmatrix} g_{21} & g_{22} & g_{23} \end{bmatrix}$. Therefore, any codeword can be generated using the relation

$$\mathbf{c} = \mathbf{bG} = \begin{bmatrix} m_1 & m_2 \end{bmatrix} \begin{bmatrix} g_1 \\ g_2 \end{bmatrix} = m_1 g_1 + m_2 g_2. \tag{2.13}$$

Using (2.13) the matrix coefficients can be computed, based on the codewords. For example, if $m = \begin{bmatrix} 1 & 0 \end{bmatrix}$ and $c = \begin{bmatrix} 1 & 1 & 0 \end{bmatrix}$ we may write $\mathbf{c} = \mathbf{m}G = m_1 g_1 + m_2 g_2 = 1 \cdot g_1 + 0 \cdot g_2 = \begin{bmatrix} 1 & 1 & 0 \end{bmatrix}$, which leads to the solution $g_1 = \begin{bmatrix} 1 & 1 & 0 \end{bmatrix}$. For $m = \begin{bmatrix} 0 & 1 \end{bmatrix}$ and $c = \begin{bmatrix} 1 & 0 & 1 \end{bmatrix}$ we have $\mathbf{c} = \mathbf{mG} = m_1 g_1 + m_2 g_2 = 0 \cdot g_1 + 1 \cdot g_2 = \begin{bmatrix} 1 & 0 & 1 \end{bmatrix}$, and therefore $g_2 = \begin{bmatrix} 1 & 0 & 1 \end{bmatrix}$. Finally, the generator matrix $\mathbf{G}$ can be written as

$$\mathbf{G} = \begin{bmatrix} 1 & 1 & 0 \\ 1 & 0 & 1 \end{bmatrix}. \tag{2.14}$$

Thus, using (2.14) it is possible to define the coded bits by

$$\begin{bmatrix} c_1 & c_2 & c_3 \end{bmatrix} = \begin{bmatrix} m_1 & m_2 \end{bmatrix} \begin{bmatrix} 1 & 1 & 0 \\ 1 & 0 & 1 \end{bmatrix} = \begin{cases} c_1 = m_1 \oplus m_2, \\ c_2 = m_1, \\ c_3 = m_2. \end{cases} \tag{2.15}$$

Since a (n, k) linear code C is a k-dimensional subspace of the vector space V_n of all the binary n-tuples, it is possible to find k linearly independent codewords, $g_0, g_1, ...g_{k-1}$ in C such that every codeword $\mathbf{c}$ in C is a linear combination of these k codewords, that is,

$$\mathbf{c} = m_0 g_0 + m_1 g_1 + \cdots + m_{k-1} g_{k-1}, \tag{2.16}$$

where $m_i = 0$ or 1 for $i = 1, .., k$. Let us arrange these k linearly independent codewords

as the rows of a $(k \times n)$ matrix as follows

$$G = \begin{bmatrix} g_{0,0} & g_{0,1} & \cdots & g_{0,n-2} & g_{0,n-1} \\ g_{1,0} & g_{1,1} & \cdots & g_{1,n-2} & g_{1,n-1} \\ & \vdots & \ddots & \vdots & \\ g_{k-2,0} & g_{k-2,1} & \cdots & g_{k-2,n-2} & g_{k-2,n-1} \\ g_{k-1,0} & g_{k-1,1} & \cdots & g_{k-1,n-2} & g_{k-1,n-1} \end{bmatrix}, \tag{2.17}$$

where $\mathbf{g_i} = (g_{i0}, g_{i1}, ..., g_{i,n-1})$ for $0 \leq i < k$. If $\mathbf{m} = (m_0, m_1, ..., m_{k-1})$ is the message to be encoded, the resulting codeword will be given by (2.11) and

$$\mathbf{c} = \mathbf{mG} = (m_0, m_1, ..., m_{n-1}) \begin{bmatrix} g_{i0} \\ g_{i1} \\ \vdots \\ g_{i,k-1} \end{bmatrix} = m_0 g_0 + m_1 g_1 + \cdots + m_{k-1} g_{k-1} \tag{2.18}$$

It follows from (2.17) that a (n, k) linear code is completely specified by the set of k rows of matrix $\mathbf{G}$.

A block code of length n and 2^k codewords is called a linear (n, k) code if and only if its 2^k codewords form a k dimensional subspace of the vector space of all the n-tuples over the field GF(2). In fact, a binary block code is linear if and only if the modulo-2 sum of two codewords is also a codeword. The block code described in table (2.1) is a $(3, 2)$ linear code [2].

A desirable property for a linear block code to possess is the systematic structure, where a codeword is divided into two parts, the message part and the redundant parity checking part. The message part consists of k unaltered information (or message) digits and the redundant checking part consists of n - k parity-check digits, which are linear combinations of the information bits. A linear block code with this structure is referred as a linear systematic block code. The $(3, 2)$ code described by (2.15) is a linear systematic block code; the rightmost two digits c_2 and c_3 of each codeword are identical to the corresponding information bits m_1 and m_2. Hence a linear systematic (n, k) code is completely specified

[2] the sum of any two codewords in this code also is a codeword

by a $k \times n$ matrix $\mathbf{G}$ given by

$$\mathbf{G} = \begin{bmatrix} g_0 \\ g_1 \\ \vdots \\ g_{k-2} \\ g_{k-1} \end{bmatrix} = \left[\begin{array}{ccccc:ccc} p_{0,0} & p_{0,1} & \cdots & p_{0,n-2} & p_{0,n-k-1} & 1 & 0\cdots 0 & 0 \\ p_{1,0} & p_{1,1} & \cdots & p_{1,n-2} & p_{1,n-k-1} & 0 & 1\cdots 0 & 0 \\ & \vdots & \ddots & \vdots & & \vdots & \vdots\ddots\vdots & \vdots \\ p_{k-2,0} & p_{k-2,1} & \cdots & p_{k-2,n-k-2} & p_{k-2,n-k-1} & 0 & 0\cdots 1 & 0 \\ p_{k-1,0} & p_{k-1,1} & \cdots & p_{k-1,n-k-2} & p_{k-1,n-k-1} & 0 & 0\cdots 0 & 1 \end{array}\right], \quad (2.19)$$

where $p_{ij} = 0$ or 1. Let I_k denote the $k \times k$ identity matrix. Then $\mathbf{G} = \left[P \vdots I_k\right]$ and $\mathbf{m} = (m_0, m_1, ..., m_{k-1})$ is the message to be encoded, the corresponding codeword is:

$$\mathbf{c} = (c_0, c_1, ..., c_{n-1}) = (m_0, m_1, ..., m_{k-1}) \cdot \mathbf{G} \quad (2.20)$$

Codes can be systematic at right or left, depending on the side where the information bits occur in the codeword. For a systematic code at right, the generator matrix $\mathbf{G}$ has a $k \times k$ identity sub-matrix I_k in the first k columns and is given by

$$\mathbf{G} = \left[I_k \vdots P\right]. \quad (2.21)$$

Obviously, for a code systematic at left results

$$\mathbf{G} = \left[P \vdots I_k\right]. \quad (2.22)$$

There is another useful matrix associated with every linear block code. For any $k \times n$ matrix $\mathbf{G}$ with k linearly independent rows exists a $(n-k) \times n$ matrix H with $n-k$ linearly independent rows that any vector in the row space of $\mathbf{G}$ is orthogonal to the rows of H. Any vector that is orthogonal to the rows of H is in the row space of $\mathbf{G}$. Hence, we can describe the (n, k) linear code generated by $\mathbf{G}$ in an alternate way as follows: An n-tuple $\mathbf{c}$ is a codeword belonging to the code generated by $\mathbf{G}$ if and only if $\mathbf{c}H^T = 0$. This matrix H is called a parity check matrix of the code. If the generator matrix of an (n, k) linear code is in the systematic form of (2.21), the corresponding parity-check matrix is

$$H = \left[P^T \vdots I_{n-k} \right]. \tag{2.23}$$

So a received set of bits $\mathbf{y}$, is a valid codeword if and only it satisfies

$$H\mathbf{y}^T = 0. \tag{2.24}$$

Another way to obtain the minimum distance with the parity-check matrix H, is to find the minimum number of columns of H needed to set the sum of all equal to zero.

Regarding the impact of these codes in system performance we can start by analysing the error probability for a ARQ system. Clearly, the retransmission probability depends on the error detection capacity. Using (2.7) we may write the probability of an erroneous detection, i.e., no retransmission in presence of errors as

$$P_w = \sum_{i=d_{min}}^{n} A_i P^i (1-P)^{n-i}, \tag{2.25}$$

where A_i are the number of words with weight i. So, for the retransmission probability results

$$P_{ret} = \sum_{i=d_{min}}^{n} \left[\binom{n}{i} - A_i \right] P^i (1-P)^{n-i}. \tag{2.26}$$

For a FEC strategy, it can be shown that the error probability is given by

$$P_w = \sum_{i=t_{max}+1}^{n} \left[\binom{n}{i} - \alpha_i \right] P^i (1-P)^{n-i}, \tag{2.27}$$

where α_i is the number of correctable error patterns and t_{max} the maximum number of correctable errors [15].

It can be shown that the power gain associated to the code is given by

$$\mathbf{G} = 10 \log(R \cdot m) \tag{2.28}$$

where $m = d_{min}$ for ARQ and $m = t + 1$ for FEC and R denotes the code's rate. As we can see the introduction of codes leads to power gains that increase with d_{min}. However,

to not compromise spectral efficiency, the code rate $R = k/n$ should not be too low.

2.3 Low-Density Parity-Check codes

Low-Density Parity-Check codes, created by Robert G. Gallager [1], are linear block codes with a very large and sparse parity-check matrix. LDPC codes were rediscovered by MacKay [6] as an alternative to turbo codes, with lower decoding complexity and similar or even better performance in high bit rate transmissions.

LDPC codes can be closer to the Shannon Limit than turbo codes, because the minimum distance increases proportionally to the code length. Since they have a higher minimum distance, the threshold of waterfall region can be lower than turbo codes. Moreover, they are also less sensitive to an error floor effect or at least, the error floor is lower since we have an higher d_{min}. It should be mentioned that the waterfall region denotes the region where the Bit Error Rate (BER) drops exponentially with any increase of SNR, as shown in fig. 2.1.

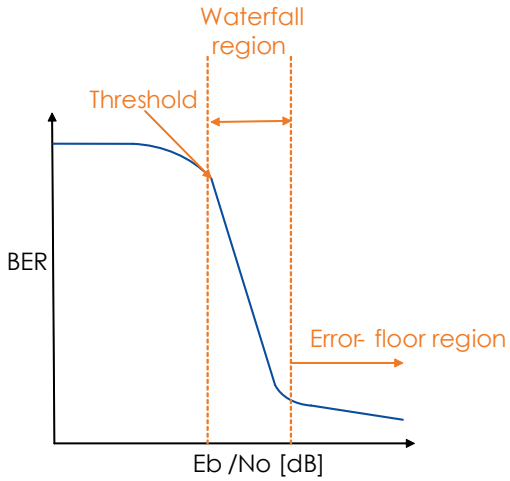

Figure 2.1: Representation of the waterfall and error-floor regions

Hence, the behavior of the minimum distance in LPDC codes is desirable to assure the intended QoS in a high bit rate transmission with very low error rate.

2.3.1 Properties

As stated before, LDPC codes are characterized by a sparse parity-check matrix H. This matrix has n columns corresponding to the number of bits in each codeword and $m = n-k$ rows related with the parity-check equations. As aforementioned, d_{min} is the number of linear independent columns of H. Hence, if the weight of the rows and columns is significantly decreased in order to attain sparseness, it will be necessary to sum more columns to assure the zero solution. Consequently, d_{min} increases as well as the error detection and correction capabilities.

2.3.2 Tanner Graphs

It is usual to describe LDPC codes with resort to Tanner graphs, which allows an easier interpretation of matrix H and can be used in both encoding and decoding processes [16]. These graphs are bipartite graphs composed by two types of nodes: check nodes and variable or bit nodes. Check nodes $f_j, j = 1, .., m$ represent each parity-check equation and are associated to the m rows of H. The variable nodes or bits nodes $x_\ell, \ell = 1, 2, .., n$ are associated to code bits and their number is equal to the number of columns of H. Connections between a bit node and a check node exist whenever the bit participates in the corresponding parity-check equation. The number of edges or connections that converge in a node is referred as node order, being dc the node order for check nodes and dv the node order for bit nodes, and the total of edges is equal to the number of "ones" of matrix H. For instance in figure 2.2, the node order of all check nodes is 3 and bit nodes have a node order of 2.

$$H = \begin{bmatrix} 1 & 1 & 0 & 1 & 0 & 0 \\ 0 & 1 & 1 & 0 & 1 & 0 \\ 1 & 0 & 0 & 0 & 1 & 1 \\ 0 & 0 & 1 & 1 & 0 & 1 \end{bmatrix}$$

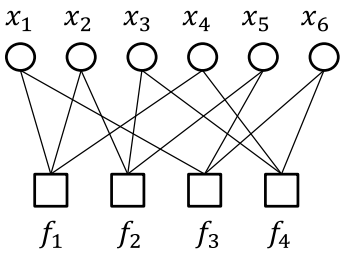

Figure 2.2: Graphical representation of a parity-check matrix with a Tanner graph

It should be mentioned that the sparseness of H also means a simplified decoding process.

Let wc and wr be the weight of columns and rows, respectively. When all rows and columns have the same weight (note that the columns and rows may have a different weights), these codes are called regular codes, otherwise are called irregular codes. In (2.29) and (2.30) are presented examples of H for regular and irregular codes, respectively.

$$H = \begin{bmatrix} 1 & 1 & 0 & 1 & 0 & 0 \\ 0 & 1 & 1 & 0 & 1 & 0 \\ 1 & 0 & 0 & 0 & 1 & 1 \\ 0 & 0 & 1 & 1 & 0 & 1 \end{bmatrix} \tag{2.29}$$

$$H = \begin{bmatrix} 1 & 1 & 0 & 1 & 0 & 1 \\ 0 & 1 & 1 & 0 & 1 & 0 \\ 1 & 0 & 0 & 1 & 1 & 1 \\ 0 & 1 & 1 & 1 & 0 & 1 \end{bmatrix} \tag{2.30}$$

In irregular codes, the weights of both rows and columns are represented by the degree of distribution polynomials $\lambda(x)$ and $\rho(x)$, since there is a different set of values for a distinct set of rows and columns. The distribution polynomials $\lambda(x)$ and $\rho(x)$ given by

$$\lambda(x) = \sum_{d=1}^{dv} \lambda_d x^{d-1}, \tag{2.31}$$

and

$$\rho(x) = \sum_{d=1}^{dc} \rho_d x^{d-1}, \tag{2.32}$$

where λ_d and ρ_d are the fraction of edges of degree d, assigned to the variable nodes and check nodes, respectively. For instance, for the irregular matrix of (2.30) the corresponding degree distribution polynomials are

$$\lambda(x) = \lambda_2 x + \lambda_3 x^2 = \frac{3}{6}x + \frac{3}{6}x^2, \tag{2.33}$$

and

$$\rho(x) = \rho_3 x^2 + \rho_4 x^3 = \frac{1}{4}x^2 + \frac{3}{4}x^3 \tag{2.34}$$

, respectively.

2.3.3 Construction

The computation of matrix H is the main process in the definition of LDPC codes. First methods were proposed by Gallager [1] and, since the H matrix is sparse, the construction is based on the desired degree distribution specified by the weight of columns and rows. Another method was proposed in [6], where the weight of the columns of H is chosen to assure the desired bit distribution. Next, columns are added one at a time from left to right, and the bit location is chosen randomly in the unfilled rows. In regular codes, a fixed number of "ones" in rows and columns of H is wanted. Therefore, if matrix is built based on algebraic operations, the complexity grows with n^2. By swapping rows and columns, we have almost a linear growth of the complexity.
Another problem is to find the corresponding generator matrix **G**. To avoid that, it can be possible to encode the message using only H, by putting this matrix in a upper triangular form by back substitution [17].

Repeat-Accumulate LDPC codes

Repeat-Accumulate (RA) codes are another construction method of LDPC codes proposed by Divsalar [18]. These codes are obtained from sparse graphs and the Repeat-Accumulate encoders are easily encodable with low complexity. In the encoding process, the value of each check-node is the addition of the adjacent bit-nodes, from which the term 'accumulate' is derived. In algebraic terms, the construction of the whole encoding process lies in the combination of two sub-matrices: one regular H_1 and another systematic H_2. The resulting parity check matrix is represented as

$$H = \left[H_1 \vdots H_2 \right], \tag{2.35}$$

where the systematic matrix H_2 has the form

$$H_2 = \begin{bmatrix} 1 & 0 & 0 & & 0 & 0 & 0 \\ 1 & 1 & 0 & \cdots & 0 & 0 & 0 \\ 0 & 1 & 1 & & 0 & 0 & 0 \\ & \vdots & & \ddots & & \vdots & \\ 0 & 0 & 0 & & 1 & 0 & 0 \\ 0 & 0 & 0 & \cdots & 1 & 1 & 0 \\ 0 & 0 & 0 & & 0 & 1 & 1 \end{bmatrix}. \tag{2.36}$$

As we can see, matrix H_2 is not regular due to its last column with corresponding weight 1. Despite this fact, for classification purposes of RA codes, whenever matrix H_1 is regular the RA code is classified as regular. Otherwise it is an Irregular Repeat-Accumulate (IRA) code. Thus, a regular RA code will be classified as (wr_1,wc_1), where wr_1 and wc_1 are the weights of the rows and columns of matrix H_1, respectively. For instance, in (2.37) it is shown a parity check matrix for a length 10 rate 1/2 (3,3)-regular RA code.

$$\begin{bmatrix} 1 & 1 & 0 & 1 & 0 & 1 & 0 & 0 & 0 & 0 \\ 1 & 0 & 1 & 0 & 1 & 1 & 1 & 0 & 0 & 0 \\ 1 & 0 & 1 & 0 & 1 & 0 & 1 & 1 & 0 & 0 \\ 0 & 1 & 1 & 1 & 0 & 0 & 0 & 1 & 1 & 0 \\ 0 & 1 & 0 & 1 & 1 & 0 & 0 & 0 & 1 & 1 \end{bmatrix}. \tag{2.37}$$

Another advantage of the codes generated by this process lies on the fact that it is easy to extract the message bits from the received code words. The same conclusion can be done based on Tanner graphs. Let us consider the Tanner graph for (2.37), shown in figure 2.3, where the bit nodes are grouped into message bit nodes and parity check bit nodes (this is possible since in codeword $\mathbf{c} = \begin{bmatrix} m_1, m_2, ..., m_k, p_1, p_2, ..., p_m \end{bmatrix}$ the first k bits contain all k message bits and the last m bits are parity-check bits). Ultimately, the greatest advantage yield by RA codes is the form of matrix H, which is built into the desired upper triangular form.

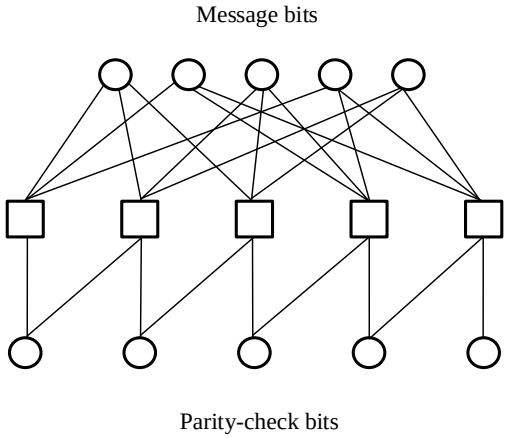

Figure 2.3: Tanner Graph representation for the RA parity-check matrix of example 2.37

2.3.4 Decoding

The decoding process of LDPC codes is based on a SISO [19]. As mentioned before, Tanner graphs can be used to decode LDPC codes. The decoding process exchanges messages between nodes iteratively [20], containing information about bit's reliability. The more edges the graph has, the more messages are transferred between nodes. However, if the connections are from neighbour nodes whose bit information is reliable, it will greatly improve the decoding process through all iterations. Bit nodes are equivalent to function variables. So, LDPC codes with a low number of "ones" on the parity-check matrix have a low number of variables therefore, are more eligible to the decoding process based on Tanner Graphs.

Sum-product algorithm

The Sum-Product (SP) Algorithm's simplification lies on a factorization of the global probability function into a product of local functions [21]. The decoding process starts by each bit node broadcasting to its neighbours nodes, the error probability of the channel, i.e., the priori probability p_i:

$$p(y_i|x_i = 1) = p_i. \tag{2.38}$$

The sent message is a "request", q_{ij}, from the bit node x_i to the connected f_j check nodes,

to know the other probabilities sent from the other nodes connected to the same check node. q_{ij} gives the probability of $x_i = 1$ for the quantity $p(y_i|x_i)$ and the previously received values

$$q_{ij} = p(x_i = 1|\ f_j, \mathbf{y}). \tag{2.39}$$

In figure 2.4 it is shown the typical exchange of messages between nodes during the iteration of the decoding process. Next, each check node connected to the bit node x_i, sends a response r_{ji} regarding the probability of $x_i = 1$ and a successful parity-check equation f_j, for a given y:

$$r_{ji} = p(x_i = 1, f_j() = 1|\mathbf{y}) \tag{2.40}$$

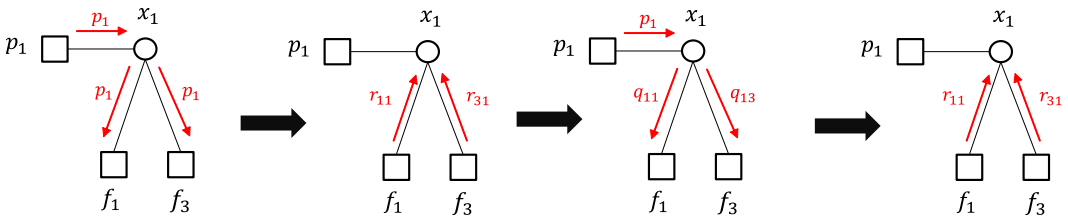

Figure 2.4: Message exchange on Tanner Graphs

So, for each decoding iteration, the message update from bit node x_i to check node f_j will be given by

$$q_{ij} = K_{ij} \prod_{j' \neq j} r_{j'i}, \tag{2.41}$$

where K_{ji} is a normalization factor. The message update from check node f_j to bit node x_i is

$$r_{ji} = \sum_{i' \neq i} \left[\prod_{i' \neq i} q_{i'j} \right], \tag{2.42}$$

and after message exchange the posteriori probability can be computed by

$$p(x_i|\mathbf{y}) = q_i = K_{ij} p_i \prod_{j' \neq j} r_{j'i}. \tag{2.43}$$

This process has a large number of operations, therefore the messages containing probabilities will be replaced by Log-Likelihood Ratios (LLR). The main reason for using LLRs is to lower the complexity by using additions instead of multiplications. The ratio between the probability of a certain bit node x_i being '1' and the probability of being '0' considering the received message bits $\mathbf{y}$ is the Log-likelihood ratio, given by

$$L(x_i|\mathbf{y}) = \ln\left[\frac{p(x_i = 1|\mathbf{y})}{p(x_i = 0|\mathbf{y})}\right]. \tag{2.44}$$

Hence, if x_i has a higher probability of being '1' results:

$$\frac{p(x_i = 1|\mathbf{y})}{p(x_i = 0|\mathbf{y})} > 1. \tag{2.45}$$

Since that $\ln(x) > 0$ if $x > 1$ and otherwise if $x < 1$, we may write

$$L(x_i|\mathbf{y}) = \begin{cases} > 0, & x_i = 1 \\ < 0, & x_i = 0 \end{cases}. \tag{2.46}$$

So, for the message from the bit node x_i to check node f_j we may write:

$$L(q_{ij}) = L(p_i) + \sum_{j' \neq j} L(r_{j'i}). \tag{2.47}$$

From check node f_j to bit node x_i we have

$$L(r_{ji}) = \Phi^{-1}\left[\prod_{i' \neq i} \Phi(q_{i'j})\right], \tag{2.48}$$

where $\Phi(x) = \tanh(-x/2)$. Finally, at the end of each iteration the a posteriori LLR will be computed as

$$L(x_i|\mathbf{y}) = L(q_i) + \sum_{j} L(r_{ji}), \tag{2.49}$$

that allows to do the final decision about the bit value.

The initialization steps for the message passing will differ according to the type of channel. The different LLRs for a Binary Erasure Channel (BEC), Binary Symmetric Channel (BSC) and BI-AWGN Channel are respectively:

$$L(q_{ij}) = L(x_i) = \begin{cases} +\infty & , y_i = 0 \\ +\infty & , y_i = 1 \\ 0 & y_i = E \end{cases} \qquad (BEC), \tag{2.50}$$

$$L(q_{ij}) = L(x_i) = (-1)^{y_i} \log\left(\frac{1-\epsilon}{\epsilon}\right) \qquad (BSC), \tag{2.51}$$

$$L(q_{ij}) = L(x_i) = 2y_i/\sigma^2 \qquad (BI-AWGNC). \tag{2.52}$$

Min-Sum algorithm

There is another method with simpler implementation and lower number of operations than SP algorithm, with only a minor performance cost [22]. This algorithm performs Maximum-Likelihood (ML) decoding and it is called as max-product or Min-Sum (MS). The main enhancement is the approximation of the LLR based on the value of $L(q_{i'j})$ that maximizes $L(r_{ji})$.

Firstly we define a new auxiliary function:

$$\phi(x) = -\log\left[\tanh(x/2)\right] = \log\left(\frac{e^x+1}{e^x-1}\right), \qquad x > 0, \tag{2.53}$$

Since for every real number y it is valid to write

$$y = sgn(y)\,|y|\,, \tag{2.54}$$

the equation (2.48) can be rewritten as

$$L(r_{ji}) = -1^{d_j}\left(\prod_{i'\neq i} sgn\left[L(q_{i'j})\right]\right)\phi\left(\sum_{i'\neq i}\phi\left(\left|L(q_{i'j})\right|\right)\right), \tag{2.55}$$

where d_j denotes the node's order.

Since ϕ is a positive function and highly decreasing as can be observed in fig. 2.5, so

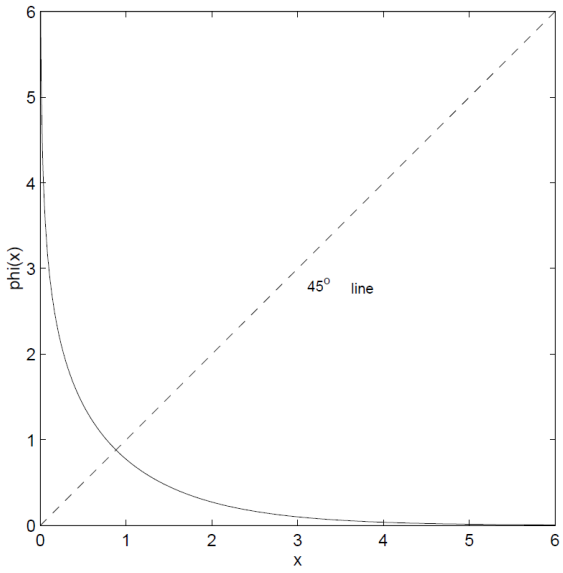

Figure 2.5: Graphical representation of the phi function

the sum of all ϕ functions it is approximately the dominant term, i.e., the minimum of $\left|L(q_{i'j})\right|$. Hence we may write

$$\phi\left(\sum_{i'\neq i}\phi\left(\left|L(q_{i'j})\right|\right)\right)\approx\phi\left(\phi\left(\min_{i'}L(q_{i'j})\right)\right)=\min_{i'\neq i}\left(\left|L(q_{i'j})\right|\right). \tag{2.56}$$

Therefore, (2.55) can be rewritten as

$$L(r_{ji})=-1^{d_j}\left(\prod_{i'\neq i}sgn\left[L(q_{i'j})\right]\right)\min_{i'\neq i}\left(\left|L(q_{i'j})\right|\right). \tag{2.57}$$

Iterative decoding

Concatenated error correction codes were proposed by Forney [23] and are derived by combining an inner code with an outer code. Concatenated codes can be used to achieve exponentially decreasing error probabilities at all data rates, with a decoding complexity that increases only algebraically with the code block length.

There are two concatenation types: Serial and Parallel. Parallel Concatenated Convolutional Codes (PCCC), first appeared in 1996 [24], and Serial Concatenated Convolutional Codes (SCCC), were presented by Divsalar [25]. The main difference between serial and parallel concatenations is that on PCCC the information bits are splited into two information streams and one of those are interleaved by an uniform interleaver of length N as

illustrated in fig. 2.7, which provides an independent weight distribution of the generated parity check bits on the two parallel encoders.

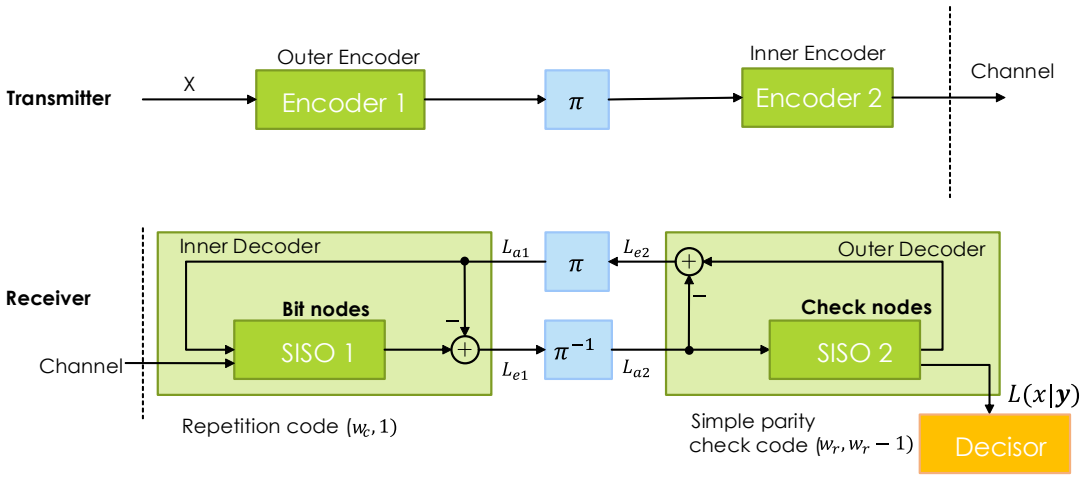

Figure 2.6: Serial concatenation diagram

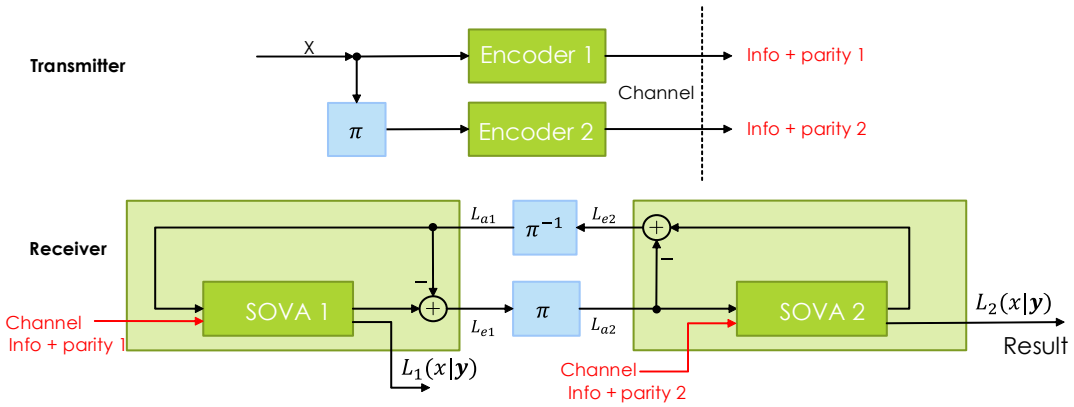

Figure 2.7: Parallel concatenation diagram

In serial concatenation the outer encoder and inner encoder are in series but separated by the uniform interleaver. The encoded bits from the outer encoder after being interleaved, will be the input of the inner encoder. So, soft decision information, LLR, is exchanged between two SISO blocks, and it is possible to define the following types of LLR:

LLR a priori

$$L_a(x) = \ln \frac{p(x=1)}{p(x=0)} \quad , \tag{2.58}$$

Conditional LLR a priori

$$L(\mathbf{y}|x) = \ln \frac{p(\mathbf{y}|x=1)}{p(\mathbf{y}|x=0)} \quad , \tag{2.59}$$

LLR a posteriori

$$L(x|\mathbf{y}) = \ln \frac{p(x=1|\mathbf{y})}{p(x=0|\mathbf{y})} \quad , \tag{2.60}$$

extrinsic LLR

$$L_e(x) = L(x|\mathbf{y}) - L_a(x) - L(\mathbf{y}|x) \quad . \tag{2.61}$$

In the first half of each iteration of the decoding process, the decoder 1 generates the extrinsic information L_{e1} which is interleaved and transformed in a priori LLR L_{a2} applied to decoder 2, and the second half, the decoder 2 makes extrinsic information L_{e2} that is de-interleaved and transformed in a priori LLR L_{a1} applied to decoder 1. Between decoders it is transferred extrinsic information only. It should be mentioned that LDPC decoding process is similar to the SCCC decoding process. In LDPC check nodes act as inner decoder and the bit nodes are equivalent to the outer decoder. Therefore, the decoding of LDPC codes can be based on two SISO blocks, with the intrinsic and extrinsic information changed between them given by the set of expressions (2.58) - (2.61).

2.4 LDPC applications

The LDPC codes have been applied in communication systems over the years, since they can surpass turbo-codes. Systems such as the Digital Video Broadcasting (DVB) uses LDPC, where in second generation, DVB-S2, the LDPC codes achieve 30% more efficiency over turbo codes.

In [26] LDPC codes for OFDM systems for AWGN channels and frequency-selective channels were proposed and the comparison with turbo-codes showed that LDPC codes achieve better performances. Same observations were made in [27] based on a comparison of LDPC with turbo codes for Rayleigh fading channels with QPSK, 8-PSK and 16-QAM for coding rates of 1/2, 2/3 and 3/4. Complexity of LDPC encoders and decoders was also analysed and compared with turbo codes in [28] with LDPC codes showing lower decoding complexity. LDPC Sum-product decoding and BCJR decoding of convolutional coded OFDM

systems where compared in [29].

Chapter 3

LDPC codes for OFDM and SC-FDE

This chapter deals with the use of LDPC codes in MC and SC systems. In sections 3.1 and 3.2 both OFDM and SC-FDE systems are characterized and the advantages of each one as well as the major differences between them are pointed out. This characterization also includes the analytical description with emphasis to the relevant properties of each modulation and the transmitter and receiver's structures suitable for each system. Section 3.3 deals with the use of LDPC codes in both systems, and it is given special emphasis to the impact of iterations and codeword's size in systems' performances. From the results we may conclude that the use of LDPC codes in iterative equalizer of SC-FDE systems allows a faster equalizer's convergence. Moreover, having in mind the performance results, the increment on complexity seems well justified due to power gains achieved by LDPC codes.

3.1 Multi-Carrier Modulation: OFDM

As stated before, spectral efficiency is one of the greatest concerns of digital communications. The simplest multi-carrier modulation is the conventional Frequency Division Multiplexing (FDM) scheme, where the spectrums related with different sub-carriers have non-overlapping bandwidths.

Let us assume that each channel uses a rectangular pulse

$$r(t) = \begin{cases} 1, & [-T_G, T] \\ 0, & \text{elsewhere} \end{cases}, \tag{3.1}$$

with the duration $T + T_G$. When the bandwidth of $R(f)$[1] is smaller than the bilateral bandwidth F, i.e., the bandwidth associated to each symbol S_k is a fraction $\frac{1}{N}$ of the total transmission band, as shown in Fig.3.1.

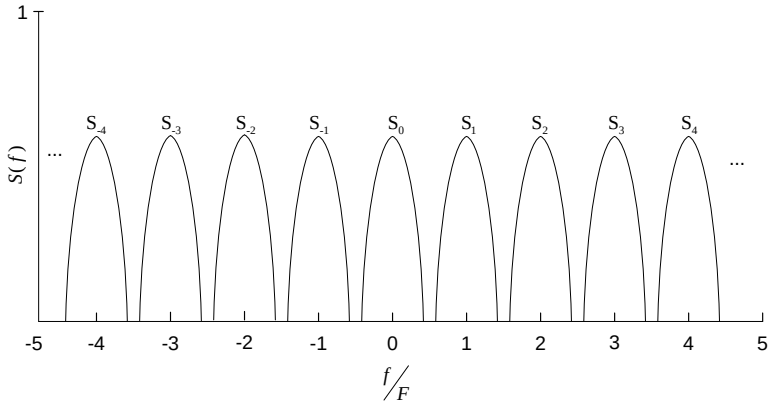

Figure 3.1: Conventional FDM

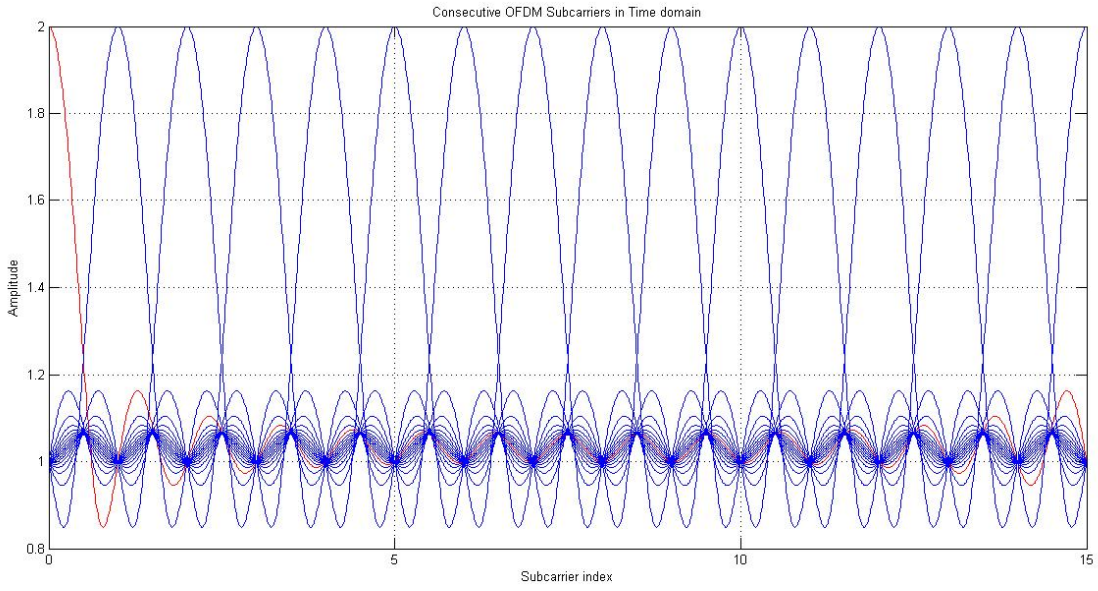

Figure 3.2: OFDM spectrum

To increase spectral efficiency it is possible to overlap channels without compromising information integrity. OFDM [30] is a MC modulation technique where information symbols

[1] $R(f)$ denotes the Fourier transform of $r(t)$

are separated into several low rate streams that are transmitted simultaneously on N narrowband sub-carriers in parallel. OFDM is very similar to FDM in some characteristics, although in OFDM sub-carriers overlap as illustrated in fig.3.2, they are orthogonal as we can see in fig.3.3.

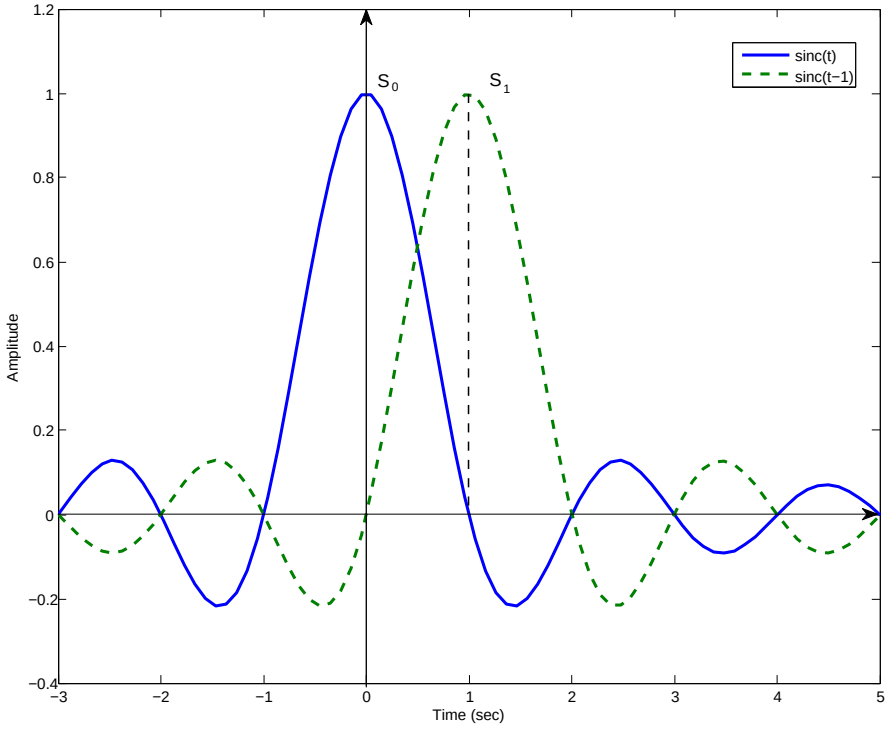

Figure 3.3: OFDM Orthogonality

Increasing the symbol period makes the signal less sensitive to Inter-Symbol Interference (ISI). Between sub-carriers the interference is null due to orthogonality since in the central frequencies of each sub-channel there is no influence from the others. The OFDM system transmits N symbols in a block with duration T_B, being N times bigger than the symbol period T_s. Each sub-carrier uses only a small portion of the total available bandwidth given by $N \times F$, with a sub-carrier spacing of $F \geq \frac{1}{T_B}$.

On SC schemes, the transmission uses a single carrier at a high symbol rate. For a linear modulation, the complex envelope of an even N-symbol burst is described by

$$s(t) = \sum_{n=0}^{N-1} s_n r(t - nT_s), \tag{3.2}$$

where $r(t)$ denotes the transmitted impulse, T_s is the symbol duration, s_n is a complex coefficient that corresponds to the n^{th} symbol of the burst, selected from a chosen constellation (for example, a Quadrature Phase-Shift Keying (QPSK) or a Quadrature Amplitude Modulation (QAM) constellation). Applying the Fourier transform (FT) to (3.2) we may write

$$S(f) = \mathcal{F}\{s(t)\} = \sum_{n=0}^{N-1} s_n R(f) e^{-j2\pi f k T_s}. \tag{3.3}$$

Hence, from (3.3), for each data symbol s_n results a transmission bandwidth equal to the bandwidth occupied by $R(f)$, where $R(f)$ is the FT of $r(t)$.

On the other hand, in a multi-carrier modulation symbols are transmitted in the frequency-domain in different sub-carriers, each one during the time interval T. The spectrum for each multi-carrier burst is:

$$S(f) = \sum_{n=0}^{N-1} S_k R(f - kF), \tag{3.4}$$

where N is the number of sub-carriers, $F = \frac{1}{T_s}$ denotes the spacing between sub-carriers and S_k refers to the k^{th} frequency-domain symbol. Clearly, (3.2) is the dual of (3.4) and the dual of (3.3) may be found applying the inverse Fourier transform to both sides of (3.4), resulting the complex envelope of the multi-carrier signal, given by

$$s(t) = \mathcal{F}^{-1}\{S(f)\} = \sum_{k=0}^{N-1} S_k r(t) e^{j2\pi k F t}. \tag{3.5}$$

Therefore, is clear that MC modulations are dual versions of SC modulations.

Due to orthogonality pulses $r(t)$ must verify the following condition

$$\int_{-\infty}^{+\infty} r(t - nT_s) r^*(t - n'T_s) dt = 0, \quad n \neq n'. \tag{3.6}$$

Using the duality property, in the frequency domain we may write the orthogonality condition as

$$\int_{-\infty}^{+\infty} R(f - kF) R^*(f - k'F) df = 0, \quad k \neq k'. \tag{3.7}$$

Using the Parseval's Theorem, (3.7) can be rewritten as

$$\int_{-\infty}^{+\infty} |r(t)|^2 e^{-j2\pi(k-k')Ft} dt = 0, \quad k \neq k'. \tag{3.8}$$

Even when signals overlap, the orthogonality may be preserved. For instance the pulse $r(t) = sinc\left(\frac{t}{T_s}\right)$ satisfies the orthogonality condition (3.6). The orthogonality cannot be verified with the pulse given by (3.1) but the sub-carriers verify the orthogonality condition within the time interval $[0, T]$, since

$$\int_0^T |r(t)|^2 e^{-j2\pi(k-k')Ft} dt = \int_0^T e^{-j2\pi(k-k')Ft} dt = \begin{cases} 1, & k = k', \\ 0, & k \neq k'. \end{cases} \tag{3.9}$$

Considering that the system has a periodic function with period T, we may write

$$s^{(p)}(t) = \sum_{n=0}^{N-1} S_k e^{j2\pi kFt} = \sum_{n=0}^{N-1} S_k e^{j2\pi \frac{k}{T} t}. \tag{3.10}$$

3.1.1 OFDM: Transmitter structure

Conceptually the OFDM transmitter is very similar to the FDM transmitter with multiple parallel single-carrier modulations in frequencies $f_k = f_c + kF$ with $k = 0, 1, ..., N-1$. The complex envelope $s^{(m)}$ may be described as a sum of bursts of duration $T_b > T$ (which are transmitted at a rate of $1/T_b < F$) given by

$$s^{Tx} = \sum_m s^{(m)}(t) h_T(t - mT_b), \tag{3.11}$$

where $S_k^{(m)}$ denotes the kth symbol of the mth burst and $h_T(t)$ denotes the adopted pulse shape. So

$$s^{(m)}(t) = \sum_{n=0}^{N-1} S_k^{(m)} r(t) e^{j2\pi kFt} = \sum_{n=0}^{N-1} S_k^{(m)} r(t) e^{j2\pi \frac{k}{T} t}. \tag{3.12}$$

In practical implementations it is used a different Inverse Discrete Fourier Transform (IDFT) block for the in-phase and quadrature components of each OFDM burst. Basically the data to be sent, is split onto N sub-carriers by a Serial/Parallel converter and transmitted by blocks, $S_k; k = 0, ..., N-1$, of size N. Then the signal has to be sampled

at the sampling rate $1/T_a$, with $T_a = \frac{T}{N}$, which results

$$s_n \equiv s(t)|_{t=nT_a} = s(t)\delta(t - nT_a) = \sum_{k=0}^{N-1} S_k e^{j2\pi \frac{k}{T} nT_a}, \quad n = 0, 1, ..., N-1. \tag{3.13}$$

Using the IDFT of S_k, (3.13) can be expressed as

$$s_n = \sum_{k=0}^{N-1} S_k e^{j\frac{2\pi kn}{N}} = IDFT\{S_k\}, \quad n = 0, 1, ..., N-1. \tag{3.14}$$

The typical structure of OFDM block is represent in figure 3.4. The cyclic prefix CP is added in the beginning of each block of N Inverse Fast Fourier Transform (IFFT) coefficients, this assures that the block has a larger size than the Channel Impulsive Response (CIR) in order to transform de multipath linear convolution into a circular convolution. This simplifies the process to change to frequency domain using the discrete Fourier transform and enabling a more simple channel estimation and equalization. Therefore, the OFDM symbol after the addition of the N_G CP samples, will be $N_G + N$ times larger, resulting in

$$s_n = \sum_{k=0}^{N-1} S_k e^{j\frac{2\pi kn}{N}}, \quad n = -N_G, 1, ..., N-1. \tag{3.15}$$

The complex envelope associated to the guard period is the repetition of the final part of the MC burst, $s(t) = s(t + T), -T_G \leq t \leq 0$, turning into a periodic signal. Due to multipath effects the received bursts will overlap with adjacent bursts as shown in figure 3.5(a), causing Inter-Block Interference (IBI). The resort to CP with a longer duration than the CIR, prevents IBI and consequently prevents ISI (fig. 3.5(b)). Then the multiple blocks are reassembled in a parallel-to-serial conversion and processed by a Digital-to-Analog Converter (DAC).

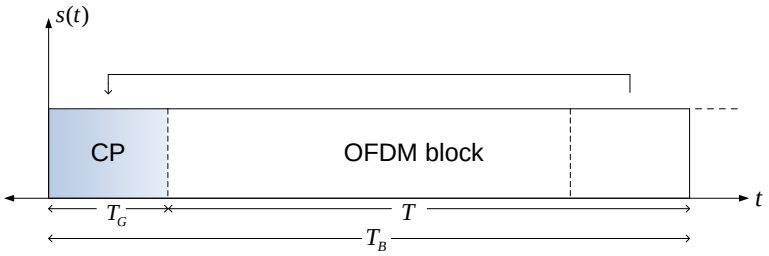

Figure 3.4: MC bursts' final part repetition in the guard interval.

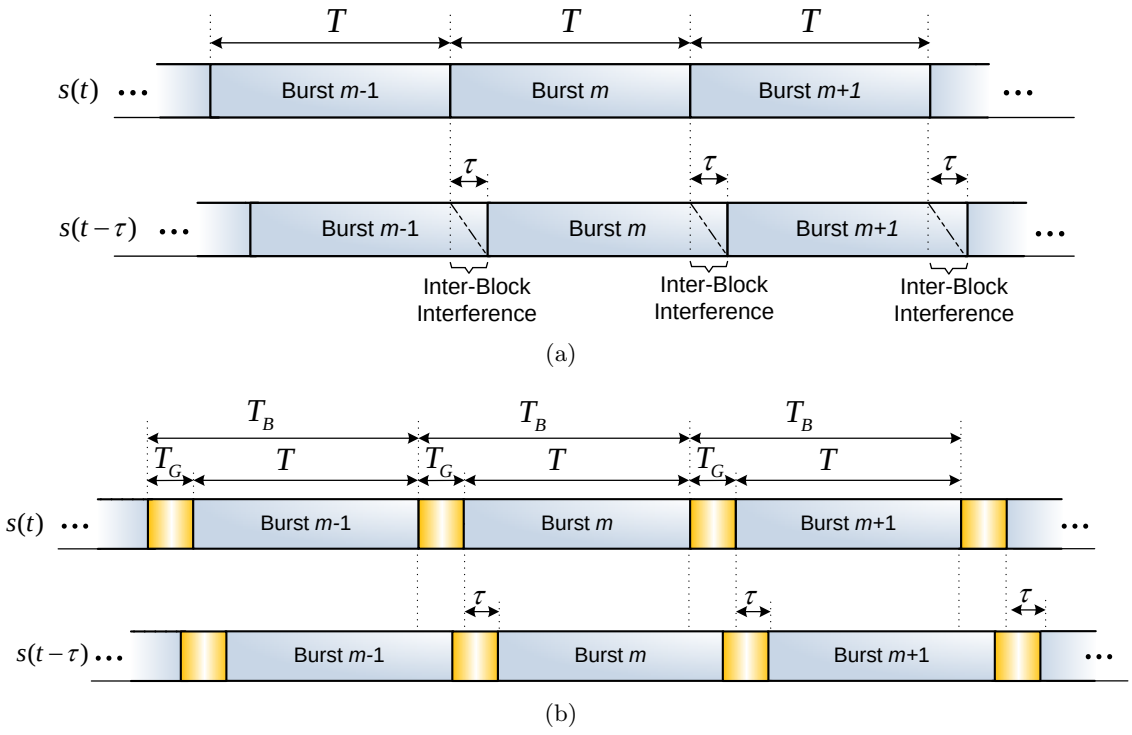

Figure 3.5: (a) Overlapping bursts due to multipath propagation; (b) IBI cancellation by implementing the cyclic prefix.

In short, it is possible to implement an OFDM transmitter, as shown in fig.3.6, where the IDFT can be implemented with an IFFT block which is more efficient[2].

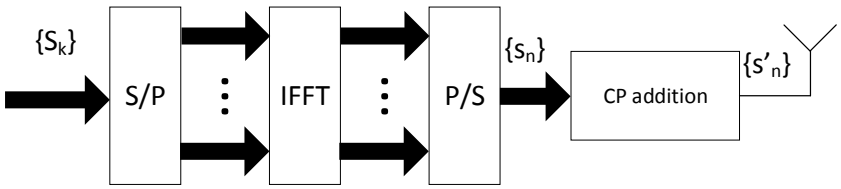

Figure 3.6: OFDM transmitter diagram

3.1.2 OFDM: Receiver structure

OFDM's receiver structure is shown in figure 3.7, where it can be seen that after receiving the incoming transmission and being converted by the Analog-to-Digital Converter (ADC), the received signal is sampled at a sampling rate $T_a = \frac{T}{N}$

[2]the number of operations of a N length IDFT, is reduced to $\frac{N}{2}\log_2 N$

$$y_n = \sum_{l=0}^{N_h-1} S_{n-l} h_l + \mathbf{v}_n, \tag{3.16}$$

where $\{s_n; n = 0, 1, ..., N-1\}$ is the block of samples associated with the transmitted burst, $\{h_n; n = 0, 1, ..., N_h - 1\}$ is the CIR with N_h denoting the length of the channel with $N_h < N$ and $\{\mathbf{v}_n; n = 0, 1, ..., N-1\}$ the Gaussian channel noise samples.

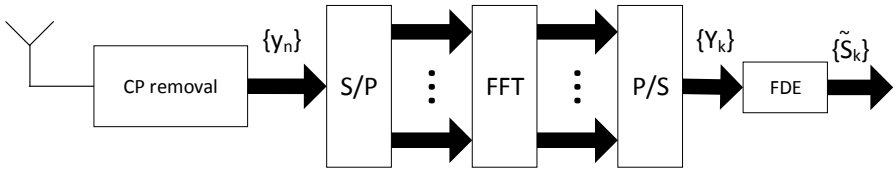

Figure 3.7: OFDM Basic FDE structure block diagram.

After the CP removal, using the FFT, y_n is converted to frequency-domain

$$Y_k = \sum_{k=0}^{N-1} y_n e^{-j\frac{2\pi kn}{N}} = H_k S_k + N_K, \quad k = 0, 1, ..., N-1, \tag{3.17}$$

where H_k denotes the overall channel frequency response for the k^{th} sub-carrier and N_k represents the additive Gaussian channel noise component.

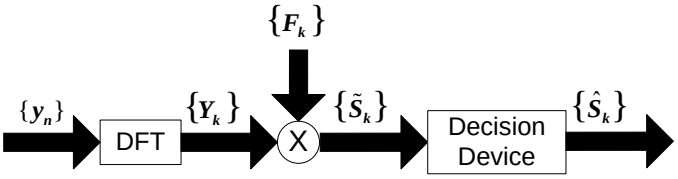

Figure 3.8: OFDM Basic FDE structure block diagram.

As aforementioned, the Frequency-Domain Equalization (FDE) is simpler than the time domain equalization since it only needs a FFT and a simple channel inversion operation. Channel distortion effects can be compensated by the FDE receiver depicted in fig. 3.8, where it is used the Zero-Forcing (ZF) criterion. The estimated data symbols will be

$$\tilde{S}_k = F_k Y_k, \tag{3.18}$$

where

$$F_k = \frac{1}{H_k} = \frac{H_k^*}{|H_k|^2}, \quad k = 0, 1, ..., N-1. \tag{3.19}$$

There is an optimized version of FDE which eliminates noise reinforcement caused by deep fadings, called Minimum Mean Square Error (MMSE) criterion. MMSE does not try to invert totally the channel effects in the presence of deep fades, instead optimizes the F_k coefficients to minimize the combined effect of ISI and channel noise. Under this conditions, the feedforward coefficients are given by

$$F_k = \frac{H_k^*}{\alpha + |H_k|^2}, \tag{3.20}$$

with α denoting the inverse of the SNR

$$\alpha = \frac{\sigma_N^2}{\sigma_S^2}, \tag{3.21}$$

where σ_N^2 is the noise variance and σ_s^2 the signal variance.

3.2 Single-Carrier Modulation: SC-FDE

Since OFDM has high envelope fluctuations, it is more susceptible to nonlinear distortion effects caused by the nonlinear amplification at the transmitter. For single-carrier modulations these fluctuations are much lower. So, SC-FDE schemes are excellent candidates for future broadband wireless systems since they can have good performance in severely time-dispersive channels without requiring complex receiver implementation [3, 4]. Not only SC-FDE has a similar transmitter and receiver structure and essentially the same performance of OFDM, but also has many advantages: it has a lower Peak to Average Power Ratio (PAPR), is less sensitive to frequency errors and has a lower complexity at the transmitter, which means that is more suitable to cellular uplink communications.

3.2.1 SC-FDE: Transmitter structure

The main difference between OFDM and SC-FDE schemes is in the transmitter where the IFFT block is moved to the receiver as shown in fig. 3.9. The complexities are similar.

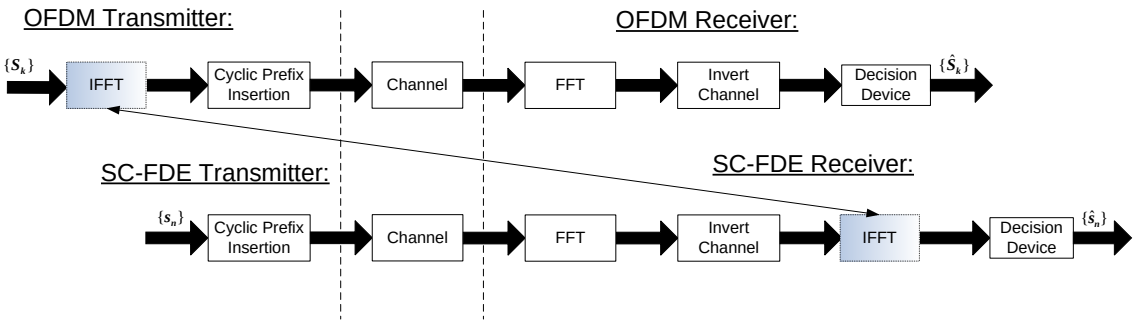

Figure 3.9: Comparison of the block diagram between OFDM and SC-FDE.

The transmission structure of an SC-FDE scheme is depicted in Fig. 3.10. As we can see, the transmitter structure will be even more simple than OFDM, with the data transmitted in blocks of N modulated symbols $\{s_n; n = 0, ..., N-1\}$. Next, a cyclic prefix with length longer that the channel impulse response is added, resulting the transmitted signal $\{s_n; n = -N_G, ..., N-1\}$. Finally, the discrete samples of the signal are converted by a DAC onto continuous signals $s^I(t)$ and $s^Q(t)$, which are then combined to generate the transmitted signal $s(t)$

$$s(t) = \sum_{n=-N_G}^{N-1} s_n r(t - nT_s), \tag{3.22}$$

where $r(t)$ is the support pulse and T_s denotes the symbol period.

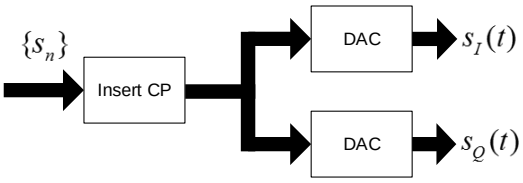

Figure 3.10: Basic SC-FDE transmitter block diagram.

3.2.2 SC-FDE: Receiver structure

In SC-FDE, the first step to do with the received data after being converted to the digital format by the ADC, is to remove the CP and process the time domain signal $\{y_n; n = 0, ..., N-1\}$ through the N-point DFT resulting in

$$Y_k = H_k S_k + N_k, \quad k = 0, 1, ..., N-1, \tag{3.23}$$

with H_k denoting the channel frequency response for the kth sub-carrier and N_k the corresponding channel noise, which means that the impact of a time-dispersive channel reduces to a scaling factor for each frequency.

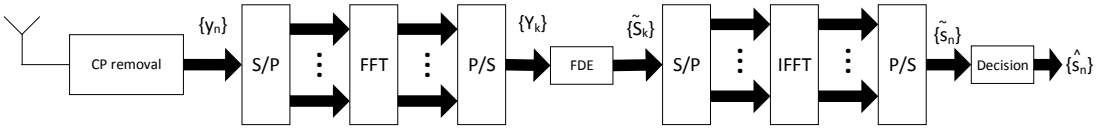

Figure 3.11: Basic SC-FDE receiver block diagram.

The receiver structure is shown in figure 3.11 and the corresponding equalizer in fig. 3.12. From this point, Y_k is ready for equalization in the frequency domain just like in OFDM scheme. After equalization, results the equalized samples $\tilde{S}_k$ for the k^{th} sub-carrier (3.18). As mentioned before, for the ZF criterion and for the MMSE criterion, coefficients F_k are defined by (3.19) and (3.20), respectively.

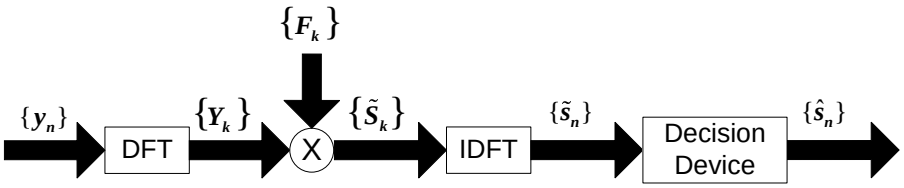

Figure 3.12: Basic SC-FDE structure block diagram.

Before the decision device the equalized samples $\{\tilde{S}_k; k = 0, 1, ..., N-1\}$ are converted again to time-domain $\{\tilde{s}_n; n = 0, 1, ..., N-1\}$ through an IFFT block.

3.2.3 IB-DFE Receivers

It is known that nonlinear equalizers surpass linear equalizers in performance. Among nonlinear equalizers the DFE is a popular choice since it provides a good tradeoff between complexity and performance. A promising IB-DFE approach for single-carrier transmission was proposed in [31] and extended to diversity scenarios and spatial multiplexing schemes [32][33]. In IB-DFE designs, both the feedforward and the feedback filters are

implemented in frequency domain as shown in fig.3.13. First IB-DFE implementations used a decision device based on hard decisions, weighted by the blockwise reliability, in the feedback loop.

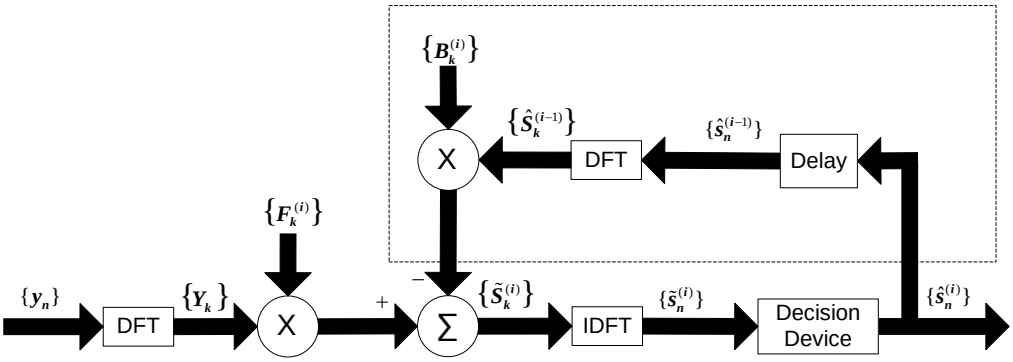

Figure 3.13: Basic IB-DFE structure block diagram .

For the i^{th} iteration, the frequency-domain block at the output of the equalizer is $\{\tilde{S}_k^{(i)}; k = 0, 1, \ldots, N-1\}$, with

$$\tilde{S}_k^{(i)} = F_k^{(i)} Y_k - B_k^{(i)} \hat{S}_k^{(i-1)}, \tag{3.24}$$

where $\{F_k^{(i)}; k = 0, 1, \ldots, N-1\}$ are the feedforward coefficients, $\{B_k^{(i)}; k = 0, 1, \ldots, N-1\}$ are the feedback coefficients and $Y_k = S_k H_k + N_k$. $\{\hat{S}_k^{(i-1)}; k = 0, 1, \ldots, N-1\}$ is the DFT of the decision block $\{\hat{s}_n^{(i-1)}; n = 0, 1, \ldots, N-1\}$ from previous iteration, related with the transmitted block $\{s_n; n = 0, 1, \ldots, N-1\}$.

The IB-DFE feedforward and feedback coefficients are chosen in order to maximize the Signal to Interference-plus-Noise Ratio (SINR). For an IB-DFE implemented with "hard-decisions", the optimum feedback coefficients are [34]

$$B_k^{(i)} = \rho^{(i-1)} \left(F_k^{(i)} H_k - 1 \right), \tag{3.25}$$

and the feedforward coefficients are

$$F_k^{(i)} = \frac{H_k^*}{\alpha + \left(1 - \left(\rho_m^{(i-1)}\right)^2\right) \left|H_k^{(l')}\right|^2}, \tag{3.26}$$

with α given by (3.21) and the correlation coefficient $\rho^{(i-1)}$ is defined as

$$\rho^{(i-1)} = \frac{E[\hat{s}_n^{(i-1)} s_n^*]}{E[|s_n|^2]} = \frac{E[\hat{S}_k^{(i-1)} S_k^*]}{E[|S_k|^2]}, \tag{3.27}$$

where $\{\hat{s}_n^{(i-1)}; n = 0, 1, \ldots, N-1\}$ is the data estimation associated to the previous iteration, $\{\tilde{s}_n^{(i)}; n = 0, 1, \ldots, N-1\} = \text{IDFT } \{\tilde{S}_k^{(i)}; k = 0, 1, \ldots, N-1\}$ are the hard decisions associated to the time-domain block at the output of the FDE. ρ is the correlation coefficient responsible of ensuring a good performance, since it measures the reliability of the estimates in the feedback loop. Mitigation of error propagation in the feedback loop is done by using the hard-decisions for each block plus the overall block reliability. For the first iteration, no information exists about s_n, which means that $\rho = 0$, $B_k^{(0)} = 0$, and $F_k^{(0)}$ coefficients are given by (3.20) (in this situation the IB-DFE receiver is equivalent to a linear FDE). After the first iteration, the feedback coefficients can be applied to reduce a major part of the residual interference (considering that the residual doesn't assume a high value). After several iterations and for a moderate-to-high SNR, the correlation coefficient will be $\rho \approx 1$ and the residual ISI will be almost vanished.

Consequently, IB-DFE techniques outperform the non-iterative methods, since they can achieve better performances [31, 32]. To have a greater improvement in the performance and to allow truly turbo FDE implementations, IB-DFE schemes with soft decisions were proposed in [34].

3.3 LDPC codes applied on OFDM and SCFDE

3.3.1 System characterization

OFDM system

To avoid the dominance of sub-carriers affected by deep fades, error correcting codes such as LDPC codes can be employed. Fig. 3.14 shows the block diagram for the OFDM transmission system. At the transmitter, the binary input data is encoded by a 1/2 rate LDPC encoder and the resulting bits are interleaved before being mapped in a symbol, belonging to a multilevel constellation[3]. Pilot symbols can be added for channel estimation

[3] e.g. a QPSK or M-QAM constellation

purposes[4]. Then the OFDM symbol is modulated onto k' sub-carriers by applying the IFFT. The output is converted to serial and a cyclic extension with duration longer than the overall delay spread of the channel is added to make the system robust to multipath propagation effects. By this, both ISI and IBI are eliminated when the cyclic prefix is discarded at the receiver.

The receiver performs the reverse operations of the transmitter. In the first step, the receiver has to estimate frequency offset and symbol timing, using special training symbols in the preamble[5]. After removing the cyclic extension, it is applied a FFT to recover the symbols of all subcarriers. The training symbols and the pilot subcarriers are used to correct the channel response and phase drifts. The symbols values are then de-mapped into the log-likelihood ratios that, after the de-interleaver operation, will be *a priori* probabilities used in the first iteration of the LDPC decoder and finally the information bits can be decoded by a SISO block.

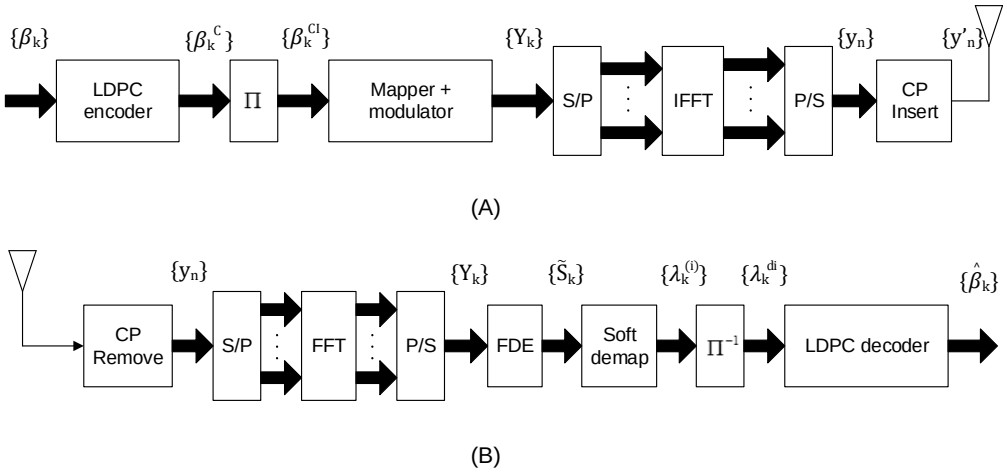

Figure 3.14: (A) OFDM transmitter; (B) Receiver structure.

[4]we omit the pilots since it is assumed perfect channel estimation
[5]it is assumed perfect time and frequency estimation

SC-FDE system and IB-DFE Receivers

It can be shown that the constellation symbols can be expressed as function of the corresponding bits as follows[6] [35]:

$$s_n = g_0 + g_1 b_n^{(1)} + g_2 b_n^{(2)} + g_3 b_n^{(1)} b_n^{(2)} + g_4 b_n^{(3)} + ... =$$

$$= \sum_{i=0}^{M-1} g_i \prod_{m=1}^{\mu} \left(b_n^{(m)} \right)^{\gamma_{m,i}}, \tag{3.28}$$

for each $s_n \in \mathfrak{S}$, where $(\gamma_{\mu,i}\ \gamma_{\mu-1,i}\ ...\ \gamma_{2,i}\ \gamma_{1,i})$ is the binary representation of i and $b_n^{(m)} = 2\beta_n^{(m)} - 1$ assuming that $\beta_n^{(m)}$ is the mth bit associated to the nth symbol and $b_n^{(m)}$ is the corresponding polar representation, i.e., $\beta_n^{(m)} = 0$ or 1 and $b_n^{(m)} = -1$ or $+1$, respectively. Since the constellation has M symbols in $\mathfrak{S}$ and M complex coefficients g_i, (3.28) is a system of M equations that can be used to obtain the coefficients g_i, $i = 0, 1, ..., \mu - 1$. Writing (3.28) in matrix format results

$$\mathbf{s} = \mathbf{W}\mathbf{g}, \tag{3.29}$$

with $\mathbf{s} = [s_1\ s_2\ ...\ s_M]^T$ and $\mathbf{g} = [g_0\ g_1\ ...\ g_{\mu-1}]^T$, where $\mathbf{W}$ denotes an appropriate Hadamard matrix. Since the array of constellation points $\mathbf{s}$ is the Hadamard transform of the array of coefficients $\mathbf{g}$ it can obtained the coefficients g_i from the inverse Hadamard transform of the array of constellation points, i.e.,

$$\mathbf{g} = \mathbf{W}^{-1}\mathbf{s} = \mathbf{W}^T\mathbf{s}/M. \tag{3.30}$$

Let us consider now the use of M-QAM in SC-FDE systems. The transmission chain is depicted in fig. 3.15-(A), where the transmitter can be based on a multi-branch structure with multiple amplifiers, followed by the cyclic prefix adding. For the sake of simplicity, we assume an ideal linear transmitter. From the receiver side, it must deal with the high sensitivity of large constellations to interference, namely the residual ISI that is inherent to imperfect equalization such as the linear FDE that is normally employed in SC-FDE

[6] It should be noted that in this subsection s_n denotes the nth constellation point but in the previous section s_n denotes the nth transmitted symbol; the same applies to $b_n^{(m)}$ (or $\beta_n^{(m)}$) that here denotes the mth bit of the n constellation point (instead of the mth bit of the nth transmitted symbol).

receivers. For this reason, we replace the linear FDE with a more powerful IB-DFE at the receiver, whose structure is depicted in figure 3.15-(B).

The signal associated to a given block is

$$s(t) = \sum_{n=-N_G}^{N-1} s_n h_T(t - nT_S), \tag{3.31}$$

with T_S denoting the symbol duration, N_G, the number of samples at the cyclic prefix, N, the number of samples at the useful part of the block and $h_T(t)$ representing the adopted pulse shape. The nth transmitted symbol[7] s_n belongs to a given size-M constellation $\mathfrak{S}$. As usual, the cyclic prefix corresponds to a periodic extension of the useful part of the block, i.e., $s_{-n} = s_{N-n}$.

At the receiver, the samples associated to the cyclic prefix are removed, which eliminates the interference between blocks when the length of the cyclic prefix is higher than the length of the overall CIR. It should be mentioned that the cyclic prefix insertion at the transmitter and its removal at the receiver is equivalent to a cyclic convolution relatively to the size-N useful part of the received block, $\{y_n; n = 0, 1, \ldots, N-1\}$. Therefore, the corresponding frequency-domain block is $\{Y_k; k = 0, 1, \ldots, N-1\}$ = DFT $\{y_n; n = 0, 1, \ldots, N-1\}$) and is given by (3.23).

For a given iteration the output samples are given by

$$\tilde{S}_k = F_k Y_k - B_k \overline{S}_k, \tag{3.32}$$

where $\{F_k; k = 0, 1, \ldots, N-1\}$ and $\{B_k; k = 0, 1, \ldots, N-1\}$ denote the feedforward and the feedback coefficients, respectively, and $\{\overline{S}_k; k = 0, 1, \ldots, N-1\}$ is the DFT of the block $\{\overline{s}_n; n = 0, 1, \ldots, N-1\}$, being $\overline{s}_n$ the average value of s_n conditioned to the FDE output associated to the previous iteration. As stated before, it is adopted a SISO block that performs the sum-product algorithm [21] to decode the LDPC code in each IB-DFE iteration. This process is repeated 10 times in SISO decoder for each iteration of IB-DFE. By taking advantage of (3.28) and the fact that the different BPSK components

[7] It should be pointed out that we have a slight abuse of notation, since in this section s_n designates the nth transmitted symbol of the block, while in sec. 4.1 s_n designates the nth symbol of the constellation.

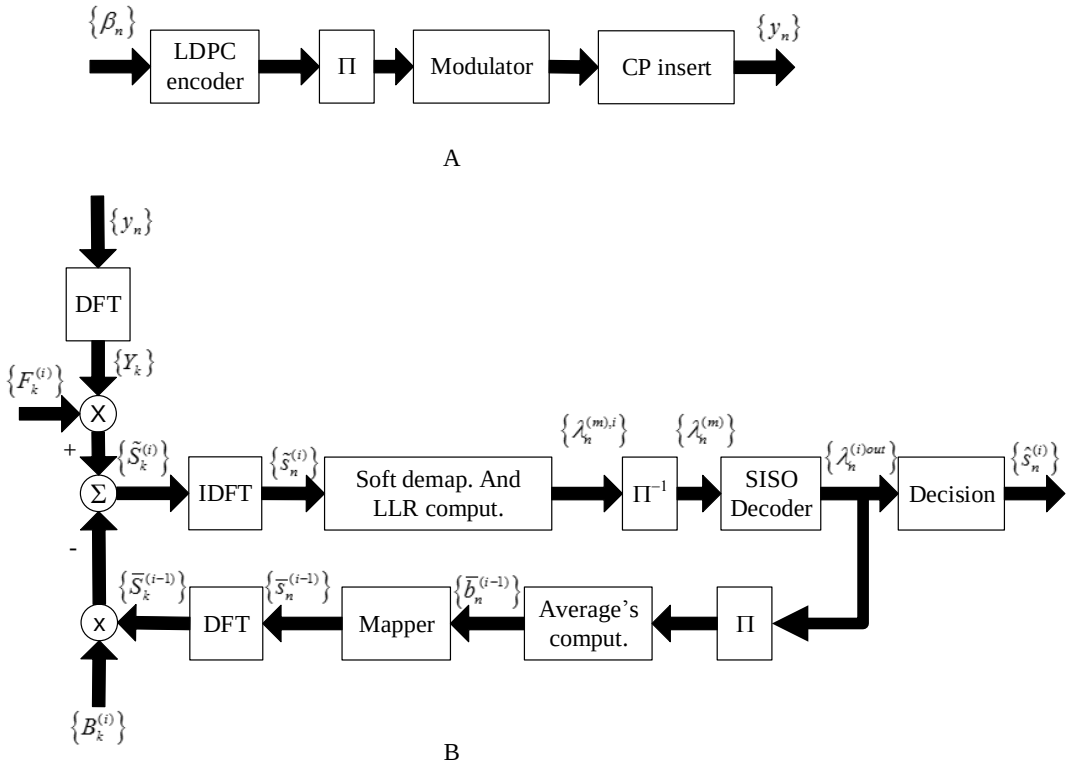

Figure 3.15: (A) - Transmitter; (B) - IB-DFE receiver with soft decisions.

are uncorrelated we may write

$$\overline{s}_n = \sum_{i=0}^{M-1} g_i \prod_{m=1}^{\mu} \overline{b}_n^{eq(m)}, \tag{3.33}$$

where the average values for the corresponding symbol's bits are given by

$$\overline{b}_n^{(m)} = \tanh\left(\frac{\lambda_n^{(m)out}}{2}\right), \tag{3.34}$$

where $\lambda_n^{(m)out}$ denotes the log-likelihood ratio of the mth bit for the nth transmitted symbol at the SISO's output. $\lambda_n^{(m)}$ denotes the log-likelihood ratio of the mth bit for the nth transmitted symbol used by iterative SISO decoding process and it is given by

$$\lambda_n^{(m)} = \log\left(\frac{\Pr(\beta_n^{(m)}=1|\tilde{s}_n)}{\Pr(\beta_n^{(m)}=0|\tilde{s}_n)}\right) = \log\left(\frac{\sum_{s\in\Psi_1^{(m)}} \exp\left(-\frac{|\tilde{s}_n-s|^2}{2\sigma^2}\right)}{\sum_{s\in\Psi_0^{(m)}} \exp\left(-\frac{|\tilde{s}_n-s|^2}{2\sigma^2}\right)}\right). \tag{3.35}$$

The sets $\Psi_1^{(m)}$ and $\Psi_0^{(m)}$ are the subsets of $\mathfrak{S}$ where $\beta_n^{(m)} = 1$ or 0, respectively (clearly, $\Psi_1^{(m)} \bigcup \Psi_0^{(m)} = \mathfrak{S}$ and $\Psi_1^{(m)} \bigcap \Psi_0^{(m)} = \emptyset$) and $\{\tilde{s}_n; n = 0, 1, ..., N-1\}$ denotes the IDFT of $\{\tilde{S}_k; k = 0, 1, ..., N-1\}$, i.e., the $\tilde{s}_n$ are the time-domain samples at the FDE output. In (3.35) σ^2 denotes the variance of the noise at the FDE output, i.e.,

$$\sigma^2 = \frac{1}{2}E[|s_n - \tilde{s}_n|^2] \approx \frac{1}{2N}\sum_{n=0}^{N-1} E[|\hat{s}_n - \tilde{s}_n|^2], \tag{3.36}$$

where $\hat{s}_n$ denotes the hard decisions associated to s_n.

It can be shown that the optimum coefficients F_k and B_k [34] are given by

$$F_k = \frac{\kappa H_k^*}{E[|N_k|^2]/E[|S_k|^2] + (1-\rho^2)|H_k|^2}, \tag{3.37}$$

and

$$B_k = F_k H_k - 1, \tag{3.38}$$

respectively, where κ is a constant that ensures that

$$\sum_{k=0}^{N-1} F_k H_k / N = 1. \tag{3.39}$$

The correlation coefficient ρ gives a measure of the reliability of the decisions employed in the feedback loop and can be characterized as

$$\rho = \frac{E[\hat{s}_n s_n^*]}{E[|s_n|^2]} = \frac{\sum_{i=0}^{M-1} |g_i|^2 \prod_{m=1}^{\mu} \left(\rho_n^{(m)}\right)^{\gamma_{m,i}}}{\sum_{i=0}^{M-1} |g_i|^2}, \tag{3.40}$$

where $\rho_n^{(m)} = |\bar{b}_n^{(m)}|$ is the reliability of the mth bit of the nth transmitted symbol.

3.3.2 Performance results

Here, a set of performance results regarding AWGN and time-varying channels is presented. The effect of the codeword length on code and system's performance is also investigated. For this purpose two possible configurations are considered $(N, K) = (528, 264)$ and $(N, K) = (1056, 528)$ LDPC encoders with rate of 1/2 and column weight of 3. At the encoder's output every codeword block are randomly interleaved before being mapped into the constellation points and distributed by the symbols of the transmitted frame. The set of constellations to be considered are QPSK, 16-QAM and 64-QAM. The block sizes of transmitted symbols depend on the modulation order and are related by $N/log2(M)$. OFDM and SC-FDE are characterized by blocks of $N_B = N/log2(M)$ useful symbols plus a cyclic prefix of 32 symbols longer than overall delay spread of the channel.

The channel is modeled as a frequency selective fading Rayleigh channel, characterized by an uniform Power Delay Profile (PDP), with 32 equal-power taps, with uncorrelated Rayleigh fading on each tap. For the sake of simplicity, it is assumed linear power amplification at the transmitter as well as perfect synchronization and channel estimation at the receiver. Results regarding performance are expressed as function of $\frac{E_b}{N_0}$, where N_0 is the one-sided power spectral density of the noise and E_b is the energy of the transmitted bits. In single carrier transmission, for time selective channels a total of three iterations are performed in the IB-FDE. Obviously, for AWGN a linear FDE is used. The number of iterations at LDPC decoder can vary between 10 or 40, but remains fixed for each system's

configuration considered here.

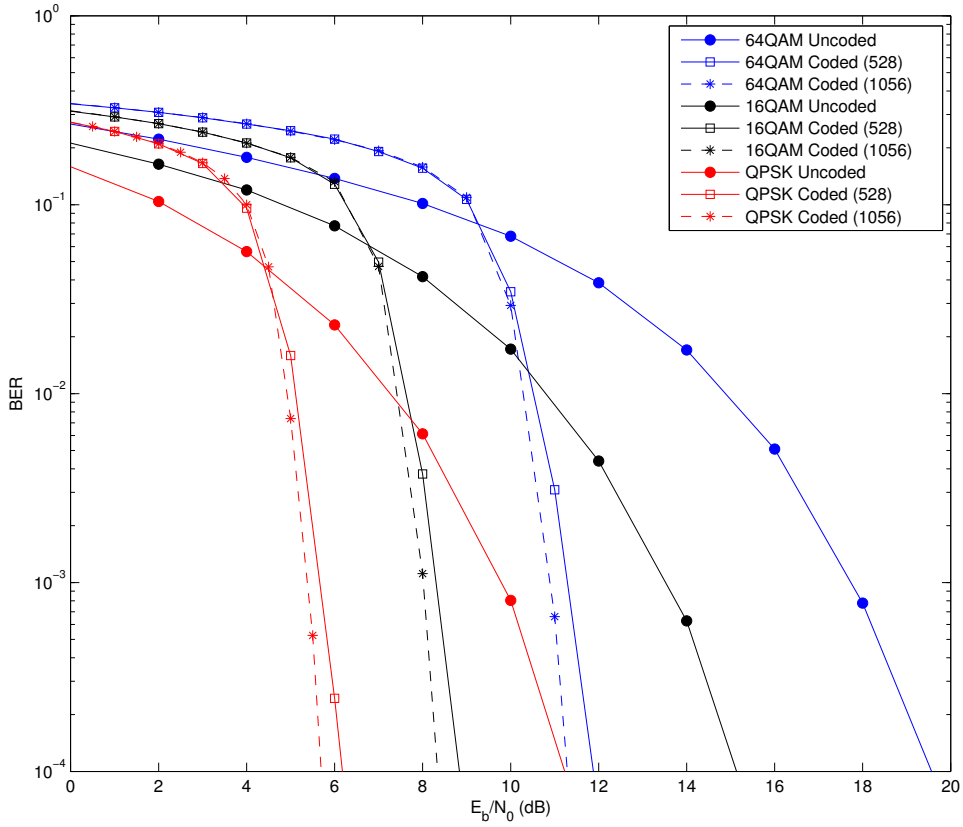

Figure 3.16: BER performance for OFDM in AWGN channel for uncoded and coded transmission with different sizes of codified blocks.

Figs. 3.16 to 3.19 show the BER performance results of OFDM and SC-FDE for both types of channels. In AWGN channel, the introduction of LDPC codes assures a substantial power gains of the coded over the uncoded schemes for all constellations sizes. It can be seen that OFDM has gains near to 5 dB, 6 dB and 7 dB for QPSK, 16-QAM and 64-QAM, respectively. SC-FDE schemes have a similar behavior, with the coded schemes showing power gains of 5 dB, 3.5 dB and 4 dB for QPSK, 16-QAM and 64-QAM, respectively. Another interesting fact common to both systems is the low performance improvement achieved by the increase of the size of the coded word. For both transmission schemes power gains attainable by the $(N, K) = (1056, 528)$ LDPC code comparatively to the $(N, K) = (528, 264)$, are near to 0.5 dB for all constellation sizes.

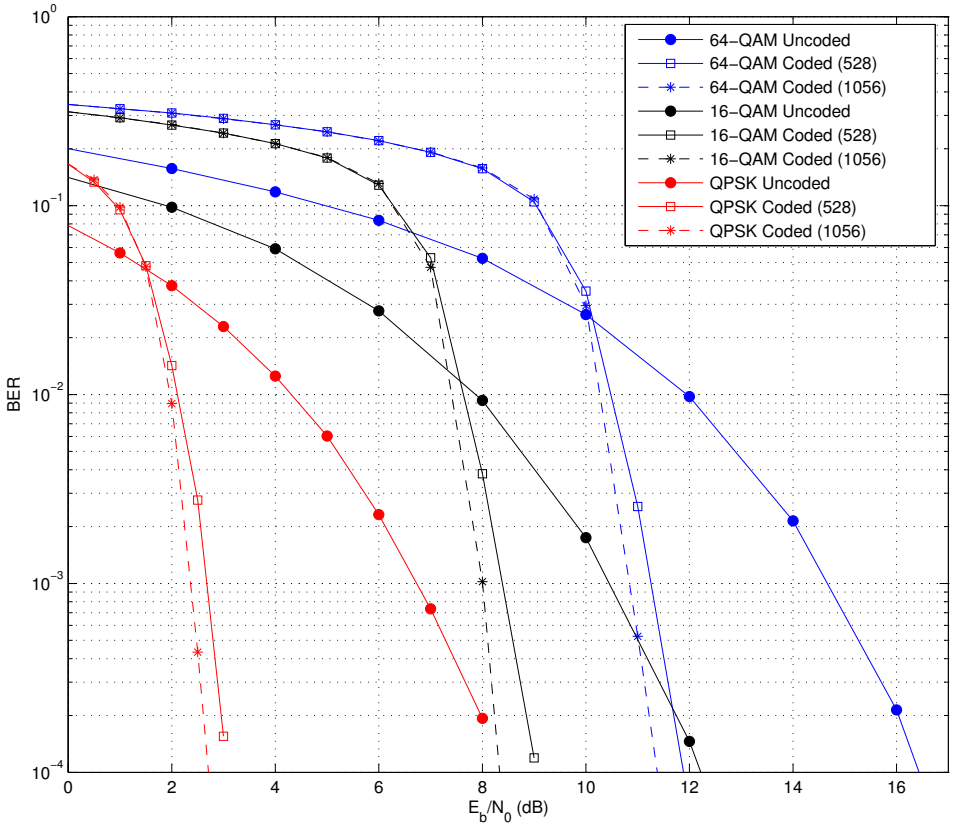

Figure 3.17: BER performance for SC-FDE in AWGN channel for uncoded and coded transmission with different sizes of codified blocks.

From figs. 3.18 and 3.19 it is clear that LDPC codes have a much bigger impact on system's performance when we have time dispersive channels. It is assumed 10 iterations in the LDPC decoder for both transmission schemes. In SC-FDE a total of 3 iterations are performed by the IB-FDE. The OFDM results from fig. 3.18 show significant improvements on performance due to LDPC codes, with coding gains near to 7 dBs for QPSK and higher than 7 dBs for other constellations sizes. Also, increments on the size of the codified block have a stronger impact in system's performance, with power gains around 2 dB for 64-QAM. For 16-QAM we have practically the same power gain and even for QPSK the power gain is higher than 1.5 dB.

Let us consider now the performance results of fig. 3.19 regarding the SC-FDE system. As it can be seen, the iterations in IB-DFE have a great impact in performance improvements

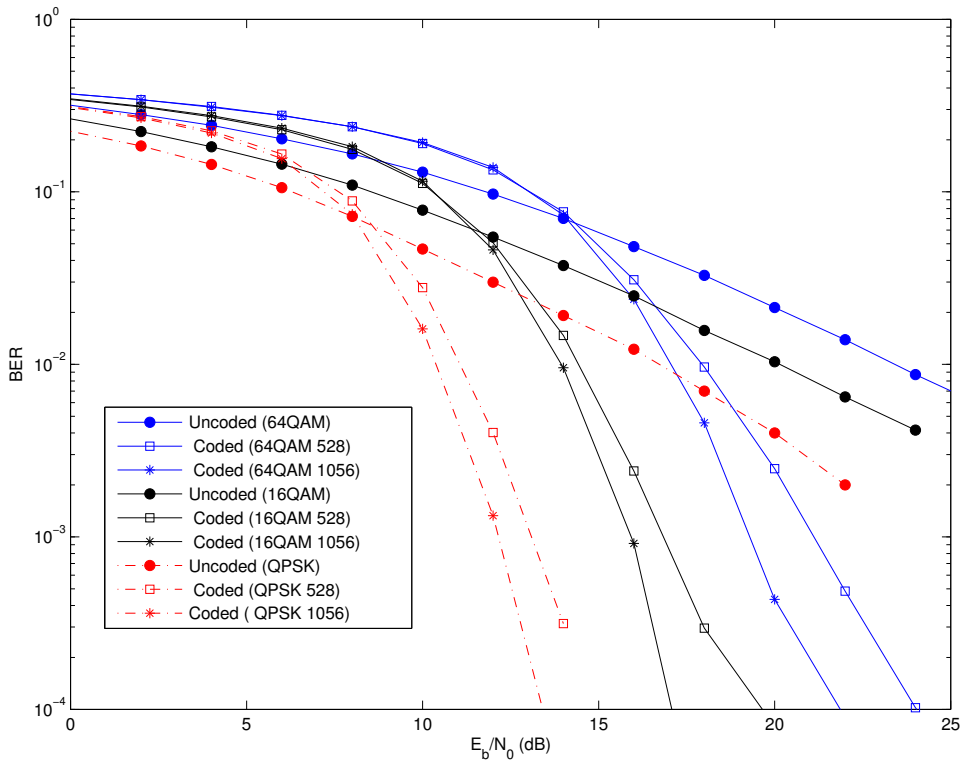

Figure 3.18: BER performance of OFDM with QPSK, 16 and 64-QAM constellations for time dispersive channel.

for uncoded schemes, with power gains near to 3.5 dB for QPSK and 4 dB for 16-QAM and 64-QAM. On the other hand, a slight degradation is observed between successive iterations of IB-DFE when are used LDPC codes. For example, power gains due to iterations are practicably non-existent for coded QPSK and only for 64-QAM we have improvements higher than 1 dB. The reason for that lies on high order modulation's sensitivity to the residual ISI, which can be compensated along the iterative equalization process. Besides this effect, the coded schemes show also good power gains when compared with uncoded schemes. For instance, it can be seen that for the third iteration the power gains due to LDPC codes are 2.5 dB, 4 dB and more than 6 dB for QPSK, 16-QAM and 64-QAM, respectively. Also, from the comparison of figs. 3.18 and 3.19 can be observed that IB-DFE outperforms OFDM, which was expectable due to the interaction between IB-DFE

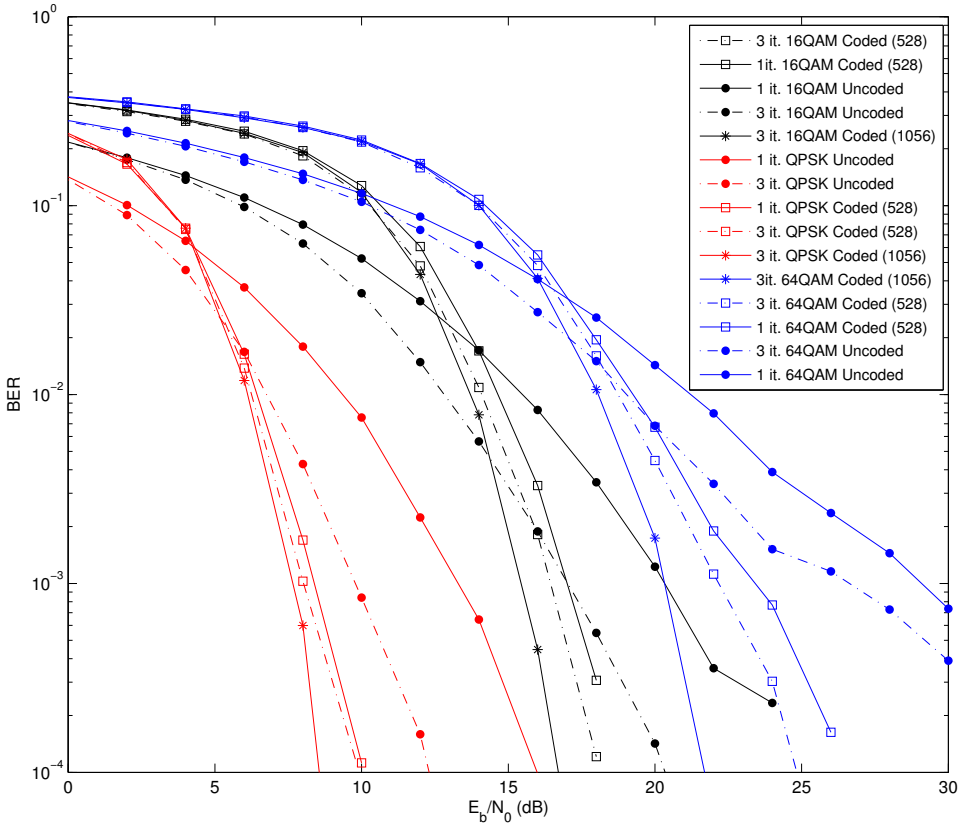

Figure 3.19: BER performance of SC-FDE with QPSK, 16 and 64-QAM constellations for time dispersive channel (IB-DFE with 1 and 3 iterations.)

and SISO decoder.

Finally, in figures Figs. 3.20 and 3.21 the influence of the iterations on LDPC decoder in the performance behavior of the proposed IB-DFE receiver is analyzed. As expected, the increment of the number of iterations does not introduce significant improvements on OFDM's BER performance. Since it is assumed perfect channel estimation, the better quality of the symbol's estimates at the decoder's output does not contribute for any improvement on the channel estimates. From figs. 3.20 and 3.21 it can be also evaluated the impact of LDPC decoding iterations in IB-DFE convergence. As we can see, adopting 40 iterations in SISO decoder on SC-FDE schemes reduces significantly the performance improvements between successive iterations of IB-DFE equalizer, which means that the effect of successive iterations in the IB-DFE becomes attenuated. Moreover, with 40

iterations in the LDPC decoder performance results for the first iteration are similar to those of the third iteration. For example, with 40 iterations the power gain achieved by the third iteration is around 0.5 dB for both constellations[8].

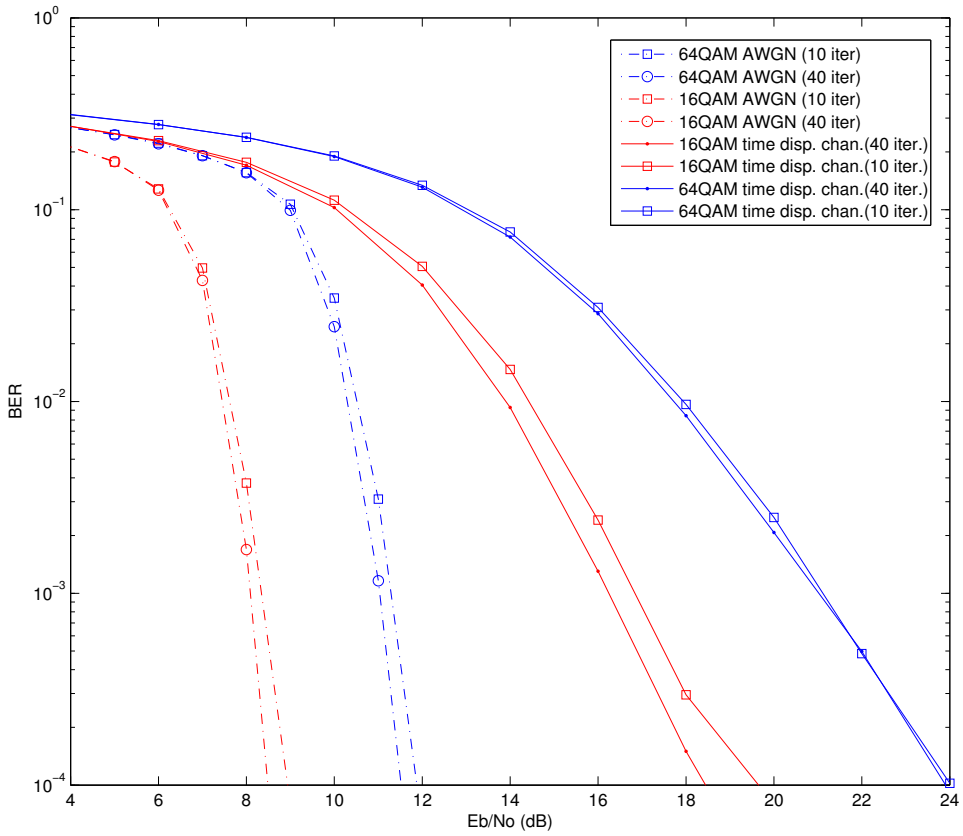

Figure 3.20: Impact of number of iterations on LDPC decoding process on OFDM's BER performance for time dispersive channel.

Having in mind the performance results presented here, this increment on complexity seems well justified when performance results of coded schemes are compared with uncoded schemes.

[8] with 10 iterations in SISO decoder the power gain allowed by a third iteration in IB-DFE is 2 dB for 16-QAM

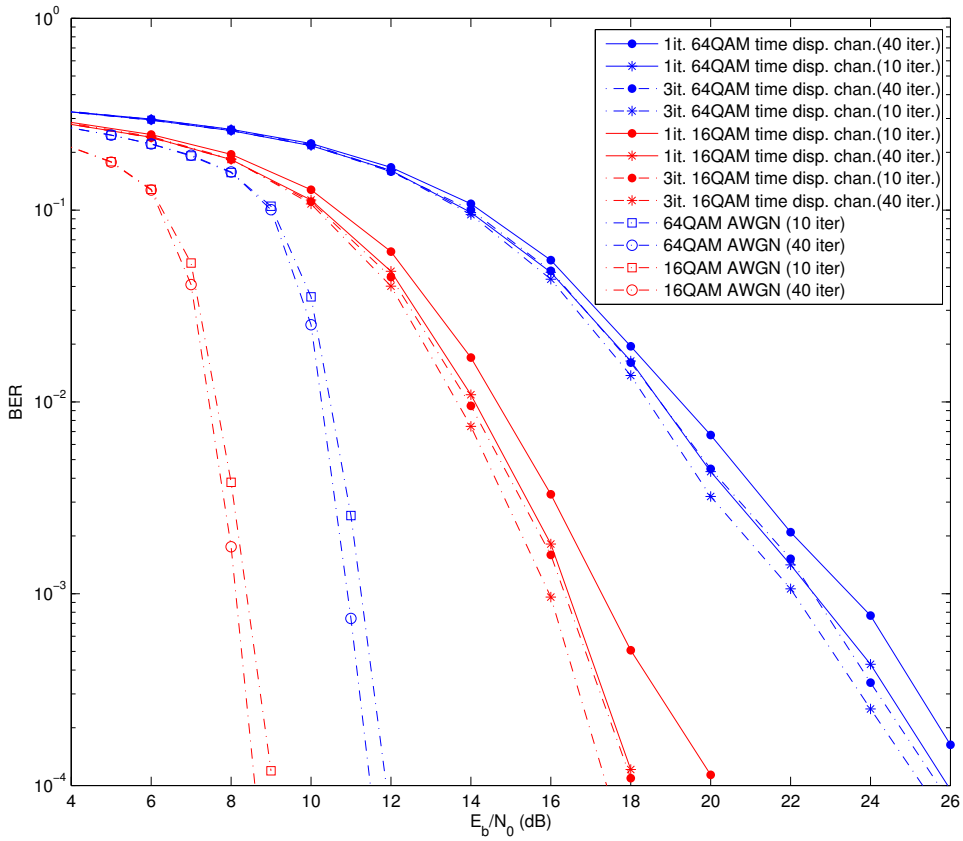

Figure 3.21: Impact of number of iterations on LDPC decoding process on SC-FDE's BER performance for time dispersive channel (3 iterations in IB-DFE).

Chapter 4

LDPC coding for phase imbalances compensation

This chapter introduces the study of techniques for compensation of phase imbalances in transmitters based structures with multi amplifiers in parallel. The first method employs LDPC codes to increase the robustness of the system against phase imbalances. We propose a receiver that combines a SISO block with a modulator that tries to compensate the phase imbalances effects in constellation symbols in order to achieve better estimates of the symbols in the feedback loop. For the second method, a receiver specially designed to implement a compensation of these phase rotations is proposed, using an iterative estimation process of the phase imbalances, practically mitigates the impact of phase imbalances due to the good accuracy of the estimates. In section 4.1 the signal characterization and the corresponding analytical decomposition are presented. In sec.4.2 will be described the new transmitter structure with a amplification method capable of grossly Nonlinear (NL) amplification is characterized. Section 4.3 characterizes the system based on LDPC codes and presents a set of performance results. Receivers specially designed to compensate phase imbalances are presented in section 4.4, where the algorithm adopted for this purpose is characterized. Finally, in subsection 4.4.1 a set of performance results and some conclusions and comparisons are presented.

4.1 Signal Characterization

As explained in section 3.3.1 the constellation symbols can be expressed by

$$s_n = g_0 + g_1 b_n^{(1)} + g_2 b_n^{(2)} + g_3 b_n^{(1)} b_n^{(2)} + g_4 b_n^{(3)} + ... =$$

$$= \sum_{i=0}^{M-1} g_i \prod_{m=1}^{\mu} \left(b_n^{(m)} \right)^{\gamma_{m,i}}, \tag{4.1}$$

and since a generic multilevel constellation has M symbols in $\mathfrak{S}$ and M complex coefficients g_i, the previous equation is a system of M equations that can be used to obtain the coefficients g_i, $i = 0, 1, ..., \mu - 1$. So, in matrix format results

$$\mathbf{s} = \mathbf{W}\mathbf{g}, \tag{4.2}$$

with $\mathbf{s} = [s_1 \ s_2 \ ... \ s_M]^T$ and $\mathbf{g} = [g_0 \ g_1 \ ... \ g_{\mu-1}]^T$, where $\mathbf{W}$ denotes an appropriate Hadamard matrix. Since the array of constellation points $\mathbf{s}$ is the Hadamard transform of the array of coefficients $\mathbf{g}$, it can obtained the coefficients g_i from the inverse Hadamard transform of the array of constellation points, i.e.,

$$\mathbf{g} = \mathbf{W}^{-1}\mathbf{s} = \mathbf{W}^T\mathbf{s}/M. \tag{4.3}$$

The array of constellation points $\mathbf{s}$ is the Hadamard transform of the array of coefficients $\mathbf{g}$. The coefficients g_i can obtained from the inverse Hadamard transform of the array of constellation points expressed in (4.3).

Using (4.2) it is possible to represent general constellation as the sum of M BPSK sub-constellations. Because power-efficient constellations have zero mean, $g_0 = 0$, $M - 1$ BPSK signals are sufficient to generate a given constellation. Nevertheless, for the case of M-QAM constellations, the decomposition only needs $\log_2(M)$ BPSK signals, since the remaining g_i coefficients are zero, e.g. a 16-QAM constellation needs only 4 BPSK signals defined by the non-zero complex set of coefficients on the table 4.1. On the other hand, for constellations with non-regular shape such as Voronoi constellations, the characterization in terms of BPSK signals is not as simple as regular constellations, since the $\mathbf{g}$ coefficients

are more likely to have non-zero values. For instance, the 16-symbol Voronoi constellation, shown in fig.4.1, is characterized by the set of 15 complex coefficients of table 4.1.

	QAM	VORONOI
g_0	0	0
g_1	0	$-0.588 + j0.572$
g_2	$2j$	$0.717 + j0.546$
g_3	j	$-0.014 - j0.124$
g_4	0	$0.029 + j0.248$
g_5	0	$-0.186 + j0.273$
g_6	0	$-0.201 + j0.149$
g_7	0	$-0.014 - j0.124$
g_8	2	$-0.100 + j0.075$
g_9	0	$0.086 - j0.199$
g_{10}	0	$0.359 + j0.273$
g_{11}	0	$0.086 - j0.199$
g_{12}	1	$-0.100 + j0.075$
g_{13}	0	$0.086 - j0.199$
g_{14}	0	$-0.100 + j0.075$
g_{15}	0	$0.086 - j0.199$

Table 4.1: g_i coefficients for 16 Symbols QAM and Voronoi constellations

4.2 Transmitter Structure

It is well known that spectral and energy efficiency are always crucial requirements in mobile communication systems. In order to achieve this, multilevel modulations can be employed together with an amplification based on NL amplifiers. Usually, NL amplifiers can be only employed when signals have constant envelope, which is the case of signals such as Continuous Phase Modulation (CPM), or offset modulations,e.g. OQPSK. However, by using OQPSK-type schemes , i.e., signals that can be written as the sum of several linear OQPSK terms [36], we can design signals with quasi-constant envelope and good spectral characteristics [37]. This technique may be applied to non-offset constellations allowing the decomposition of multilevel constellations onto a sum of constant or practically constant envelope signals. Therefore, it is possible to use grossly NL amplifiers in a new transmitter structure that relies on the mentioned decomposition methods for multilevel constellations (M-QAM, M-PSK, Voronoi or other) as a sum of constant envelope components[35] that can be amplified independently and, posteriorly, combined to generate the multilevel constellation.

Having in mind these considerations, the transmitter will have multiple parallel amplifi-

cation stages. So firstly, the considered signal is given by

$$x(t) = \sum_{n=0}^{N-1} a_n r(t - nT), \tag{4.4}$$

where $r(t)$ represents the modulation pulse and a_n denotes the data symbol associated to the chosen constellation. It is easy to conclude that $x(t)$ has envelope fluctuations for M-QAM and for Voronoi constellations (see figure 4.1 where it is possible to see the different magnitudes of constellation's symbols). However, through a proper selection of the modulation pulse $r(t)$, we can design BPSK signals with constant or quasi-constant envelope [38]. For instance, if it is selected a Minimum Shift Keying (MSK) pulse shape, all the sub-constellations, in which M-QAM or even Voronoi are decomposed, have constant envelope and can be separately amplified with nonlinear amplifiers. Even for the rectangular pulse shape general BPSK signals still have envelope fluctuations (since the pulse shape is an approximation of rectangular shape). Although, those envelope fluctuations are much lower when compared with the resultant constellations from the combination of all components.

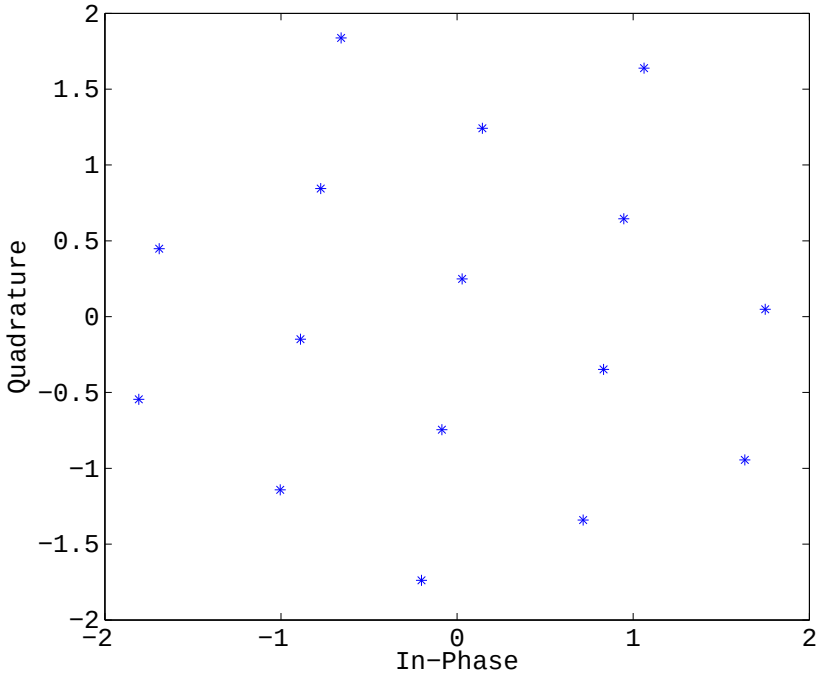

Figure 4.1: Optimum known Voronoi constellations with size 16.

Let us define a_n as

$$a_n = \sum_{m=0}^{M-1} g_i b_n^{eq(m)}, \quad with \quad b_n^{eq(m)} = \prod_{m=1}^{\mu} \left(b_n^{(m)} \right)^{\gamma_{m,i}}, \tag{4.5}$$

where b_n^{eq} represents the phase (± 1) from the correspondent BPSK component and g_i the amplifier amplitude gain. Merging (4.4) and (4.5) it is possible to write $x(t)$ as

$$x(t) = \sum_{n=0}^{N-1} \sum_{m=0}^{M-1} g_i b_n^{eq(m)} r(t - nT) \tag{4.6}$$

Considering that all BPSK signals have small envelope fluctuations at the input of each amplifier,it is possible to use high power nonlinear amplifiers to assure power amplification efficiency and at same time a simple implementation. After the amplification stage with M amplifiers in parallel, all the signals are combined to generate the symbol of the high order constellation, as shown if fig. 4.2. Nevertheless, this amplification structure imposes some

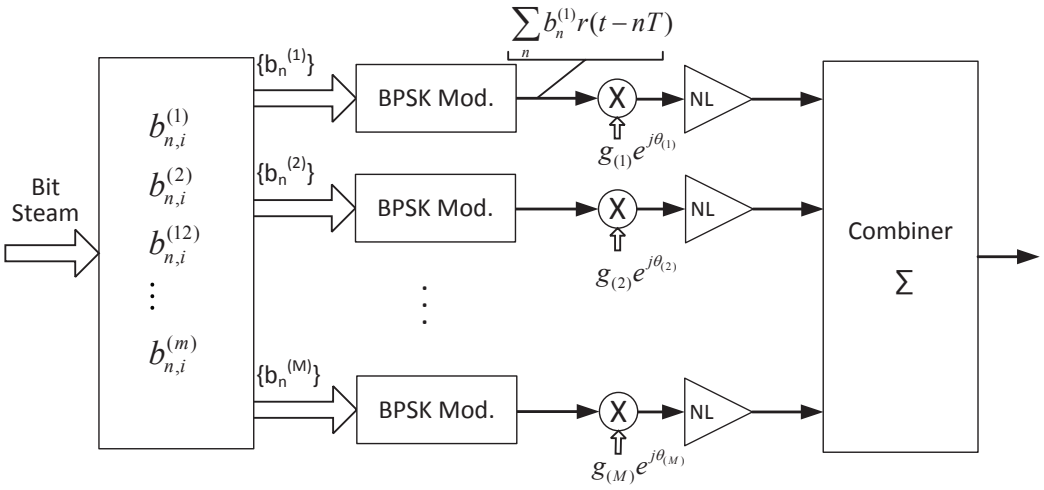

Figure 4.2: Separate amplification of BPSK components..

restrictions to the amplifiers, since gains and phases must take well-defined values to avoid imbalances between them which can lead to performance's degradation. Phase imbalances can occur when the signals in different amplification branches, have different delay values at the combiner input. Under these conditions, the symbols associated to each amplification

branch will suffer different phase rotations that can distort the resulting constellations after the combiner. Due to cumulative changes in the distances between constellation's symbols, phase imbalances will compromise the system performance and may have higher impact on high order constellations. Since in high order constellations symbols have a bigger number of adjacent symbols, phase imbalances will be have a higher impact when compared with smaller constellations [39].

Obviously, for specification purposes it is important to evaluate the impact of these imbalances as well as to measure amplifiers's accuracy requirements. Besides that, it is also important to achieve good tolerance against these imbalances. To increase system robustness against these phase imbalances, we can adopt the following approaches:the first is to tighten up the implementation requirements for amplification design and hardware implementation. It is worth to mention that in general, phase errors below 1^o are achievable with current technologies. The second is to implement at the receiver a compensation method of these phase rotations based on a error correcting code to help the estimates of the received symbols or the adoption of an iterative estimation process of the phase imbalances. Therefore, in next section the use of LDPC codes and their capability to minimize any effect of phase imbalances in system's performance is analyzed.

Because most of regular and non-uniform large constellations are very sensitive to interference, ISI, a receiver based on a SC-FDE capable to cope with the effects of highly time-dispersive channels is used. As mentioned before in Chapter 3, the IB-DFE receiver with soft decisions outperforms the non-iterative receivers and for large constellations it is expected to achieve significant performance improvements. Therefore, for both approaches is adopted an IB-DFE receiver that uses the outputs of LDPC decoder or the estimates of phase imbalances block estimator to compute the reliability of each block, in the feedback loop. It is worth to mention that the resulting complexity of both receivers (with LDPC or with phase imbalance block estimator) does not increase system's complexity and can be used for the computation of the receiver parameters for any constellation.

4.3 LDPC and phase imbalance effects compensation on systems

The impact caused by those imbalances must be evaluated and to measure the requirements on the accuracy of the amplifiers matching it is assumed that the phase mismatches between different amplifiers are uncorrelated zero-mean Gaussian random variables with variance σ_θ^2.

For evaluation purposes we consider both AWGN and time-varying channels. In the simulations regarding time varying channels, is considered a coded SC-DFE system based on multilevel modulations. The transmitter encodes data bits using an $(N, K) = (528, 264)$ LDPC encoder with rate 1/2 and column weight of 3. In each block the coded bits are randomly interleaved before being mapped into the constellation points and distributed by the symbols of the transmitted frame (the constellations can be 16-QAM or 64-QAM). The block sizes of transmitted symbols depend on the modulation order and are related with then by $N/log2(M)$. SC-FDE modulation is characterized by blocks of $N_B = N/log2(M)$ useful symbols and a cyclic prefix of 32 symbols longer than overall delay spread of the channel. The severely time-dispersive channel is characterized by an uniform PDP, with 32 equal-power taps, with uncorrelated Rayleigh fading on each tap. For simplicity purposes, it is considered linear power amplification at the transmitter, perfect synchronization and channel estimation at the receiver. Results regarding performance tolerance against phase imbalances are expressed as a function of phase errors. Performance results are expressed as function of $\frac{E_b}{N_0}$, signal-to-noise ratio, where N_0 is the one-sided power spectral density of the noise and E_b is the energy of the transmitted bits. For time selective channels a total of three iterations are performed in the IB-FDE receiver, with 10 iterations in the LDPC decoder for each IB-FDE iteration. Obviously, for AWGN the receiver have a linear FDE with 10 iterations at LDPC decoder (in this case the channel response is unitary)[1].

First it is measured the impact of phase errors on the BER performance for an ideal AWGN channel depicted in figs. 4.3 and 4.4, respectively (the E_b/N_0 values are selected to ensure BER in the vicinity of 10^{-4} with the different constellations when the amplifiers

[1]It should be noted that the selection of the number of iterations adopted in the SISO decoding process took into consideration the best compromise between convergence of the process, complexity and power efficiency when compared with higher number of iterations.

are perfectly matched). From BER comparison of coded and uncoded cases becomes obvious that, LDPC codes allow higher tolerance to phase mismatches. As illustrated on fig. 4.3, for AWGN channel the use of LDPC codes can achieve an almost invariant BER until 2.5^o for 16-QAM. This effect is valid independently the constellation size, as it shows from the results of figs. 4.3, where due to LDPC code the BER of 64-QAM remains unaffected for phase imbalances as well, near to 1.8^o. Without LDPC codes the BER is severely affected for imbalances higher than 0.5^o for both 16-QAM and 64-QAM.

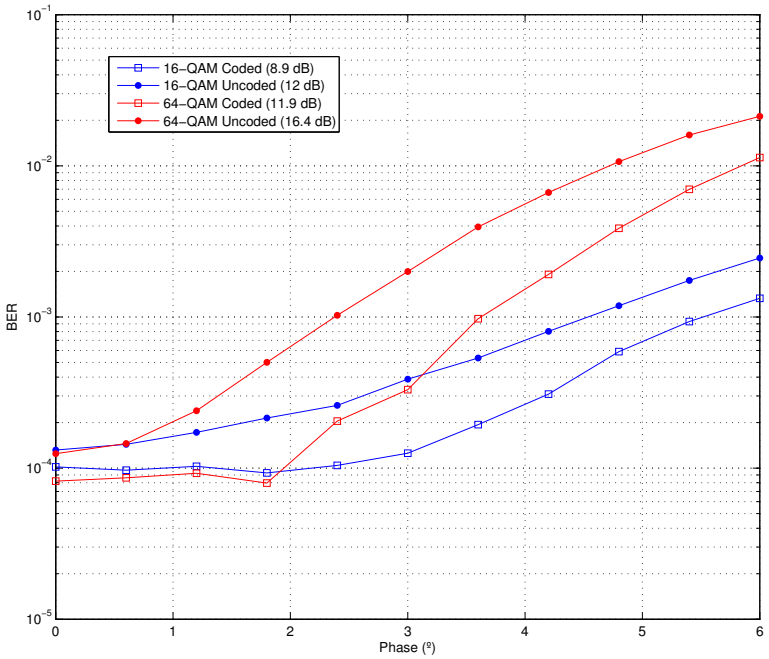

Figure 4.3: Phase imbalance impact on performance for AWGN channel

The tolerance's increase to phase imbalances with LDPC codes becomes higher for time dispersive channels where the BER of 16-QAM remains unaffected until 4^o. This means an increase of more than 2.5^o when compared with the uncoded scheme. The same conclusion applies to 64-QAM since the BER remains unaltered until 2.5^o. The main reason for that reliable behavior lies in the iterative decoding process of LDPC that can correct a large part of the bit errors caused by phase imbalances.

Let us consider now the BER performance results from figs. 4.5 to 4.8.

In an AWGN channel, the first observed effect of LDPC codes is the BER decreasing into the asymptotic value not until 6 dB for 16-QAM and 8 dB for 64-QAM. This is expected

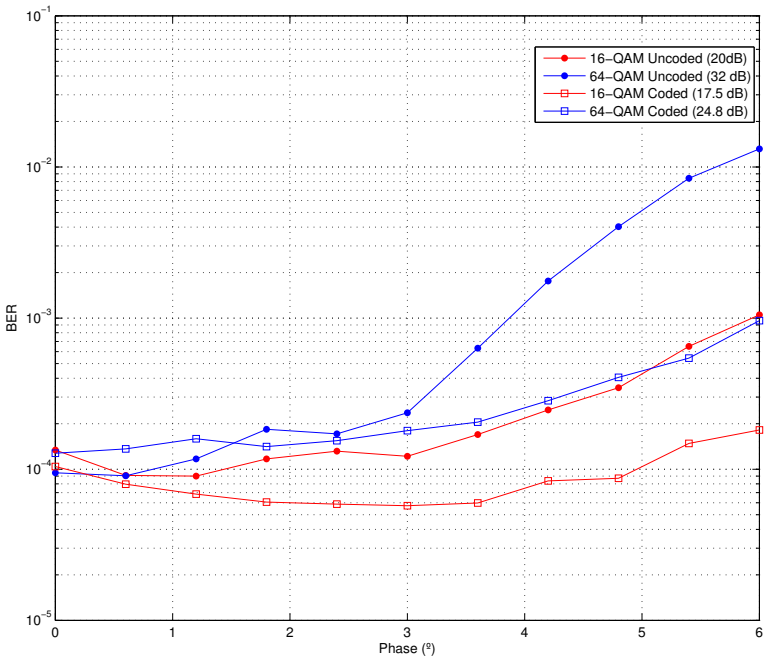

Figure 4.4: Phase imbalance impact on performance for time dispersive channel

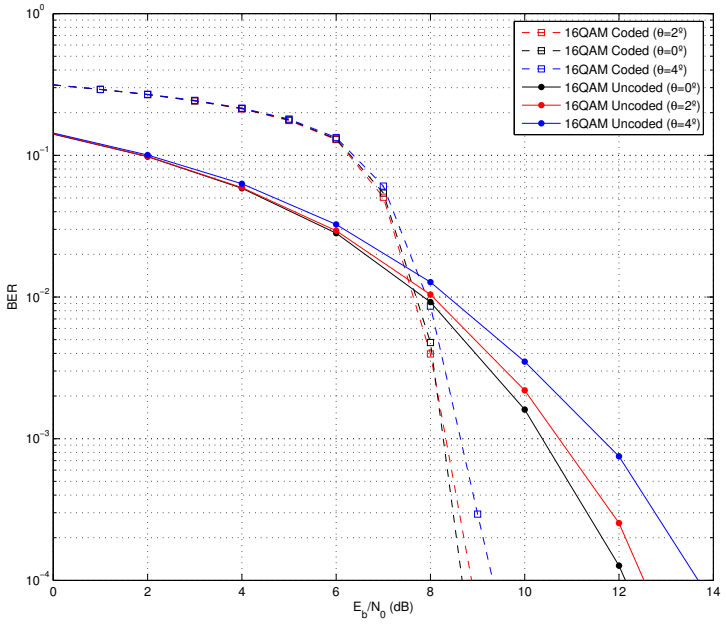

Figure 4.5: BER performance of 16-QAM constellations with AWGN channel

for regular constellations. Although this effect can be devalued since for bigger E_b/N_0 values, the error-correcting starts to have more impact. The power gains achieved by

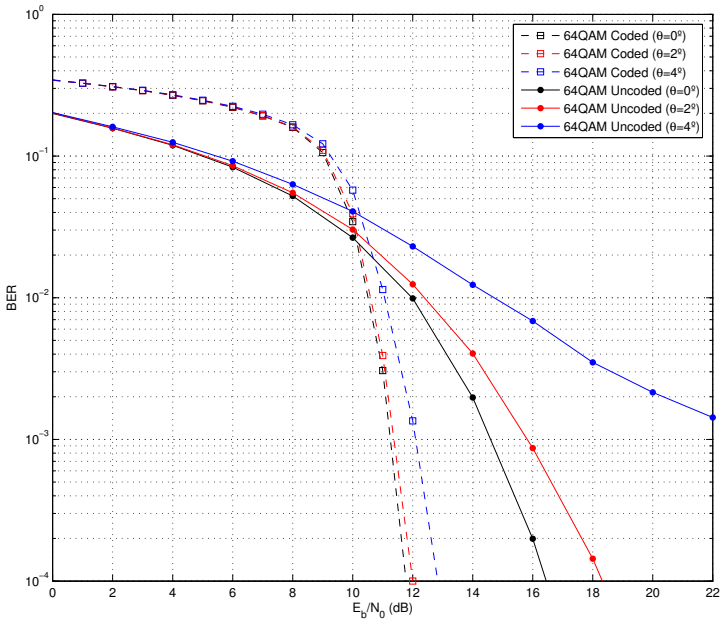

Figure 4.6: BER performance of 64-QAM constellations with AWGN channel

LDPC codes for phase imbalances of 4^o are 5 dB and more than 8 dB for 16-QAM and 64-QAM, respectively. Another positive effect of LDPC codes is the reduction on power degradation associated to phase imbalances for both constellations' sizes. For instance, in coded schemes the degradation is less than 0.75 dB for the maximum phase imbalance. On the opposite, uncoded schemes have bigger degradations of 2 dB for 16-QAM and more than 8 dB for 64-QAM. The effect of LDPC codes against phase imbalances, improving the robustness and reliability of the transmission becomes evident. Therefore, the better quality of bit estimates at output of LDPC decoder means better symbol estimates of the original constellation and consequently faster convergence in IB-DFE performance. Hence, it can be expected a low number of iterations at IB-DFE, more precisely it is predicted a lower improvement on performance as the number of IB-FDE iterations grows. Moreover, simulation results show also small performance differences between different phase imbalances which confirms the better tolerance to phase imbalances already shown in fig. 4.5.

Finally, are considered figs. 4.7 and 4.8 for time dispersive channel. From the comparison of performance results for coded and uncoded schemes it may be concluded that the

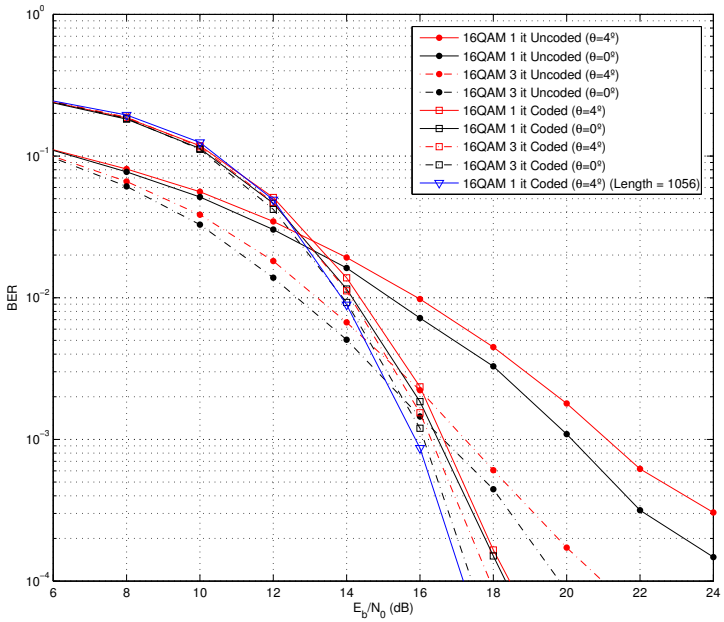

Figure 4.7: BER performance of 16-QAM constellations with time dispersive channel

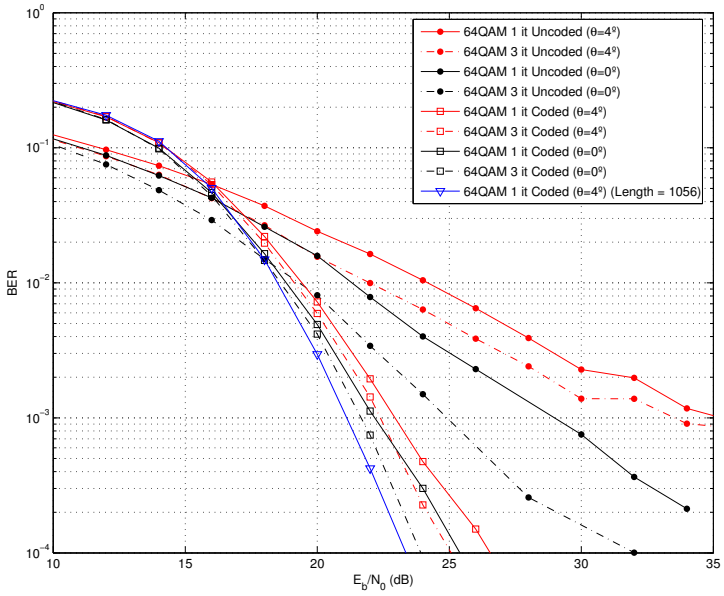

Figure 4.8: BER performance of 64-QAM constellations with time dispersive channel

power gains achieved by LDPC codes are similar to those associated to AWGN channel. For instance, for 16-QAM there is a power gain of 2 dB and more than 8 dB for 64-QAM. Once more, due to LDPC codes as error-control coding method, the system has a lower

performance improvement between successive iterations of IB-DFE. The performance of LDPC decoding process, in the first iteration bit estimation, is given with higher quality than uncoded case. The performance advantage is more significant as the codeword length increases. Another important aspect shown in fig. 4.7 is the slight difference on performances of coded schemes for the different phase imbalances, which justifies the better tolerance against imbalances of coded 16-QAM. Clearly, the IB-DFE iteration's impact on system's performance is lower when the LDPC codes are used. This behaviour becomes obvious from the comparison of BER results for both code and uncoded schemes.
It becomes clear that, although the lower tolerance against phase imbalances of the proposed transmitter, the use of LDPC codes increases significantly the margin for phase errors for both types of constellations. Thus, due to LDPC codes the complexity of iterative equalization process can be reduced as well, by considering a lower number of iterations at the IB-DFE. As it was already mentioned, in practical implementations of amplifiers, the phase errors below 1^o are achievable with current technologies [40]. Therefore, the tolerance range allowed by the coded schemes, achieves more flexibility in the requirements for the transmitter implementation.

4.3.1 Block length behavior

To analyze the impact of the codeword length in the BER performance, the block length was increased twice. The transmitter now encodes data bits using an $(N, K) = (1056, 528)$ LDPC encoder with rate 1/2 and column weight of 3 as well.
On AWGN channel, the BER performance for a 16-QAM constellation, depicted in figure 4.9 is slightly better, around 0.3 dB, than the BER achieved by a block length of 528 in fig. 4.5. A slimly improvement, 0.5 dB, is attained for a 64-QAM constellation as we can see in fig. 4.10 (in comparison with fig.4.6 which has a codeword half the size).

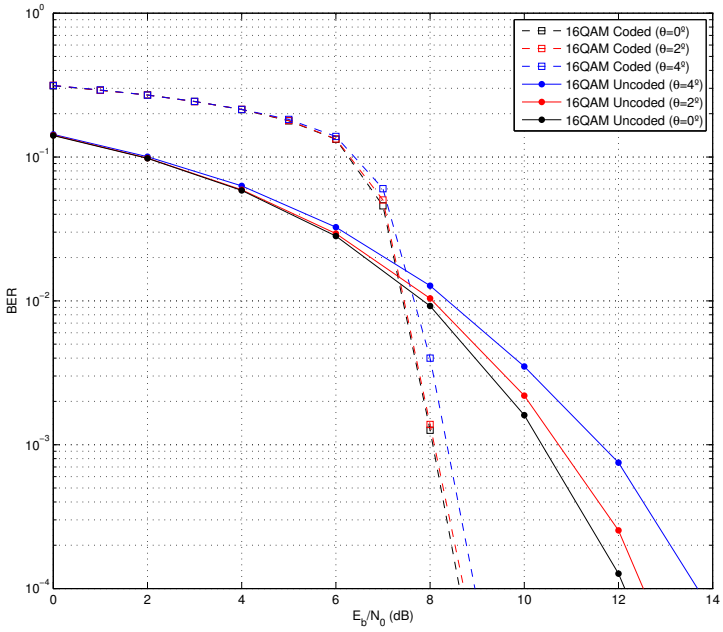

Figure 4.9: BER performance of 16-QAM constellations with AWGN channel for code length of 1056

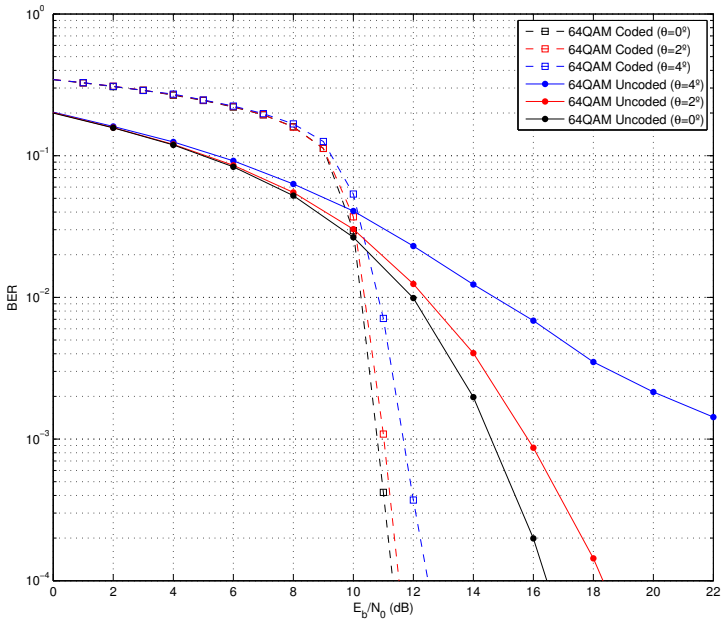

Figure 4.10: BER performance of 64-QAM constellations with AWGN channel for a code length of 1056

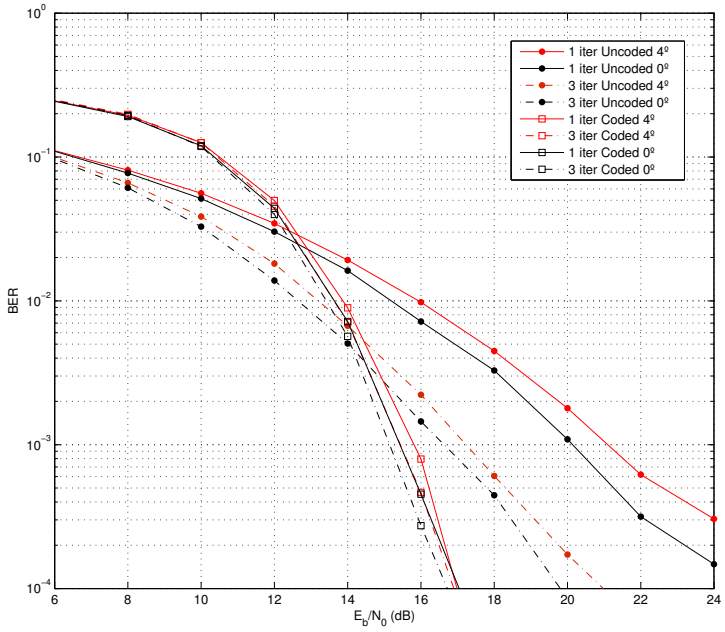

Figure 4.11: BER performance of 16-QAM constellations with time dispersive channel for code length of 1056

Considering a time dispersive channel and a 16-QAM constellation, from the comparison of figure 4.11 with fig. 4.7 (whose block has half of the length), it can be seen that the 1056 block length code has a performance around 1 dB better, and for 4^o phase imbalances, it shows an improvement near to 1.5 dB. BER performances for each imbalance are slightly more tolerant than the 528-length codeword. For a 64-QAM constellation, the comparison of fig. 4.12 with fig. 4.8 shows that the margin of performance enhancement is bigger with improvements between 2 dB and 3dB and there is also a small increase in tolerance against phase imbalances. It is clear that the codeword's size has a big effect in the BER performance in time dispersive channel (in contrast the improvements achieved in an AWGN channel were not significant).

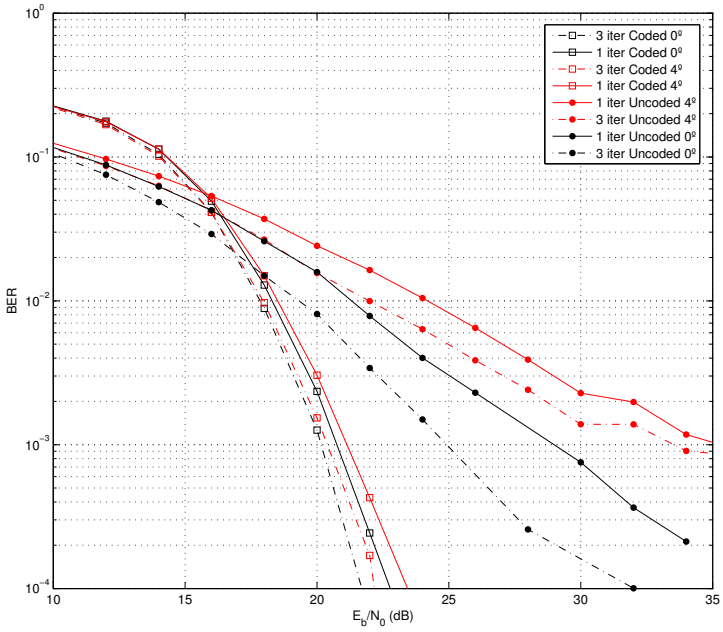

Figure 4.12: BER performance of 64-QAM constellations with time dispersive channel for a code length of 1056

4.3.2 Number of the decoder iterations behavior

The LDPC decoder considered for the preceding simulations had 10 iterations, however in this section it will be used 20 and 40 iterations on the LDPC decoding process within each IB-DFE iteration. For 0^o and 4^o phase imbalances are examined what is the impact on the BER performance on AWGN and time dispersive channel.

Firstly for an AWGN channel for a 16-QAM and 64-QAM constellation, respectively represented on figs. 4.13 and 4.14. It can be observed that the power gains for both constellations are around 0.1 and 0.2 dB when doubling the number of iterations on the decoder.

For both constellation sizes, i.e., 16-QAM and 64-QAM, performances results only consider 10 and 40 iterations in LDPC decoder. Results are shown in figs. 4.15 and 4.16. For 16-QAM the improvement of using 40 instead of 10 iterations is between 0.1dB and 0.2dB approximately, and for 64-QAM is between 0.2dB and 0.5dB.

It can be seen that, for a significant increase of iterations' number, the improvements on BER are few tenths of a decibel. Therefore, increasing complexity and decoding time by

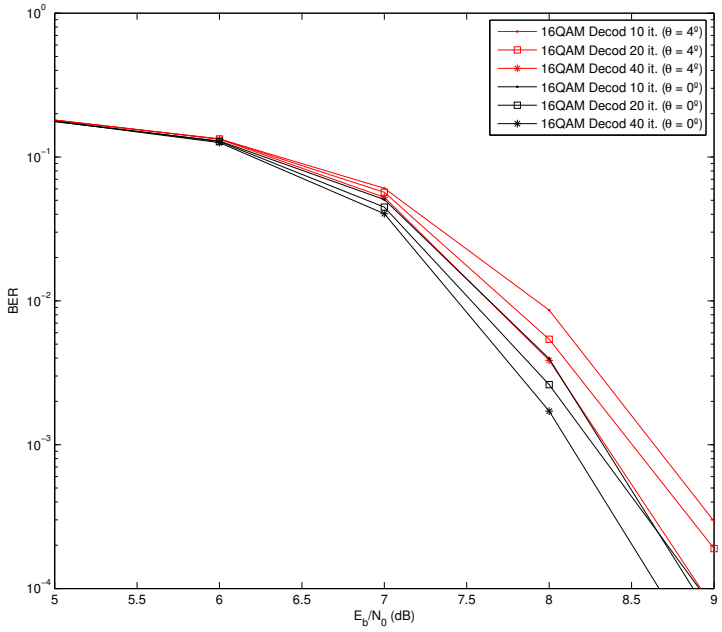

Figure 4.13: BER performance of 16-QAM constellations with AWGN channel for 10, 20 and 40 decoding iterations

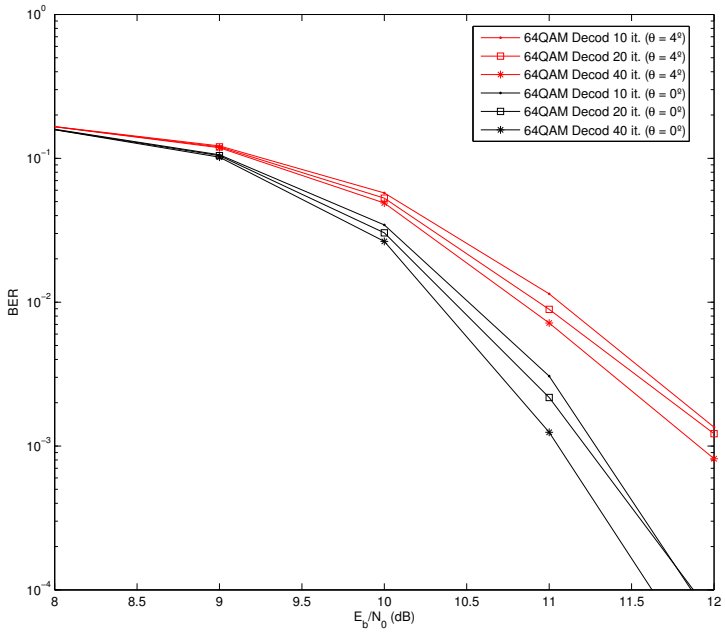

Figure 4.14: BER performance of 64-QAM constellations with AWGN channel for 10, 20 and 40 decoding iterations

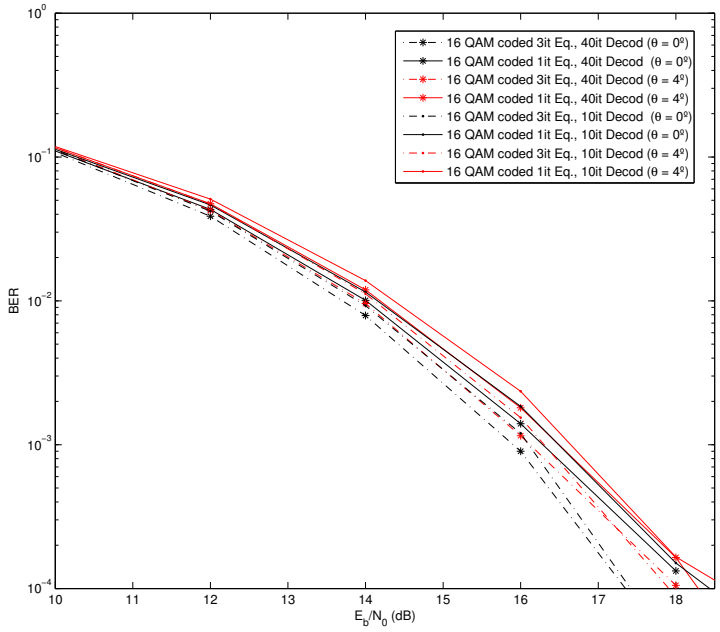

Figure 4.15: BER performance of 16-QAM constellations with time dispersive channel for 10, 20 and 40 decoding iterations

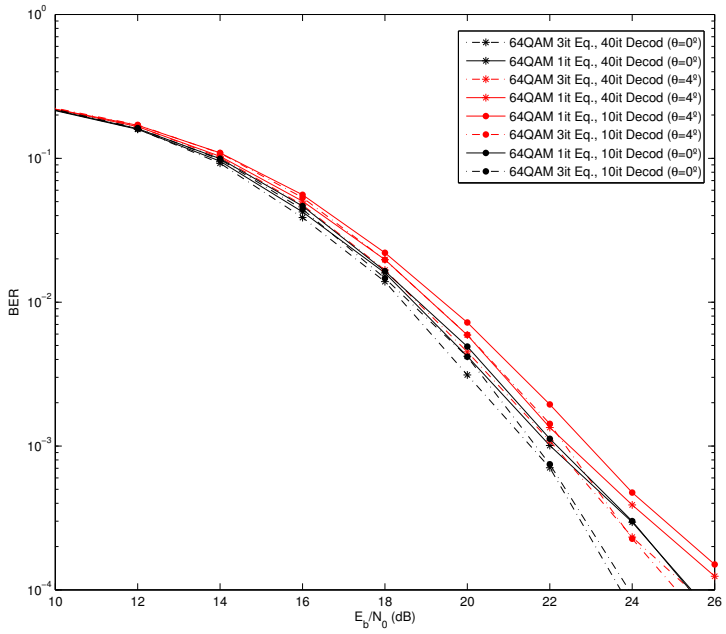

Figure 4.16: BER performance of 64-QAM constellations with time dispersive channel for 10, 20 and 40 decoding iterations

setting 40 iterations in LDPC's decoder it is avoidable.

4.4 Receiver with Phase imbalance estimator block

In the decomposition of multilevel constellations, all the BPSK components used to define the 2^M-QAM symbols belong to one quadrant. This property leads to the conclusion that the training sequence for phase imbalances estimation shall include, at least, all the symbols from one quadrant. Thus, for 16-QAM and 64-QAM the length of corresponding training sequences are 4 and 16, respectively. The minimum error allowed for phase imbalances estimation, that does not have significant impact on system's performance, it is another aspect to take into account. The choice of this value must follow two criteria: the first, is the computational complexity associated to the estimation process and the second, is the maximum phase estimation error allowed. Current self biased amplifiers implementations may have phase imbalances upper bounded by $\pm 1.0^o$. Still, these phase imbalances can affect power efficiency of the system, mainly when constellation sizes are high[2]. Therefore, it seems reasonable to consider phase imbalances between $\pm 2^o$ and a maximum phase estimation error of 0.5^o [3]. Since the number of symbols in the training sequence is $2^M/4$, the phase estimation algorithm will compare the training sequence with the sequences resulting from all the combinations of phase imbalances. To reduce complexity we assume that each amplifier may suffer phase imbalances belonging to a set with $Q = 4$ quantified values, i. e., $[-1^0, -0.5^0, 0^0, 0.5^0, 1^0]$. Under these conditions, the number of possible phase imbalances combinations for M' amplifiers is $Q^{M'}$. Thus, the algorithm computes $Q^{M'}$ possible training sequences with $Q^{M'}2^M/4$ symbols and selects the set of phase imbalances that assures the minimum Euclidean distance between the estimate and the received training sequence. For instance, for 16-QAM we will have 256 possible training sequences and for 64-QAM, the number will be 4096. The schematic representation of this algorithm is shown in figure 4.17, where we can see the three fundamental steps: computation of all possible phase imbalances combinations, computation of all training sequences, computation of all Euclidean distances to the received training

[2] 64-QAM constellations have 6 amplifiers in parallel that may have independent phase imbalances
[3] results show that performance degradation is lower than 0.1 dB for 64-QAM

sequence and selection of the phase imbalances that lead to the minimum Euclidean distance. The set of estimated phase imbalances will be used by the IB-DFE to compensate the phase imbalances in the received data block symbols. Obviously, the receiver starts with the estimation process and only after that, starts with the iterative equalization process. In figure 4.18 it can be seen the structure for the proposed receiver. It should be noted that it is assumed that phase imbalances remain almost constant during all the duration of each data block. Nevertheless, we admit that the operating characteristics of the amplifiers change with time. However, due to the small duration of each data block we can consider that the estimates of phase imbalances will be valid for several consecutive data blocks. For instance, in simulation results of subsection 4.4.1 it is assumed amplifiers characteristics remain almost constant during at least 10 block.

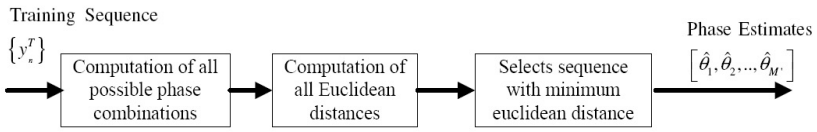

Figure 4.17: Phase estimation algorithm steps

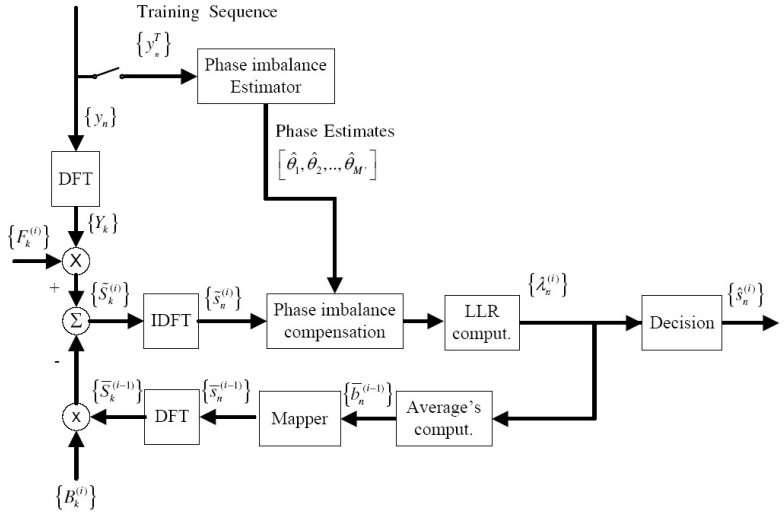

Figure 4.18: Receiver with phase estimation block

4.4.1 Phase Estimator behavior

To evaluate the impact of phase imbalances and measure the performance of the proposed algorithm for phase imbalance estimation, we consider uncorrelated phase imbalances θ between different amplifiers. For 16-QAM random phase imbalances are between 0^o and 4^o and for 64-QAM phase imbalances are limited to 2^o.

As for LDPC codes in section 4.3 we consider both AWGN and time-varying channels. For time varying channels, we have a SC-DFE system based on multilevel modulations, characterized by blocks of 256 useful symbols and a cyclic prefix of 32 symbols longer than overall delay spread of the channel. The severely time-dispersive channel is characterized by an uniform PDP, with 32 equal-power taps, with uncorrelated Rayleigh fading on each tap. For sake of simplicity, it is assumed linear power amplification at the transmitter, perfect synchronization and channel estimation at the receiver. Again, performance results are expressed as function of $\frac{E_b}{N_0}$, where N_0 is the one-sided power spectral density of the noise and E_b is the energy of the transmitted bits. For time selective channels a total of three iterations are performed in the IB-FDE. Obviously, for AWGN we have a linear FDE (in this case the channel response is unitary).

We start with the BER results for 16-QAM and 64-QAM constellations, regarding an ideal AWGN channel and depicted in figs. 4.19 and 4.20. For comparison purposes, receivers with and without the proposed estimation algorithm are considered. As we can see, a phase imbalance of $\theta \leq 2^o$ has low impact on system's performance for 16-size constellations. Despite this fact, we can see from the results of fig. 4.19, that the receiver with phase estimation algorithm compensates very well the phase imbalances, since the performances for $\theta = 2^o$ and $\theta = 0^o$ are practically the same (when compared with the receiver without phase imbalance compensation the power gain is around 0.5 dB). Even for imbalances of 4^o, this algorithm improves the performance by 1.75 dB. Same conclusions are valid for 64-size constellations. From the results of fig. 4.20, it is clear that phase imbalances estimation algorithm reduces significantly the impact of any phase imbalance on system's performance. For example, the power gains achieved by the estimator of phase imbalances are 0.25 dB for $\theta = 1^o$ and more than 1.25 dB for $\theta = 2^o$, respectively.

Let us consider now the results of fig. 4.21 and 4.22 regarding the time dispersive chan-

nel. An interesting effect introduced by the phase estimator, is the reduction of power improvements between successive iterations of IB-DFE. The reason for that lies on the good quality of phase estimates at output of phase estimator, which means better symbol estimates of the original constellation and consequently faster convergence in IB-DFE's equalization. Moreover, simulation results show also small performance differences between different phase imbalances which confirms the better tolerance to phase imbalances already shown in fig. 4.19 and 4.20. Once again, power improvements due to phase imbalance estimator are lower for small constellations due to the lower number of amplification branches used at the transmitter. Another important aspect to refer is the slight difference on performances for different phase imbalances when we have 16-QAM. On the contrary, the degradation in 64-QAM reaches practically 1.5 dB.

It is easy to conclude that the algorithm for phase imbalance estimation reduces significantly the impact of phase imbalances in a transmission system based on M amplifiers in parallel. From simulation results, it becomes obvious that the use of a receiver that compensates phase imbalances based on the estimates increases significantly the tolerance range against phase imbalances of the proposed transmitter. It should be also mentioned that, for 16-QAM performance degradation due to phase imbalances is almost cancelled and for 64-QAM degradations are limited to 0.25 dB in the worst case. Therefore, it becomes clear, that despite the lower tolerance against phase imbalances of the proposed transmitter, the use of the estimation algorithm relaxes significantly the range of phase imbalances for both types of constellations and allows to use error correcting codes, such as LDPC codes, when it is needed to improve system's power performance.

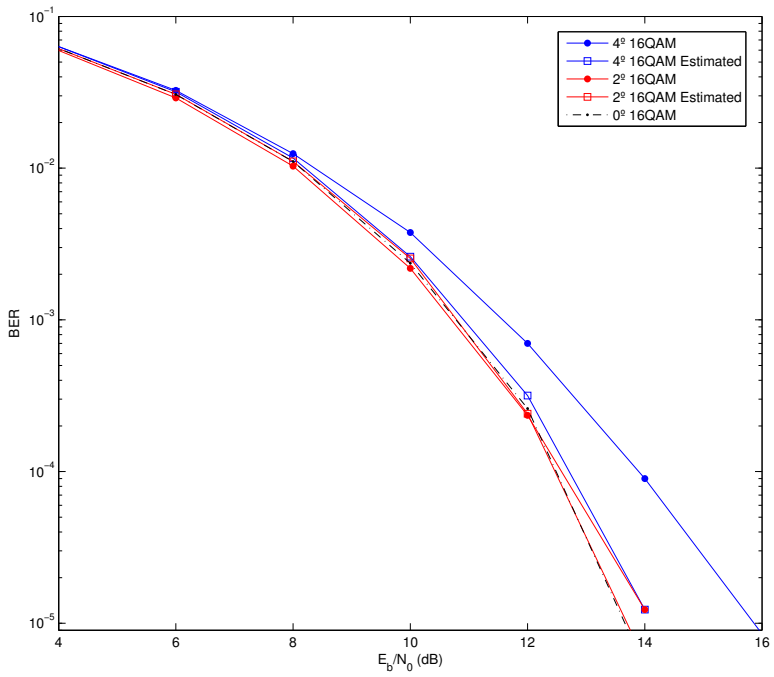

Figure 4.19: Phase imbalance impact on BER performance of 16-QAM constellations with AWGN channel

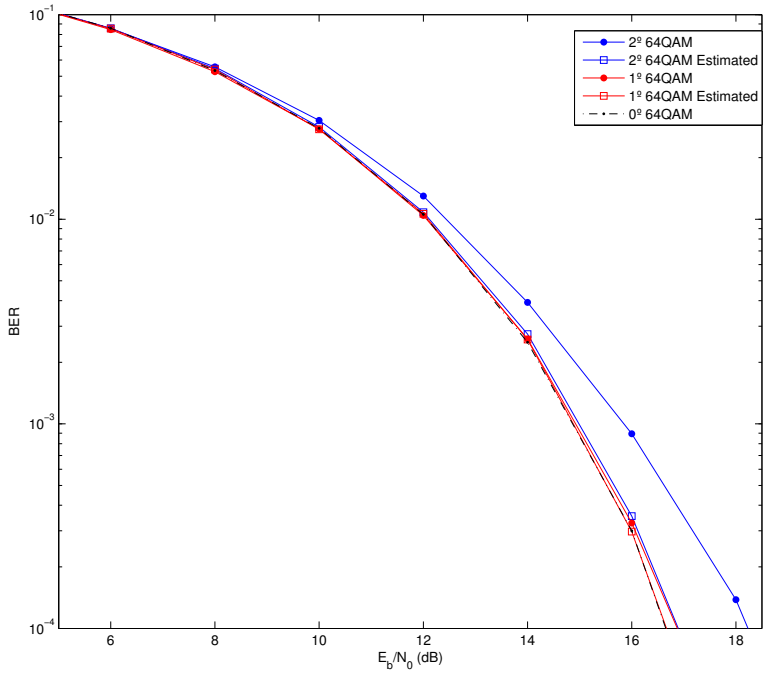

Figure 4.20: Phase imbalance impact on BER performance of 64-QAM constellations with AWGN channel

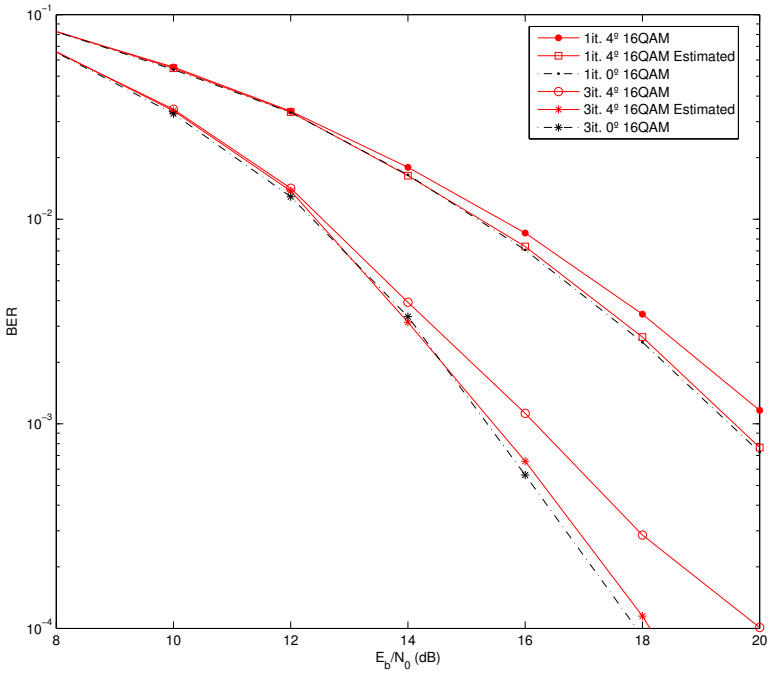

Figure 4.21: Phase imbalance impact on BER performance of 16-QAM constellations with time dispersive channel

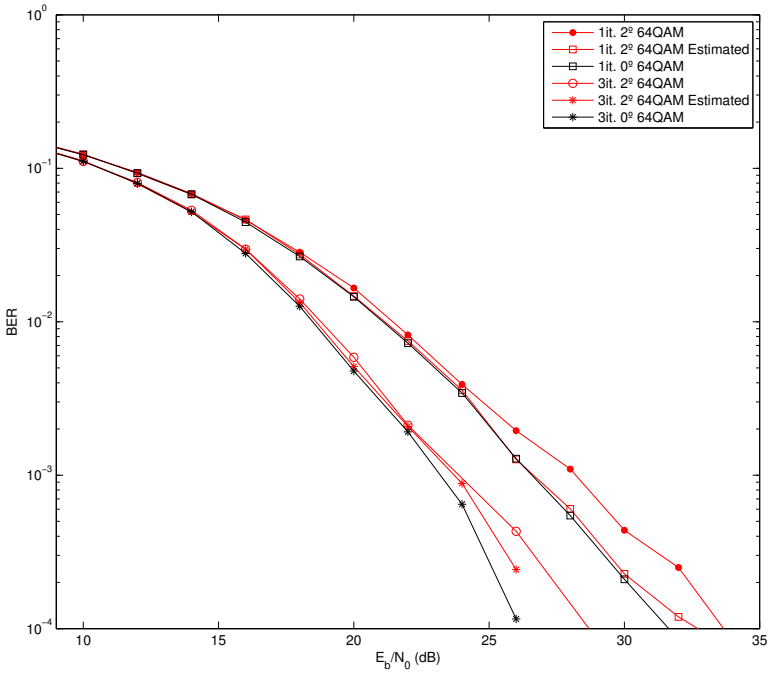

Figure 4.22: Phase imbalance impact on BER performance of 64-QAM constellations with time dispersive channel

Chapter 5

Conclusions and Future Work

5.1 Conclusions

The main objective of this thesis is focused on the study and development of LDPC codes for MC and SC schemes with IB-DFE receivers, in order to achieve great performances when transmitting, while maintaining a low system complexity and computational process.

Chapter 2 introduced the characterization of error correcting codes' principles and key aspects of LDPC codes such as the construction methods and decoding processes. It was also pointed out that RA codes are a good construction method due to an almost linear encoding process' time. As for the decoding method, the MS algorithm provides a good solution with a reliability similar to the SP algorithm but with less complexity.
In chapter 3 the basic principles of MC and SC modulations were characterized. The main objective was to perceive if by applying LDPC codes to each one of the modulations, it has a sufficient enhancement to the system performance. It is shown that, both OFDM and SC-FDE schemes with LDPC codes can have significant improvements on error rate without significant increase on decoding's complexity. This conclusion is valid for non-iterative and iterative receivers. LDPC codes were also considered to improve the convergence of the IB-DFE. Simulation results, even for small block sizes, show that the iterative equalization can be optimized together with the iterative decoding of LDPC to improve greatly the reliability when compared to uncoded schemes. In addition, the proposed coded IB-DFE scheme outperforms coded OFDM and has similar performance to uncoded IB-DFE, even

for lower number of iterations in the iterative equalization block, which means that we can reduce the computational load at the receiver's side. It becomes obvious that the use of LDPC codes increases significantly the power efficiency of both systems. However, the higher impact is in IB-DFE where due to LDPC codes the complexity of iterative equalization process can be reduced. This effect is more significant for a higher number of iterations in SISO block. Therefore, a lower number of iterations in IB-DFE allows a less complex equalization in SC systems. Overall, the resort to LDPC codes allows significant power improvements in both MC and SC schemes with only a small increase of the system complexity.

Some parts of the work presented in chapter 3 were accepted for presentation in a international conference's proceeding [41] (see Appendix A).

In chapter 4, several techniques to compensate phase imbalances between amplifiers, including the use of LDPC codes were analyzed. The study showed that LDPC codes can be used to compensate phase imbalances in amplification stages based on multiple amplifiers in parallel. The use of these codes increases the robustness against phase mismatches and simulation results showed that the resulting transmission system can achieve higher tolerance to phase imbalances without significant increase in system's complexity. Aspects such as the effects of codeword's size and number of iterations in the LDPC decoder were evaluated. Simulation results showed that codeword's size has a higher impact in time dispersive channel while in AWGN channel it is only tenths of a decibel. Also, from simulation results it is clear that a increment on decoding iterations does not lead to significant improvements on BER. Therefore, incrementing the number iterations on the decoder is not advantageous since any improvement implies an higher computational load.

Besides the use of LDPC codes, it was also proposed a algorithm for phase imbalance estimation that achieves good accuracy in the estimates. Simulation results showed that phase imbalance's impact in performance is negligible since errors on estimates are lower than 0.5^o. It was already pointed out, that phase errors below 1^o are achievable with current technologies. Therefore, the tolerance range allowed by LDPC codes or by the phase estimation algorithm allows more flexible requirements in transmitter's implementation.

It should be mentioned that both techniques can be combined in a receiver where first we perform the phase imbalances estimates and the LDPC codes are used to compensate any residual error that may results from the phase imbalance estimator block.
Some parts of the work presented in chapter 4 were accepted for presentation in a international conference's proceeding [42] (see Appendix A).

5.2 Future Work

Having in mind the considerations presented before, future research subjects should include the following topics:

- **LDPC ensemble optimization**

  The construction of the parity-check matrix was based on the RA codes and only regular ones were used. It is known that the irregular ensembles have a better performance. Therefore, we can expect that this kind of construction could provide bigger improvements.

- **Voronoi constellations**

  In this thesis, we considered only regular constellations such as QPSK, 16-QAM and 64-QAM. Irregular designs such as Voronoi constellations, where the modulated symbols are selected from the transmitted data according to a mapping rule that optimizes energy efficiency, suffer severely with phase imbalances. Therefore, the use of LDPC codes or the resort to phase imbalance algorithms could greatly improve system's performance.

- **Design of phase and gain estimation algorithms**

  In chapter 4 was presented a algorithm for phase estimation that despite the simplicity, leads to estimates with a negligible error. However, we can have gain and phase imbalances at same time. Therefore, it seems crucial the design of algorithms

for joint estimation of these two imbalances, keeping low at the same time the computational load required to decode each data block at the receiver.

Appendix A

Publications

In this appendix, we present the articles submitted in international conferences.

- **Chapter 3**

  "Low complexity LDPC coded IB-DFE for multilevel modulations and coded OFDM: comparison and complexity trade-offs" – The work presented in this chapter will be published in the *2014 International Conference on Telecommunications and Multimedia (TEMU2014)*[41].

- **Chapter 4**

  "Robust Frequency-Domain Receivers for A Transmission Technique with Directivity at the Constellation Level" – The work presented in this chapter was published in the *2014 IEEE 80th Vehicular Technology Conference (VTC2014-Fall)* [42].

Low complexity LDPC coded IB-DFE for multilevel modulations and coded OFDM: comparison and complexity trade-offs

Paulo Montezuma[1,2,3], Daniel Marques[1] and Rui Dinis[1,2]

[1] DEE, FCT Universidade Nova de Lisboa, Portugal
[2] IT, Instituto de Telecomunicações, Av. Rovisco Pais, Lisboa, Portugal.
[3] Uninova, Instituto de Desenvolvimento de Novas Tecnologias, Quinta da Torre, Caparica, Portugal.

Abstract - In this paper, we propose IB-DFE receiver (Iterative Block Decision Feedback Equalization) with iterative SISO LDPC decoding (soft-input soft-output - Low Density Parity Code) suitable for SC-FDE (Single-Carrier with Frequency-Domain Equalization) with offset modulations. This scheme can be implemented in a simple way with resort to an analytical characterization where the any multilevel constellation is represented as a sum of BPSK (Bi-Phase Shift Keying) sub-constellations. This decomposition also allows energy efficient amplification compatible with grossly nonlinear amplifiers where BPSK component is amplified independently). The proposed system is compared with LDPC-coded OFDM (Orthogonal Frequency Division Multiplexing) with similar complexity. It is shown that the proposed system allows significant improvements on error rate performance without significant increase on decoding process' complexity. The simulation results show that the iterative equalization together with the iterative decoding of LDPC improves the performance significantly when compared with uncoded schemes, even for small block sizes. In addition, the proposed coded IB-DFE scheme outperforms coded OFDM and has similar performance to uncoded IB-DFE even for lower number of iterations in the iterative equalization process, which can contribute for reductions in the computational load at the receiver's side.

Index Terms: Multilevel constellation, SC-FDE with offset modulations, LDPC decoding, coded OFDM, computational load.

I. Introduction

In modern mobile communication systems high bit rate transmission is required together with high quality communications. Orthogonal Frequency Division Multiplexing (OFDM), which divides the signal bandwidth into many narrow band subchannels that are transmitted in parallel, is an attractive technique for high bit rate transmission over time dispersive channels, since ISI (Inter-Symbol Interference) can be eliminated by adding a guard interval with length higher than overall delay spread of channel. Moreover, frequency selective effects of the channel can be also easily compensated through a simple equalizer implemented in frequency domain. Still, frequency selective channels with deep fades affecting several sub-carriers can compromise system performance. In such situation even though most subcarriers may be detected without errors the overall BER (Bit Error Rate) of the system is dominated by the weakest sub-carriers.

SC-FDE schemes (Single-Carrier with Frequency-Domain Equalization) [1] have lower PMEPR (Peak to Mean Power Ratio) which allows reduction in power consumption and cost in mobile terminals. Alike OFDM the equalization in SC-FDE is also done in frequency domain. For that, the received signal is transformed from the time domain to the frequency domain using the DFT (Discrete Fourier Transform). On the other hand, the high bandwidth efficiency required in modern wireless communications can be achieved by multilevel modulations at the expense of an higher PMEPR that compromises power efficiency. Obviously a lower PMEPR can allows reductions in the total power consumption of the devices due to a more efficient amplification. Further reductions on PMEPR can be achieved by employing offset modulations which combined with SC-FDE are excellent transmission schemes for the uplink of broadband wireless systems. Another solution is to use multilevel modulations with multi-branch amplifiers structures at the transmitter. However, conventional FDE receivers do not cope with the residual interference between the in-phase and quadrature components at the sampling instants. To overcome this problem, FDE receivers specifically designed for offset modulations were proposed in [2], [3]. On the other hand, to cope with the very high residual ISI of multilevel modulations, the DFE (Decision Feedback Equalizer) with frequency domain feedforward and feedback filters is a more efficient solution. Thus, IB-DFE receivers (Iterative Block Decision Feedback Equalization) [4], [5], [6] optimized for non-offset constellations should be adopted to minimize the residual ISI and IQI (In-phase/Quadrature Interference) interferences associated to multilevel modulations. Alike OFDM the performance can be limited by the weakest symbols affected by the deep fades of multipath environment. Hence, becomes crucial the use of forward-error correction coding techniques such as convolutional codes [7] or turbo codes [8] to avoid this domination by the weakest subcarriers.

Low-density parity-check (LDPC) codes proposed by Gallager [9] have performance very close to the Shannon limit for large block lengths [10]. Moreover, LDPC codes have

better block error performance than turbo codes because the minimum distance increases proportional to the code length with high probability [10]. It should be mentioned, that waterfall probability of turbo codes depends directly of the minimum distance of the concatenated codes. Hence, the minimum distance behavior of LPDC codes is desirable to assure the intended QoS (quality of Service) on an high bit rate transmission, i. e., very low bit error rate. In this paper we adopt LDPC for both multi carrier and single carrier systems. Since it is assumed perfect channel estimation, only in single carrier option the LDPC decoder will interact with the IB-DFE receiver, where in each iteration the soft outputs from LDPC decoder are provided to the iterative equalizer, which achieves better estimates of the transmitted symbols in the feedback loop. We start by characterizing the analytical description of multilevel modulations into sub-constellations as well the transmission architectures adopted OFDM and and SC-FDE systems. For both systems are proposed low complexity algorithms for decoding based on an analytical decomposition of multilevel constellations. As we shall see the simulation results show better performance for both transmission schemes even for small block lengths and small number of iterations at cost of low complexity increase.

The rest of this paper is organized as follows: following this introduction in section II is made the characterization of analytical tool for multilevel constellations description. Systems characterizations are presented in Sec. III. Sub sections III-A and III-B, characterize the receivers suitable for both types of signals. In sec. IV a brief overview of LDPC codes is presented. A set of performance results and the corresponding analysis are presented in sec. V. Finally, Sec. VI presents the conclusions.

II. Constellation Design

Any multilevel constellation can be represented as a sum of two BPSK (Bi Phase Shift Keying) components in quadrature. Therefore it becomes obvious that the constellation symbols can be expressed as function of the corresponding bits as follows[1]:

$$\begin{aligned} s_n &= g_0 + g_1 b_n^{(1)} + g_2 b_n^{(2)} + g_3 b_n^{(1)} b_n^{(2)} + g_4 b_n^{(3)} + ... \\ &= \sum_{i=0}^{M-1} g_i \prod_{m=1}^{\mu} \left(b_n^{(m)} \right)^{\gamma_{m,i}} = \sum_{m=0}^{M-1} g_i b_n^{eq(m)}, \end{aligned} \quad (1)$$

with $b_n^{eq(m)} = \prod_{m=1}^{\mu} \left(b_n^{(m)} \right)^{\gamma_{m,i}}$, where $(\gamma_{\mu,i} \ \gamma_{\mu-1,i} \ ... \ \gamma_{2,i} \ \gamma_{1,i})$ is the binary representation of i and $b_n^{(m)} = 2\beta_n^{(m)} - 1$. Since we have M constellation symbols in $\mathfrak{S}$ and M complex coefficients g_i, (1) is a system of M equations that can be used to obtain the coefficients g_i, $i = 0, 1, ..., \mu - 1$. Writing (1) in matrix format results

$$\mathbf{s} = \mathbf{W}\mathbf{g}, \quad (2)$$

where $\mathbf{s} = [s_1 \ s_2 \ ... \ s_M]^T$, $\mathbf{g} = [g_0 \ g_1 \ ... \ g_{\mu-1}]^T$ and $\mathbf{W}$ is a Hadamard matrix with dimensions $M \times M$. Therefore, for a given constellation we can obtain the corresponding coefficients g_i from the inverse Hadamard transform of the vector of constellation points.

To characterize M-QAM (Quadrature Amplitude Modulation) or M-OQAM (Offset-QAM) constellations we only need $\log_2(M)$ BPSK signals, since the remaining g_i coefficients are zero. For instance, for 16-QAM with Gray mapping we only need four BPSK signals defined by the set of non-zero complex coefficients $g_2 = \pm 2j$, $g_3 = \pm j$, $g_8 = \pm 2$ and $g_{12} = \pm 1$ (actually, this corresponds to only two QPSK (Quadrature Phase Shift Keying) or two OQPSK (Offset-QPSK) sub-constellations in the case of 16-OQAM). Assuming that all BPSK signals at the input of each amplifier have small envelope fluctuations, we can employ grossly nonlinear power amplifiers which have higher amplification efficiency, higher output power and are simpler to implement. After the amplification stage, with M amplifiers in parallel, all the signals are combined to generate the high order constellation, as shown in fig. 1. Obviously the transmitter structure based on M amplifiers can be employed in single carrier modulations without significant increment on complexity.

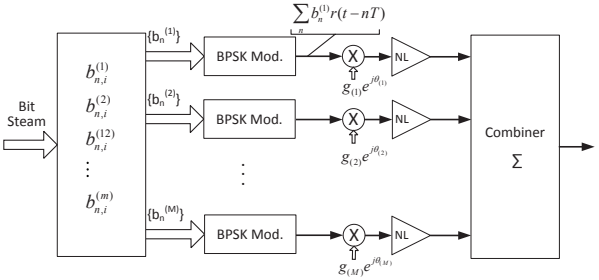

Fig. 1: Transmitter structure with M amplification branches in parallel.

III. System Characterization

A. OFDM transmission system

To avoid the dominance of subcarriers affected by deep fades LDPC codes are applied. Also to increase spectral efficiency multilevel constellations are considered for each subcarrier. Fig. 2 shows the block diagram for the OFDM transmission system. At the transmitter the binary input data is encoded by a $1/2$ rate LDPC encoder and the resulting bits are interleaved. After interleaving, the binary values are converted to QPSK or M-QAM values. Pilot symbols can be added for channel estimation purposes (we omit the pilots since it is assumed perfect channel estimation and synchronization at the receiver). The OFDM symbol is modulated onto k' subcarriers by applying the IFFT (Inverse Fast Fourier Transform). The output is converted to serial and a cyclic extension with duration longer than the overall delay spread of the channel is added to make the system robust to multipath propagation effects. By this the ISI and IBI (Inter Block Interference) are eliminated when the cyclic prefix is discarded at the receiver. The resulting signal is then converted to analog, amplified, and transmitted through the antenna. The receiver performs the reverse operations of the transmitter. In the first step, the

[1] It should be noted that s_n denotes the nth constellation point and not the nth transmitted symbol; the same applies to $b_n^{(m)}$ (or $\beta_n^{(m)}$) that here denotes the mth bit of the n constellation point.

receiver has to estimate frequency offset and symbol timing (which we assume that are perfect), using training symbols in the preamble. After removing the cyclic extension, is applied a FFT to the signal to recover the symbols of all subcarriers. The symbols values are then demapped into the log-likelihoods that after the de-interleaver operation will be the *a priori* probabilities used in the first iteration of the LDPC decoder, i.e. the SISO decodr (Soft-In Soft Out).

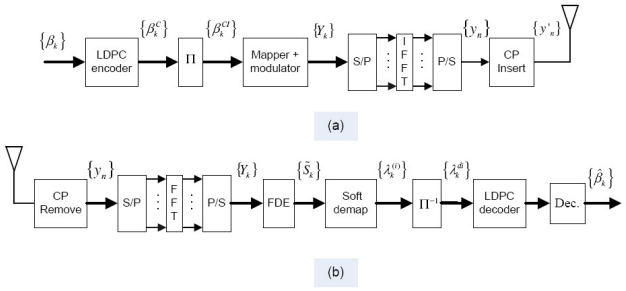

Fig. 2: (A) OFDM transmitter; (B) Receiver structure.

B. SC-FDE and IB-DFE Receivers

Let us consider now the use of M-QAM in SC-FDE systems. The transmission chain is depicted in fig. 3-(A), where the transmitter can be based on the multi-amplifier structure presented in section II, followed by the cyclic prefix adding. For the sake of simplicity, we assume an ideal linear transmitter (this can be achieved with the transmitter structure of fig. 1, provided that we have perfect balance between the different amplifiers). From the receiver side, it must deal with the high sensitivity of large constellations to interference, namely the residual ISI. For this reason, we replace at the receiver the linear FDE by a more powerful IB-DFE depicted in fig. 3-(B). The signal associated to a given block is given by

$$s(t) = \sum_{n=-N_G}^{N-1} s_n h_T(t - nT_S), \tag{3}$$

with T_S denoting the symbol duration, N_G denoting the number of samples at the cyclic prefix, N denoting the number of samples at the useful part of the block and $h_T(t)$ denoting the adopted pulse shape. The nth transmitted symbol[2] s_n belongs to a given size-M constellation $\mathfrak{S}$. As usual, the cyclic prefix corresponds to a periodic extension of the useful part of the block, i.e., i.e., $s_{-n} = s_{N-n}$.

At the receiver, the samples associated to the cyclic prefix are removed, which eliminates the interference between blocks. It should be mentioned that the cyclic prefix insertion at the transmitter and removal at the receiver is equivalent to a cyclic convolution relatively to the size-N useful part of the received block, $\{y_n; n = 0, 1, \ldots, N-1\}$. Hence, the corresponding frequency-domain block is $\{Y_k; k = 0, 1, \ldots, N-1\}$ = DFT $\{y_n; n = 0, 1, \ldots, N-1\}$), where

$$Y_k = S_k H_k + N_k, \tag{4}$$

[2]It should be pointed out that we have a slight abuse of notation, since in this section s_n designates the nth transmitted symbol of the block, while in sec. II s_n designates the nth symbol of the constellation.

with H_k denoting the channel frequency response for the kth subcarrier and N_k the corresponding channel noise, which means that the impact of a time-dispersive channel reduces to a scaling factor for each frequency.

To cope with these channel effects we will consider the IB-DFE receiver depicted in fig. 3-(B).

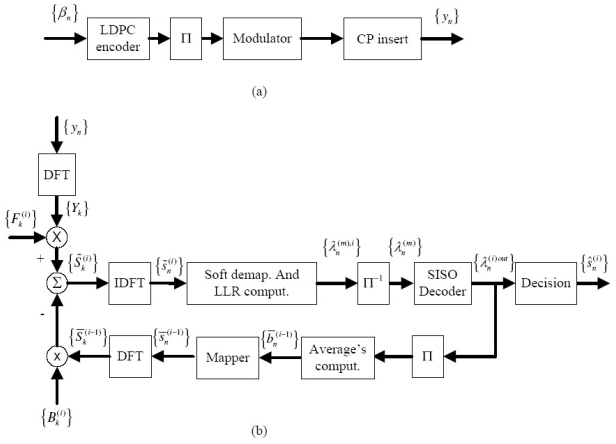

Fig. 3: (A) - Transmitter; (B) - IB-DFE receiver with soft decisions.

For a given iteration the output samples are given by

$$\tilde{S}_k = F_k Y_k - B_k \overline{S}_k, \tag{5}$$

where $\{F_k; k = 0, 1, \ldots, N-1\}$ and $\{B_k; k = 0, 1, \ldots, N-1\}$ denote the feedforward and the feedback coefficients, respectively, and $\{\overline{S}_k; k = 0, 1, \ldots, N-1\}$ is the DFT of the block $\{\overline{s}_n; n = 0, 1, \ldots, N-1\}$, with $\overline{s}_n$ denoting the average value of s_n conditioned to the FDE output associated to the previous iteration. As stated before, we adopt a SISO block that performs the sum-product algorithm [11] to decode the LDPC code in each IB-DFE iteration. This process is repeated 10 times in SISO decoder for each iteration of IB-DFE. By taking advantage of (1) and the fact that the different BPSK components are uncorrelated we have

$$\overline{s}_n = \sum_{i=0}^{M-1} g_i \prod_{m=1}^{\mu} \overline{b}_n^{eq(m)}, \tag{6}$$

where the average values for the corresponding symbol's bits are given by

$$\overline{b}_n^{(m)} = \tanh\left(\frac{\lambda_n^{(m)out}}{2}\right). \tag{7}$$

$\lambda_n^{(m)out}$ denotes the log-likelihood ratio of the mth bit for the nth transmitted symbol at the SISO's output. $\lambda_n^{(m)}$ denotes the log-likelihood ratio of the mth bit for the nth transmitted symbol used by iterative SISO decoding process and is given

by

$$\lambda_n^{(m)} = \log\left(\frac{\Pr(\beta_n^{(m)}=1|\tilde{s}_n)}{\Pr(\beta_n^{(m)}=0|\tilde{s}_n)}\right) = \log\left(\frac{\sum_{s\in\Psi_1^{(m)}}\exp\left(-\frac{|\tilde{s}_n-s|^2}{2\sigma^2}\right)}{\sum_{s\in\Psi_0^{(m)}}\exp\left(-\frac{|\tilde{s}_n-s|^2}{2\sigma^2}\right)}\right). \quad (8)$$

The sets $\Psi_1^{(m)}$ and $\Psi_0^{(m)}$ are the subsets of $\mathfrak{S}$ where $\beta_n^{(m)}=1$ or 0, respectively (clearly, $\Psi_1^{(m)}\bigcup\Psi_0^{(m)}=\mathfrak{S}$ and $\Psi_1^{(m)}\bigcap\Psi_0^{(m)}=\emptyset$) and $\{\tilde{s}_n; n=0,1,...,N-1\}$ denotes the IDFT of $\{\tilde{S}_k; k=0,1,...,N-1\}$, i.e., the $\tilde{s}_n$ are the time-domain samples at the FDE output. In (8) σ^2 denotes the variance of the noise at the FDE output, i.e.,

$$\sigma^2 = \frac{1}{2}E[|s_n-\tilde{s}_n|^2] \approx \frac{1}{2N}\sum_{n=0}^{N-1}E[|\hat{s}_n-\tilde{s}_n|^2], \quad (9)$$

where $\hat{s}_n$ denotes the hard decisions associated to s_n.

From [12], results the optimum coefficients F_k and B_k given by

$$F_k = \frac{\kappa H_k^*}{E[|N_k|^2]/E[|S_k|^2]+(1-\rho^2)|H_k|^2}, \quad (10)$$

and

$$B_k = F_k H_k - 1, \quad (11)$$

respectively, where κ ensures that

$$\sum_{k=0}^{N-1}F_k H_k/N = 1. \quad (12)$$

The correlation coefficient ρ gives a measure of the reliability of the decisions employed in the feedback loop and can be characterized as

$$\rho = \frac{E[\hat{s}_n s_n^*]}{E[|s_n|^2]} = \frac{\sum_{i=0}^{M-1}|g_i|^2\prod_{m=1}^{\mu}\left(\rho_n^{(m)}\right)^{\gamma_{m,i}}}{\sum_{i=0}^{M-1}|g_i|^2}, \quad (13)$$

where $\rho_n^{(m)}=|\bar{b}_n^{(m)}|$ is the reliability of the mth bit of the nth transmitted symbol.

IV. LDPC Codes

LDPC codes are recognized as good error-correcting codes with performance near Shannon limit. In fact, LDPC codes are linear block codes using a sparse parity-check matrix with a very small number of 1's per column and row. These codes are classified into two groups, regular and irregular LDPC codes. Regular LDPC codes have a uniform column and row weight, while irregular LDPC codes have a nonuniform column and row weight. A regular (N, K) LDPC code has a code rate $R=K/N$. An LDPC code is defined by an $M\times N$ parity-check matrix H, where $K=N-M$ and that matrix is linearly independent. LDPC codes can be represented by a Tanner graph with two types of nodes: the bit nodes and the check nodes. Each bit node corresponds to a column of the parity check matrix. Let us consider the example shown in fig.4 with an parity check matrix and the corresponding Tanner graph for a block code (7,3). As it can seen in fig. 4b that check nodes correspond to the rows of the parity check matrix of fig. 4a. Edges between a bit node and a check node exits when the bit is present in the parity check equation associated to the check node. For instance, the check node f_1 corresponds to the 1^{st} line of H and the same applies for the remainder check nodes.

$$H=\begin{bmatrix}1&1&0&1&0&0\\0&1&1&0&1&0\\1&0&0&0&1&1\\0&0&1&1&0&1\end{bmatrix}$$

(a) Parity Matrix H

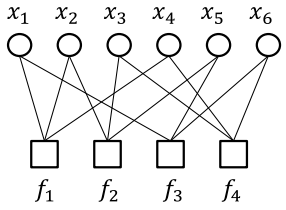

(b) Tanner Graph

Fig. 4: Parity matrix H and corresponding Tanner Graph

A. Sum-product algorithm

In this paper we adopt the sum-product algorithm [11] to decode the LDPC code. Here we provide a brief revision of the sum-product algorithm. Let $f_{j,\ell}$ denote a check node connected to the bit node x_ℓ ($f_{j,\ell}$ represents the jth parity check equation where the bit β_ℓ is present, i.e. the positions corresponding to the ones in the parity check matrix). In sum-product algorithm, and message passing in general, bit nodes and check nodes exchange messages iteratively. A check node f_j gets messages $q_{j,\ell}(\beta_\ell), \beta_\ell=0,1$ from its neighbors ($q_{j,\ell}(\beta_\ell)$ denotes the probability information that the bit node x_ℓ sends to the check node f_j, indicating $P(\beta_\ell=i), i=0,1$), processes the messages, and sends the resulting messages $r_{j,\ell}(\beta_\ell)$ back to its neighbors. $r_{j,\ell}(\beta_\ell)$ denotes the probability information that the check node f_j gathers about the ℓ^{th} bit being i and sent to bit node x_ℓ. So, $r_{j,\ell}(\beta_\ell)$ represents the likelihood information for $\beta_\ell=i$ that results from the parity-check equation f_j, when the probabilities for other bits are represented by $q_{j,\ell}(\beta_\ell)$. Similarly, a bit node x_ℓ receives a set of messages $r_{j,\ell}(\beta_\ell)$ from its neighbors, processes the messages, and sends messages back to its neighbors. Each output message of a variable or a check node is a function of all incoming messages to the node except the incoming message on the edge where the output message will be sent out. This two-step procedure is repeated many times. After such iterations, the variable node decodes its associated bit based on all information obtained from its depth-subgraph of neighbors. Let us assume that we have binary codes. Using the analytical characterization referred above on II, for a multilevel constellation at the input of SISO decoder in the IB-DFE we have (8). For the OFDM system $\lambda_k^{(m)}$ denotes the log-likelihood ratio of the mth bit for the kth transmitted symbol, which is

$$\lambda_k^{di,(m)} = \log\left(\frac{\Pr(\beta_k^{(m)}=1|Y_k)}{\Pr(\beta_k^{(m)}=0|Y_k)}\right) = \log\left(\frac{\sum_{s\in\Psi_1^{(m)}}\exp\left(-\frac{|Y_k-\tilde{s}_k|^2}{2\sigma^2}\right)}{\sum_{s\in\Psi_0^{(m)}}\exp\left(-\frac{|Y_k-\tilde{s}_k|^2}{2\sigma^2}\right)}\right), \quad (14)$$

where $\Psi_1^{(m)}$ and $\Psi_0^{(m)}$ are the subsets of $\mathfrak{S}$ where $\beta_k^{(m)} = 1$ or 0, respectively and $\{\tilde{S}_k; k = 0, 1, ..., N-1\}$, are the frequency-domain samples at the equalizer output.

V. Performance Results

Here we present a set of performance results for time-varying channels. Simulations include coded and uncoded transmission for both OFDM and SC-DFE systems with multilevel modulations.

The effect of the code word length on the performance is also investigated. For this purpose two possible configurations are considered $(N, K) = (528, 264)$ and $(N, K) = (1056, 528)$ LDPC encoders with rate $1/2$ and column weight of 3. At the output of encoder every codeword block are randomly interleaved before being mapped into the constellation points and distributed by the symbols of the transmitted frame (the constellations can be QPSK, 16-QAM or 64-QAM). OFDM and SC-FDE are characterized by blocks of $N_B = N/log2(M)$ useful symbols plus a cyclic prefix of 32 symbols longer than overall delay spread of the channel. The channel is modeled as a frequency selective fading Rayleigh channel characterized by an uniform PDP (Power Delay Profile), with 32 equal-power taps, with uncorrelated rayleigh fading on each tap. For sake of simplicity, it is assumed linear power amplification at the transmitter, perfect synchronization and channel estimation at the receiver. Results regrading performance are expressed as function of $\frac{E_b}{N_0}$, where N_0 is the one-sided power spectral density of the noise and E_b is the energy of the transmitted bits. In SC-FDE systems a total of three iterations are performed in the IB-FDE. The number of iterations at LDPC decoder can vary between 10 or 40, but remains fixed for each configuration of the transmission systems considered here.

From figs. 5 and 6 it is clear the higher impact of LDPC codes in system performance for both systems. It is assumed 10 iterations in the LDPC decoder for both transmission schemes. In SC-FDE a total of three iterations are performed in the IB-FDE, with 10 iterations in the LDPC decoder. The OFDM results from fig. 5 show significant improvements on performance due to LDPC codes, with coding gains near to 7 dBs for QPSK and higher than 7 dBs for the other constellations sizes. Also, the increments on the size of the codified block have stronger impact o system performance with power gains around 2dB for 64-QAM (for 16-QAM we have practically the same power gain and even for QPSK the power gain is higher than 1.5 dB). Let us consider now the performance results from fig. 6 regarding the SC-FDE system. As we can see iterations in IB-DFE have strong impact in performance improvements for uncoded schemes, with power gains near to 3.5 dB for QPSK and 4 dB for 16-QAM and 64-QAM. On the other hand, slight improvements are observed between successive iterations of IB-DFE when are used LDPC codes. For example, power gains due to iterations are practicably inexistent for coded QPSK and only for 64-QAM we have an impact higher than 1 dB (the reason for that lies in the sensitivity of 64-QAM to the residual ISI, which can be compensated along the iterative equalization process). Besides this effect, the coded schemes show also good power gains when compared with uncoded schemes. For instance, it can be seen that for the third iteration the power gains due to LDPC codes are 2.5 dB, 4 dB and more than 6 dB for QPSK, 16-QAM and 64-QAM, respectively. Also, from the comparison of figs. 5 and 6 it can be seen that IB-DFE outperforms OFDM, which was expectable due to the interaction between IB-DFE and SISO decoder. Another interesting fact, common to both systems, is the low performance improvement achieved by the increase of the size of the coded word (for both transmission schemes power gains attainable by the $(N, K) = (1056, 528)$ LDPC code are near to 0.5 dB for all constellation sizes).

Let us now analyze the influence of the iterations on LDPC decoder in the performance behavior of the proposed IB-DFE receiver. Figs. 7 and 8 show the behavior of performance with the number of iterations applied in the LDPC decoder (Additive White Gaussian Noise (AWGN) channel it is also considered). As expected, the increment of the number of iterations does not introduces significant improvements on OFDM's BER. Since we assumed perfect channel estimation, the better quality of the symbol estimates at the decoder's output do not contribute for any improvement on the channel estimates. Per contrary, on SC-FDE schemes adopting 40 iterations in SISO decoder reduces significantly the performance improvements achieved by successive iterations of IB-DFE equalizer. Moreover, the performance results for the first iteration are similar to those of third iteration when we have 10 iterations in the LDPC decoder. For example, with 40 iterations the power gain achieved by the third iteration is around 0.5 dB for both constellations (for instance with 10 iterations on LDPC decoder the power gain allowed by the third iteration is 2 dB for 16-QAM).

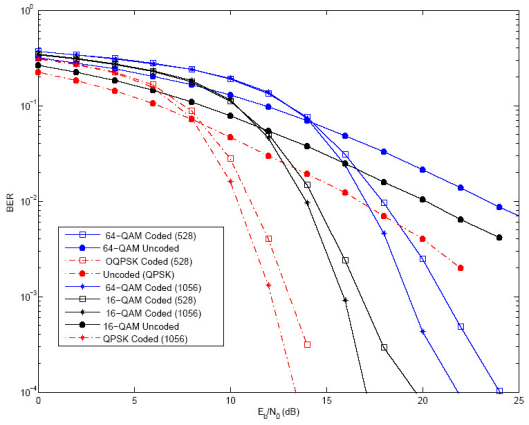

Fig. 5: BER performance of OFDM with QPSK, 16 and 64-QAM constellations for time dispersive channel.

VI. Conclusions

In this paper we presented an comparative analysis of the impact of LDPC codes in OFDM and SC-FDE with iterative receivers. LDPC codes were considered not only to improve the power efficiency as well as to improve the convergence of the IB-DFE. From simulation results, it becomes obvious that the use of LDPC codes increases significantly the power efficiency of both systems. However, the higher impact is in IB-DFE where due to LDPC codes the complexity of iterative equalization process can be reduced. This effect is more significant for an higher number of iterations in SISO block.

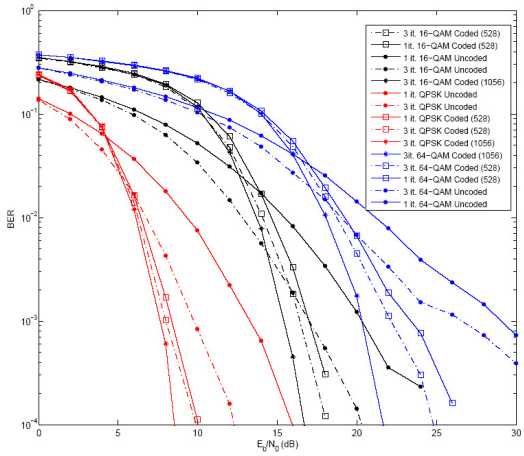

Fig. 6: BER performance of SC-FDE with QPSK, 16 and 64-QAM constellations for time dispersive channel (IB-DFE with 1 and 3 iterations.)

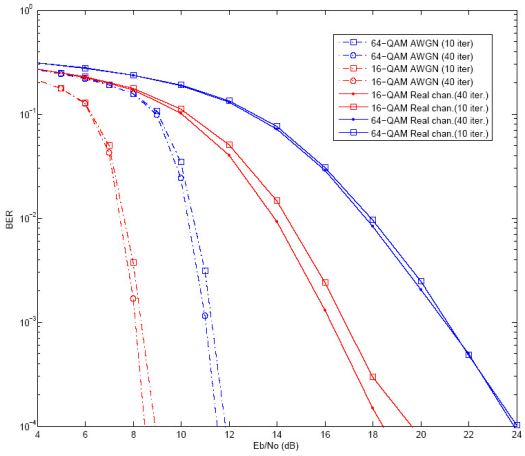

Fig. 7: Impact of number of iterations on LDPC decoding process on OFDM's BER performance for time dispersive and AWGN channels.

The resort to LDPC codes allows a less complex equalization in single carrier systems (i.e. lower number of iterations in IB-DFE) and significant power improvements in both systems at cost of a slight increase on system complexity.

ACKNOWLEDGMENTS

This work was supported in part by FCT (pluriannual funding from Uninova and IT and project GLANC (EXPL/EEI-TEL/1582/2013).

REFERENCES

[1] H. Sari, G. Karam and I. Jeanclaude, "An Analysis of Orthogonal Frequency-division Multiplexing for Mobile Radio Applications", *In Proc. IEEE Vehic. Tech. Conf., VTC'94*, pp. 1635–1639, Stockholm, June 1994.

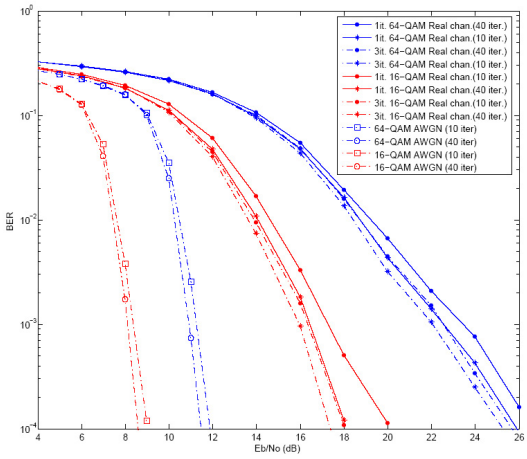

Fig. 8: Impact of number of iterations on LDPC decoding process on SC-FDE's BER performance for time dispersive and AWGN channels (3 iterations in IB-DFE).

[2] R. Dinis, M. Luzio and P. Montezuma, "On the Design of Frequency-Domain Equalizers for OQPSK Modulations", *33rd IEEE Sarnoff Symposium*, April 2010.

[3] M. Luzio, R. Dinis and P. Montezuma "On the Design of Linear Receivers for SC-FDE Schemes Employing OQPSK Modulation", *72nd IEEE VTC'10 - Fall*, Ottawa, September 2010.

[4] N. Benvenuto and S. Tomasin, "Block Iterative DFE for Single Carrier Modulation", *IEE Elec. Let.*, Vol. 39, No. 19, pp. 1144–1145, Sep. 2002.

[5] R. Dinis, A. Gusmão and N. Esteves, "On Broadband Block Transmission over Strongly Frequency-Selective Fading Channels", *Proc. Wireless 2003*, Calgary, Canada, July 2003.

[6] R. Dinis, R. Kalbasi, D. Falconer and A. Banihashemi, "Iterative Layered Space-Time Receivers for Single-Carrier Transmission over Severe Time-Dispersive Channels", *IEEE Comm. Letters*, Vol. 8, No. 9, pp. 579–581, Sep. 2004.

[7] J. Proakis, *Digital Communications*. McGraw-Hill, 1995.

[8] C. Berrou and A. Glavieux, "Near optimum Error Correcting Coding and Decoding: Turbo-Codes", *IEEE Trans. on Comm.*, Vol. 44, No. 10, pp. 1261–1271, Oct. 1996.

[9] Robert G. Gallager, *Low Density Parity Check Codes*. Monograph, M.I.T. Press, 1963.

[10] David J. C. MacKay, "Good Error-Correcting Codes Based on Very Sparse Matrices", *In IEEE Trans. on Information Theory*, Vol. 45, No. 2, pp.399-431, February 1999.

[11] Frank R. Kschischang, Brendan J. Frey and Hans-Andrea Loeliger, "Factor Graphs and the Sum-Product Algorithm", *In IEEE Trans. on Information Theory*, Vol. 47, No. 2, February 2001.

[12] A. Gusmão, P. Torres, R. Dinis and N. Esteves, "A Turbo FDE Technique for Reduced-CP SC-Based Block Transmission Systems, *IEEE Trans. on Comm.*, Vol. 55, No. 1, pp. 16-20, Jan. 2007.

Robust Frequency-Domain Receivers for A Transmission Technique with Directivity at the Constellation Level

Paulo Montezuma[1,3], Daniel Marques[1], Vitor Astucia[1], Rui Dinis[1,2], and Marko Beko [1,3]

[1] DEE, FCT Universidade Nova de Lisboa, Portugal
[2] IT, Instituto de Telecomunicações, Av. Rovisco Pais, Lisboa, Portugal.
[3] Uninova, Instituto de Desenvolvimento de Novas Tecnologias, Quinta da Torre, Caparica, Portugal.

Abstract - It was shown recently that we can decompose multilevel constellations as the sum of constant-envelope components which can be amplified and transmitted by separate antennas, allowing power-efficient transmitters, together with directivity at the constellation level without changing on the radiation pattern associated to the set of antennas. However, errors in the direction estimates can lead to substantial performance performance degradation since the constellations seen at the receiver can be substantially distorted.

In this paper we present an improved receiver that is designed taking into account constellation distortion effects inherent to errors in direction estimates. It is shown that these "smart" receivers, optimized taking into account the apparent constellation at the receiver side can substantially outperform conventional receivers that assume that assume undistorted constellations.

Index Terms: Multilevel modulations, directivity, SC-FDE, constellation configuration.

I. Introduction

Spectral and power efficiency and low interference level are critical aspects in wireless communication systems. Spectral efficiency can be assured by multilevel modulations, despite the fact that this increased spectral efficiency usually comes at the expense of a reduced power efficiency. However due to envelope fluctuations of multilevel constellations amplifiers must be over dimensioned to avoid nonlinear effects [1]. Therefore, a decomposition of multilevel modulations into a sum of quasi constant or constant envelope components will allow the use of nonlinear amplifiers in such operation, which can maximize the power efficiency of the transmission system [2], [3].

On the other hand, low interference can be assured through a directive beam of radiation, with nulls in the directions of interfering signals. A common solution to achieve this is to configure elementary radiators into an array [4] to suppress the side lobe level whereas preserving the gain of the main beam. A quite different approach was proposed in [5] with the directivity introduced in the transmitted information, being the constellation optimized for the desired direction. Now, the directivity is implicitly on the constellation's symbols arrangement associated to each transmission direction. Moreover, efficiency on power amplification it is also assured since the constellations are decomposed into several BPSK (Bi-Phase Shift Keying) or OQPSK components (Quadri Phase Shift Keying) that can be separately amplified by non linear amplifiers and transmitted independently by each antenna. Obviously, there is no change in radiation pattern since the transmitted signals by the antennas are uncorrelated. It should be noted that despite the M transmitted signals in parallel, the system transmission rate remains unchanged since each transmitted signal is a component of the original constellation (remark that the coefficients associated to each array element are the coefficients associated to the elementary BPSK or QPSK sub-constellations).

Therefore, the receiver must know the constellation coefficients, associated to the amplification stage as well as the array configuration, otherwise receives a degenerated constellation. Logically, the performance of a receiver without knowledge on the transmission direction will be strongly affected. The impact of angle errors on performance can be minimized adopting a receiver that knows the transmission direction, denoted as "smart receiver". The present study specifically focuses on these two types of receivers and additionally provides a full comparison of performance of both.

It is well known that large constellations in general and non-uniform constellations in particular are very sensitive to interference, namely the residual ISI (Inter-Symbol Interference) at the output of a practical equalizer that does not invert completely the channel effects (e.g., a linear equalizer optimized under the MMSE (Minimum Squared Mean Error)). To cope with channel effects we consider the use of SC-FDE (Single-Carrier with Frequency-Domain Equalization) schemes, because its frequency-domain receiver implementation makes them appropriate to severely time-dispersive channels [6]. To cope with the overall residual interference between the in-phase and quadrature components (IQI- In-phase/Quadrature Interference) at the sampling instants as well as overall residual interference ISI plus IQI, FDE receivers specifically designed for offset modulations were proposed in [7], [8]. Despite this optimization, lower levels of residual ISI and IQI can be achieved by IB-DFE (Iterative Block Decision Feedback Equalization) approach for SC transmission

[9], [10], [11]. Obviously, the IB-DFE receivers considered her must be optimized for offset constellations to minimize the residual ISI and IQI interferences associated to multilevel Offset modulations.

In this paper we investigate the performance of both receivers ("smart" and "normal") under angle errors against the direction in which the constellations are optimized. We also provide a comparison among the two receivers. This paper is organized as follows: We begin in II by reviewing some relevant aspects regarding the decomposition of a multi-level constellation in BPSK components. This decomposition is employed in sec. III into the definition of transmitter structure and its implications on receivers' side. IV, presents IB-DFE receivers suitable for general constellations. The simulation parameters and performance evaluation of the proposed receivers are described in sec. V. Results are discussed in Sec. V. VI resumes this paper.

II. Multi-level constellation decomposition

Let us consider now two OQPSK signals (Offset Quadri Phase Shift Keying), $x_p(t)$ and $x_{p'}(t)$, with complex envelope given by

$$x_p(t) = \sum_{n'} b_{n'}^{(p)} x^{(p)}(t - n'T), \tag{1}$$

and

$$x_{p'}(t) = \sum_{n'} b_{n'}^{(p')} x^{(p')}(t - n'T). \tag{2}$$

We assume the same pulse shape for both signals, i.e. $x^{(p)}(t) = k_p r(t)$ and $x^{(p')}(t) = k_{p'} r(t)$, where $r(t)$ represents a pulse shape that guarantees null ISI) at the matched filter's output and g_p and $g_{p'}$ are complex coefficients (it is assumed that $g_p \neq g_{p'}$). From (1) and (2) results

$$x(t) = \sum_{n'} b_{n'}^{(p)} g_p r(t - n'T) + \sum_{n'} b_{n'}^{(p')} g_{p'} r(t - n'T) \tag{3}$$

with each OQPSK signal associated to a QAM constellation (Quadrature Amplitude Modulation) . Thus, for each sampling instant we may write

$$g_p b_{n'}^{(p)} + g_{p'} b_{n'}^{(p')} = a_{n'}^{'}, \tag{4}$$

where $a_n^{'}$ can assume the values $\pm|g_p| \pm |g_{p'}|$, $\pm j|g_p| \pm |g_{p'}|$, $\pm|g_p| \pm j|g_{p'}|$ and $\pm j|g_p| \pm j|g_{p'}|$, which correspond to the four sub-sets of 4 symbols from a 16-OQAM constellation. Similarly, a 64-OQAM constellation can be viewed as a sum of 3 OQPSK signals $x_p(t)$, $x_{p'}(t)$ and $x_{p''}(t)$ with $g_p \neq g_{p'} \neq g_{p''}$.

It turns out that the constellation symbols can be expressed as function of the corresponding bits as follows[1]:

$$\begin{aligned} a_n &= g_0 + g_1 b_n^{(1)} + g_2 b_n^{(2)} + g_3 b_n^{(1)} b_n^{(2)} + g_4 b_n^{(3)} + ... \\ &= \sum_{i=0}^{M-1} g_i \prod_{m=1}^{\mu} \left(b_n^{(m)} \right)^{\gamma_{m,i}} = \sum_{i=0}^{M-1} g_i b_n^{eq(m)}, \end{aligned} \tag{5}$$

[1]It should be noted that a_n denotes the nth constellation point and not the nth transmitted symbol; the same applies to $b_n^{(m)}$ (or $\beta_n^{(m)}$) that here denotes the mth bit of the n constellation point.

with $b_n^{eq(m)} = \prod_{m=1}^{\mu} \left(b_n^{(m)} \right)^{\gamma_{m,i}}$. For each $a_n \in \mathfrak{a}$, where $(\gamma_{\mu,i}\ \gamma_{\mu-1,i}\ ...\ \gamma_{2,i}\ \gamma_{1,i})$ is the binary representation of i and $b_n^{(m)} = 2\beta_n^{(m)} - 1$. Since we have M constellation symbols in $\mathfrak{S}$ and M complex coefficients g_i, (5) is a system of M equations that can be used to obtain the coefficients g_i, $i = 0, 1, ..., \mu - 1$. Putting (5) in matrix format a general constellation can be written as the sum of $M/2$ OQPSK or M BPSK based on

$$\mathbf{a} = \mathbf{W}\mathbf{g}, \tag{6}$$

where $\mathbf{a} = [a_1\ a_2\ ...\ a_M]^T$, $\mathbf{g} = [g_0\ g_1\ ...\ g_{\mu-1}]^T$ and $\mathbf{W}$ is a Hadamard matrix with dimensions $M \times M$.

III. Transmitter Structure

Based on (5) it is possible to write $x(t)$ as

$$x(t) = \sum_{n=0}^{N-1} \sum_{m=0}^{M-1} g_i b_n^{eq(m)} r(t - nT). \tag{7}$$

Constant envelope signals can be assured by assuming a MSK pulse shape for all OQSPK components. As referred before, any M-OQAM constellation can be decomposed as the sum of several OQPSK or BPSK components (see (5)) with quasi-constant or constant envelope, that can be separately amplified with an non-linear amplifier. Therefore, it is possible to employ non linear amplifiers in each component, Under these conditions, results a transmitter with a structure similar to the transmitter proposed in [5] composed by M grossly NL amplifiers and M isotropic antennas that transmit M uncorrelated signals as shown if fig. 1. It is also assumed equally spaced antennas by $d/\lambda = 1/4$. Hence, the coefficients that affect each antenna depend on the coefficients associated to the sub-constellations and on the progressive phase that affect the antennas given by $\alpha_A = 2\pi n \cos\left(\frac{\pi}{2} + \Theta\right) \frac{d}{\lambda}$. Taking into consideration (5) and α_A we may write

$$a_n^A = \sum_{m=0}^{M-1} g_i^A b_n^{eq(m)}, \tag{8}$$

where $g_i^A = g_n e^{\alpha_A}$ are the coefficients affected by the phase rotations associated to each antenna. Therefore, each transmitted sub-constellation suffers a different rotation that depends on the antenna position in the array and sort order adopted along the M branches. For instance, the sub-constellation arrangements along the array for 16 QAM and Voronoi constellations may have the coefficients distributions presented in table I.

Clearly, it can be expected great impact on system performance when there are errors in relation to the direction in which the constellation is optimized. Moreover, constellations with higher dimensions will be more sensitive to the effect of angle errors to the radiation direction θ due to the highest number of BPSK components. In figs. 2, 3 and 4 are shown the effects of an angle error of 4^o relative to the transmission direction θ in which the constellation is optimized. It can be seen that in both cases the resulting constellations are degenerated (this effect is stronger for higher constellations sizes). For the same size, it is also clear the higher sensitivity of Voronoi constellations to errors on the transmitted direction θ.

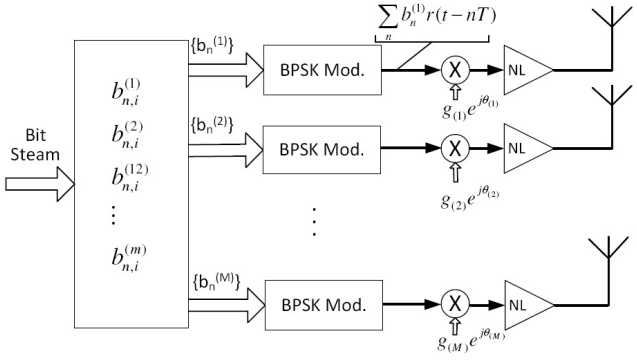

Fig. 1. Structure of Power optimized directive transmitter for generalized constellations

TABLE I. GAIN VALUES FOR TWO DIFFERENT SORT ORDERS

Sort=LINEAR			Sort=CENTER		
Gain	QAM	VORONOI	Gain	QAM	VORONOI
g^A0	2j	0,717+j 0,546	g0	0	-0,100+j 0,075
g^A1	2	-0,588+j 0,572	g1	0	-0,014-j 0,124
g^A2	j	0,359+j 0,273	g2	0	-0,014-j 0,124
g^A3	1	-0,186+j 0,273	g3	0	0,086-j 0,199
g^A4	0	-0,201+j 0,149	g4	0	0,086-j 0,199
g^A5	0	0,029+j 0,248	g5	0	-0,201+j 0,149
g^A6	0	0,086-j 0,199	g6	j	0,359+j 0,273
g^A7	0	0,086-j 0,199	g7	2j	0,717+j 0,546
g^A8	0	0,086-j 0,199	g8	2	-0,588+j 0,572
g^A9	0	0,086-j 0,199	g9	1	-0,186+j 0,273
g^A10	0	-0,014-j 0,124	g10	0	0,029+j 0,248
g^A11	0	-0,100+j 0,075	g11	0	0,086-j 0,199
g^A12	0	-0,014-j 0,124	g12	0	0,086-j 0,199
g^A13	0	-0,100+j 0,075	g13	0	-0,100+j 0,075
g^A14	0	-0,100+j 0,075	g14	0	-0,100+j 0,075
g^A15	0	0,000	g15	0	0,000

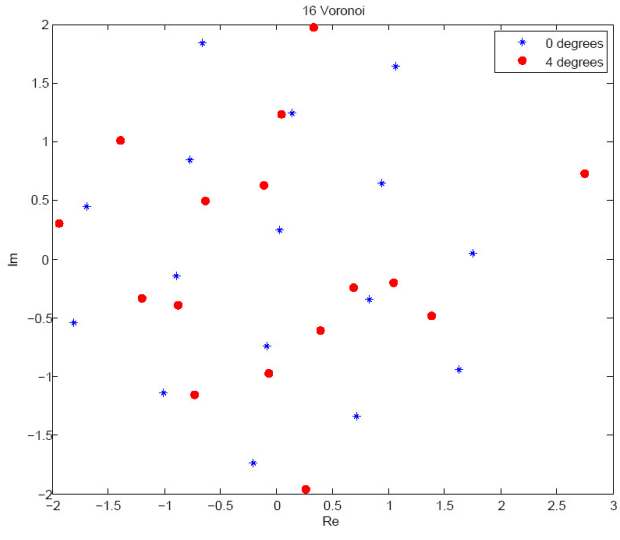

Fig. 2. Impact of an angle error regarding to the transmission direction θ in a 16-Voronoi constellation using a centered array configuration at the transmitter

IV. RECEIVER DESIGN

At the receiver, besides the IB-DFE two different approaches can be adopted. The first one assumes that the receiver do not knows nothing about the direction in which the information is optimized. In the second one, denoted as "smart receiver", the receiver knows the direction in which the constellation is optimized. So, the receiver is aware about the configuration of the transmitter array and consequently knows the phase rotations that affect each sub-constellation at the transmitter and tries to compensate them. As referred previously, at the receiver it is adopted an IB-DFE due to it's capacity to cope with multilevel constellations' sensitivity to interference. We assume an ideal linear transmitter (this can be achieved with the transmitter structure of fig. 1, with constant envelope signals in each amplification branch). The

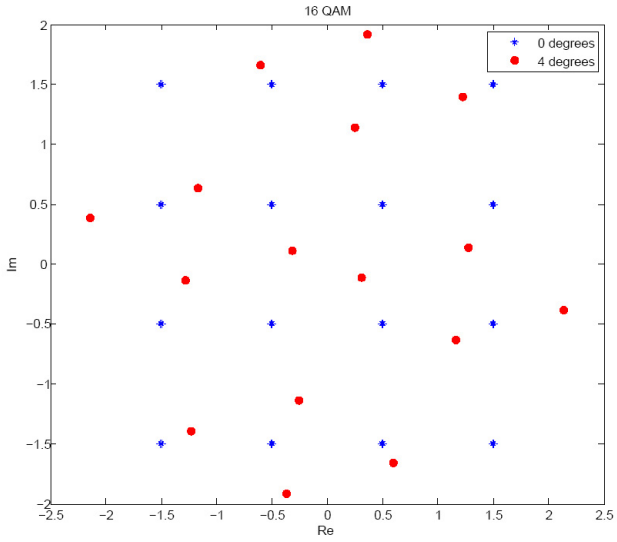

Fig. 3. Impact of an angle error regarding to the transmission direction θ in a 16-QAM constellation using a centered array configuration at the transmitter

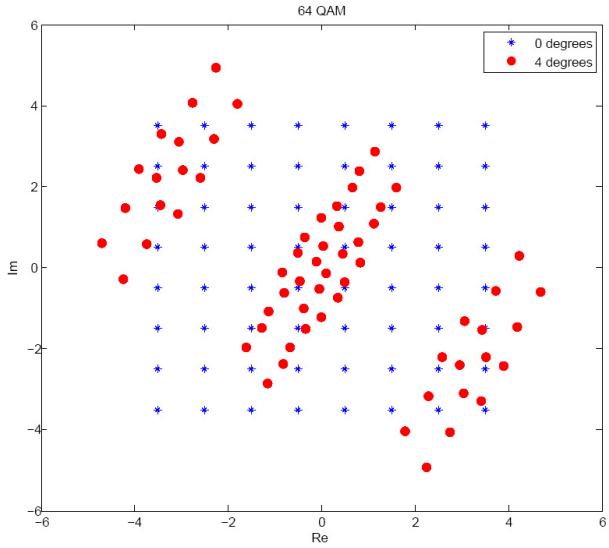

Fig. 4. Impact of an angle error regarding to the transmission direction θ in a 64-QAM constellation using a centered array configuration at the transmitter

signal associated to a given block is

$$s(t) = \sum_{n=-N_G}^{N-1} s_n h_T(t - nT_S), \tag{9}$$

with T_S denoting the symbol duration, N_G denoting the number of samples at the cyclic prefix, N denoting the number of samples at the useful part of the block and $h_T(t)$ denoting the adopted pulse shape. The nth transmitted symbol s_n belongs to a given size-M constellation $\mathfrak{S}$. It should be mentioned that the cyclic prefix corresponds to a periodic extension of the useful part of the block, i.e., $s_{-n} = s_{N-n}$, that are discarded at the receiver (this means that there is no interference between blocks when the length of the cyclic prefix is higher than the length of the overall channel impulse response). Therefore, results the frequency-domain block $\{Y_k; k = 0, 1, \ldots, N-1\}$ = DFT $\{y_n; n = 0, 1, \ldots, N-1\}$), where

$$Y_k = S_k H_k + N_k, \tag{10}$$

with H_k denoting the channel frequency response for the kth subcarrier and N_k the corresponding channel noise, which means that the impact of a time-dispersive channel reduces to a scaling factor for each frequency. The IB-DFE receiver structure is depicted in fig. 5.

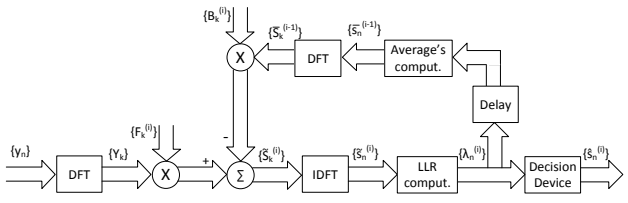

Fig. 5. *IB-DFE receiver with soft decisions*

For a given iteration the output samples are given by

$$\tilde{S}_k = F_k Y_k - B_k \overline{S}_k, \tag{11}$$

where $\{F_k; k = 0, 1, \ldots, N-1\}$ and $\{B_k; k = 0, 1, \ldots, N-1\}$ denote the feedforward and the feedback coefficients, respectively, and $\{\overline{S}_k; k = 0, 1, \ldots, N-1\}$ is the DFT of the block $\{\overline{s}_n; n = 0, 1, \ldots, N-1\}$, with $\overline{s}_n$ denoting the average value of s_n conditioned to the FDE output associated to the previous iteration. It can be shown that the optimum coefficients F_k and B_k are given by (see [12], [13])

$$F_k = \frac{\kappa H_k^*}{E[|N_k|^2]/E[|S_k|^2] + (1-\rho^2)|H_k|^2}, \tag{12}$$

and

$$B_k = F_k H_k - 1, \tag{13}$$

respectively, where κ is selected to ensure that $\sum_{k=0}^{N-1} F_k H_k / N = 1$.

The correlation coefficient ρ [13], is given by

$$\rho = \frac{E[\hat{s}_n s_n^*]}{E[|s_n|^2]} = \frac{\sum_{i=0}^{M-1} |g_i|^2 \prod_{m=1}^{\mu} \left(\rho_n^{(m)}\right)^{\gamma_{m,i}}}{\sum_{i=0}^{M-1} |g_i|^2}, \tag{14}$$

where $\rho_n^{(m)} = \left|\tanh\left(\frac{\lambda_n^{(m)}}{2}\right)\right|$ represents the reliability of the mth bit of the nth transmitted symbol, with the log-likelihood ratio of the mth bit for the nth transmitted symbol given by

$$\lambda_n^{(m)} = \log\left(\frac{\sum_{s\in\Psi_1^{(m)}} \exp\left(-\frac{|\tilde{s}_n - s|^2}{2\sigma^2}\right)}{\sum_{s\in\Psi_0^{(m)}} \exp\left(-\frac{|\tilde{s}_n - s|^2}{2\sigma^2}\right)}\right), \tag{15}$$

where $\Psi_1^{(m)}$ and $\Psi_0^{(m)}$ are the subsets of $\mathfrak{S}$ where $\beta_n^{(m)} = 1$ or 0, respectively (clearly, $\Psi_1^{(m)} \bigcup \Psi_0^{(m)} = \mathfrak{S}$ and $\Psi_1^{(m)} \bigcap \Psi_0^{(m)} = \emptyset$) and $\{\tilde{s}_n; n = 0, 1, ..., N-1\}$ denotes the IDFT of $\{\tilde{S}_k; k = 0, 1, ..., N-1\}$, i.e., the $\tilde{s}_n$ are the time-domain samples at the FDE output. In (15) σ^2 denotes the variance of the noise at the FDE output, i.e.,

$$\sigma^2 \approx \frac{1}{2N} \sum_{n=0}^{N-1} E[|\hat{s}_n - \tilde{s}_n|^2], \tag{16}$$

where $\hat{s}_n$ denotes the hard decisions associated to s_n.

Being the different BPSK components uncorrelated, from [13] we may write

$$\overline{s}_n = \sum_{i=0}^{M-1} g_i \prod_{m=1}^{\mu} \left(\tanh\left(\frac{\lambda_n^{(m)}}{2}\right)\right)^{\gamma_{m,i}}. \tag{17}$$

V. Simulation Results

We consider an SC-FDE modulation with blocks of N = 256 useful symbols and a cyclic prefix of 32 symbols longer than overall delay spread of the channel. The modulation symbols belong to a M-QAM or Voronoi constellation and are selected from the transmitted data according to a mapping rule that optimizes energy efficiency. We have a one dimensional non-uniform array with equal spaced antennas by $d/\lambda = 1/4$ and amplifiers gains following the sort order which appears in Table I. We consider both "normal" and "smart" receivers (remark that table I only applies to constellations of size 16).

Two channel types are considered. The first one is a AWGN channel and the second is a severely time-dispersive channel characterized by an uniform PDP (Power Delay Profile), with 32 equal-power taps, with uncorrelated rayleigh fading on each tap. For both channel types the IB-DFE structure is the same. We also make the practical assumption of linear power amplification at the transmitter, perfect synchronization and channel estimation at the receiver. Our performance results are expressed as function of $\frac{E_b}{N_0}$, where N_0 is the one-sided power spectral density of the noise and E_b is the energy of the transmitted bits.

Performance results for AWGN channel (Additive White Gaussian Noise) are shown in figures 6 and 7. As we can see the constellation directivity has a major impact on system performance when the receiver does not know the transmitting direction θ. From the results it can be seen the lower impact of angle errors on system performance of "smart receiver", since it uses the direction of transmission reconstruct the original constellation. It is also obvious the good tolerance against angle errors showed by the "smart" receiver when are employed M-QAM constellations. As example, for 16 and 64-QAM the performance remains almost constant for angle errors until 2^o. On the other hand, for Voronoi constellations the

knowledge of the direction of transmission it is not sufficient to avoid performance degradation, even for small values of angle errors (in fig. 7 the performance degradation can't be avoided even for very small angle errors). This behavior confirms our expectations, since the impact of these angle errors will be stronger for constellations with an higher number of sub-constellations (the explanation for that lies on the higher number of BPSK components and consequently more sub-constellations suffer phase rotations in the transmitter. This has implications on system sensitivity to the transmission direction and make them a good choice to increase the system's directivity). On the other hand, the performance of "normal receiver" is severely affected for all sizes and types of constellations, independent of the angle error values.

Next we focus on the performance results for a severely time-dispersive channel. In figures 8, 9 and 10 are shown the BER performance results for both constellations types as function of angle error. As expected, constellations with higher dimensions show more sensitivity to angle errors relative to the transmission direction θ. As previously mentioned, for the same size, Voronoi constellations have higher directivity. Simulation results from figs. 8 and 9 lead us to conclude that "smart receiver" together with the iterations of IB-DFE can cope with estimate errors of θ without significant performance degradation (for 3 iterations and 16-QAM there is no degradation on performance even for an angle error of 4^o, and for 64-QAM the performance degradation is lower than 0.5 dB). This is special valid for regular M-QAM constellations (for Voronoi even knowing θ any angle error has high impact on system performance). Hence, simulation results demonstrate the efficiency of "smart" receiver to cope with angle estimation errors as well as his higher tolerance against these errors. On the other hand, the significant degradation associated to the "normal receiver" confirms the higher sensitivity to a strictly directive communication with the information only optimized in the desired direction θ.

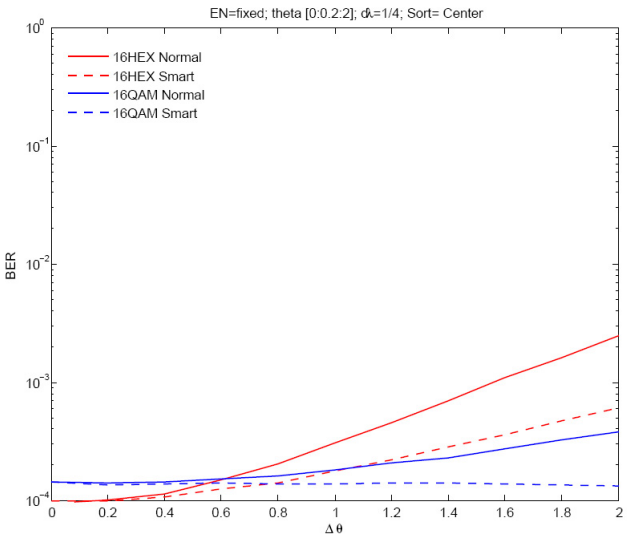

Fig. 6. Impact of an angle error regarding to the transmission direction θ in BER performance of size-16 constellations using a contered array. ($E_b/N_0 = 12dB$)

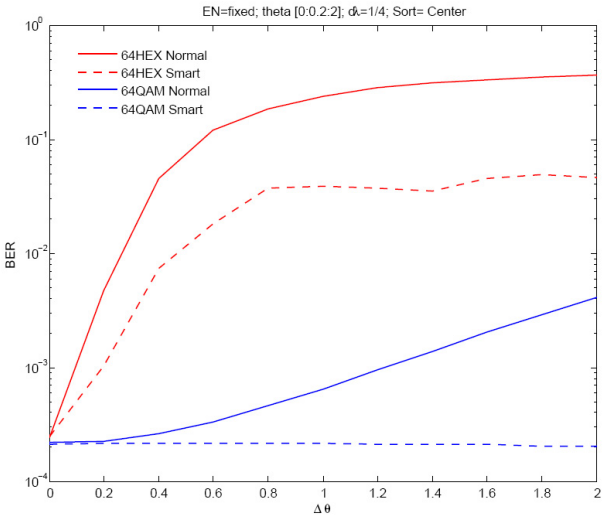

Fig. 7. Impact of an angle error regarding to the transmission direction θ in BER performance of size-64 constellations using a centered array. ($E_b/N_0 = 16dB$)

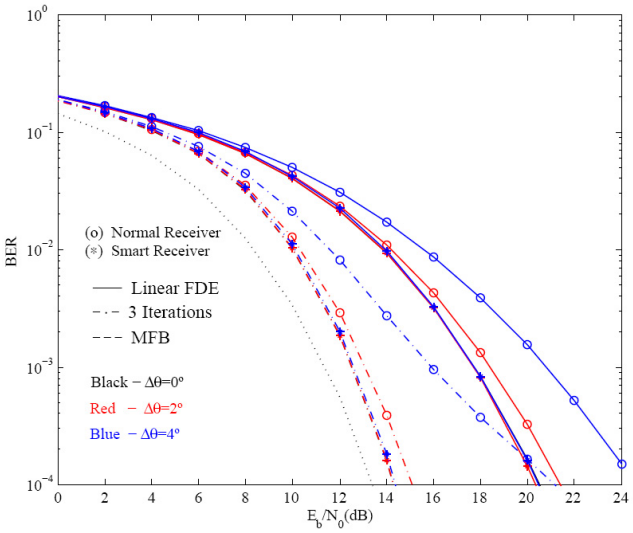

Fig. 8. Centered array: BER performance for size-16 constellations with a frequency selective channel and an angle error regarding to the transmission direction θ

VI. Conclusions

In this paper firstly we proposed a new scheme for a receiver suitable for information directive transmissions, denoted as "smart receiver". We also included an comparative analysis of two types of receivers in a transmission system in which directivity is introduced at the transmitted information. The comparison was extended to AWGN channels and severely dispersive channels and considered both rectangular M-QAM and Voronoi constellations. It is worth to mention that when are used Voronoi constellations any angle error has a major impact on system performance independently of receivers' type. The initial assumptions regarding the directivity sensivity of non regular constellations were confirmed by simulation results for both types of channels and receivers. However, for rectangular M-QAM constellations the "smart receiver" showed a very

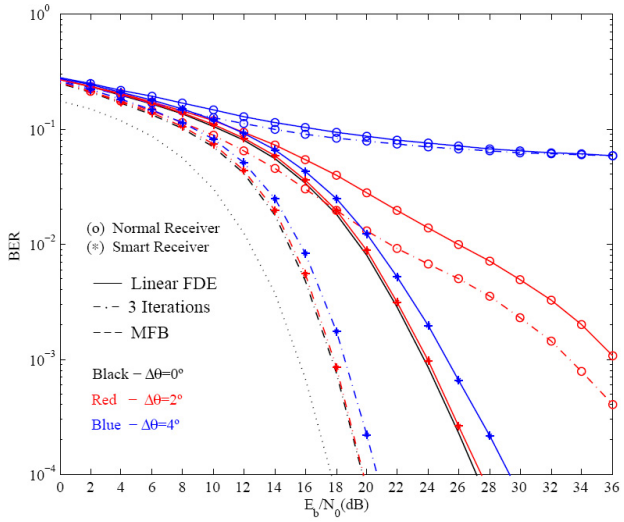

Fig. 9. Centered array: BER performance for 64-QAM constellations with a frequency selective channel and an angle error regarding to the transmission direction θ

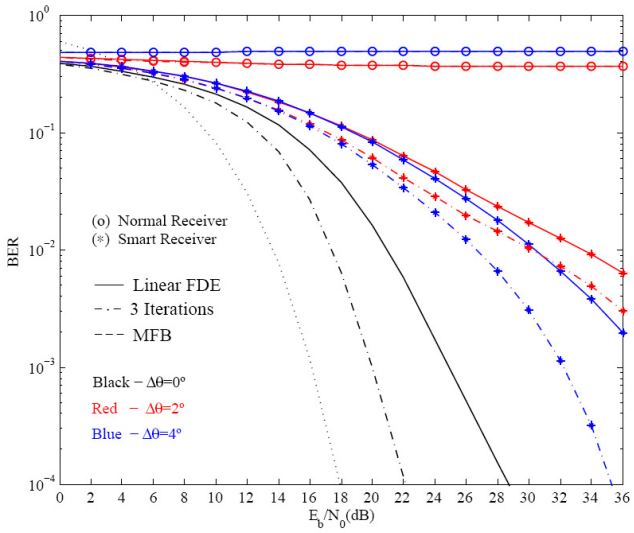

Fig. 10. Centered array: BER performance for 64-size Voronoi constellations with a frequency selective channel and an angle error regarding to the transmission direction θ

good tolerance against angle errors, with a practically constant performance over the angle errors between 0 and 2 degrees. Therefore, we may conclude that when it is intended better tolerance to angle errors this "smart receiver" must be used together with regular constellations. However, simulation results also show that if it is intended a higher tolerance against angle errors, for both types of constellations, other receiver designs must be considered (since the performances of both receivers are very sensitive when are used Voronoi constellations). As final remark we should say that we admit a previous knowledge of the direction θ for the "smart receiver". Further studies will cover the design of receivers with iterative process to estimate the direction θ.

ACKNOWLEDGMENTS

This work was supported in part by FCT (pluriannual funding) from Uninova (PEst-OE/EEI/UI0066/2011) and IT (PEst-OE/EEI/LA0008/2011) and projects MP-SAT (PTDC/EEA-TEL/099074/2008) and Opportunistic-CR, (PTDC/EEA/TEL/115981/2009)).

REFERENCES

[1] P. S. K. Leung and K. Feher, "F-QPSK - A Superior Modulation Technique for Mobile and Personal Communications", *IEEE Trans. Broadcast.*, Vol. 39, pp. 288-294, June 1993.

[2] P. Montezuma and A. Gusmão, "Design of TC-OQAM Schemes Using a Generalised Nonlinear OQPSK-type Format",*IEE Elect. Letters*, Vol. 35, No. 11, pp. 860-861, May 1999.

[3] P. Montezuma and A. Gusmão, "On Analytically Described Trellis-Coded Modulation Schemes", ISCTA'01, Ambleside, UK, ,July 2001.

[4] C. A. Balanis, *Antenna theory analysis and design*, Wiley, New York, 1997.

[5] P. Montezuma, V. Astucia and R. Dinis, "On the use of Multiple Amplifiers and Antennas for efficient Directive Transmission with large Constellations", *33rd IEEE Milcom'2013*, San Diego, November 2013.

[6] H. Sari, G. Karam and I. Jeanclaude, "An Analysis of Orthogonal Frequency-division Multiplexing for Mobile Radio Applications", *In Proc. IEEE Vehic. Tech. Conf., VTC'94*, pp. 1635–1639, Stockholm, June 1994.

[7] R. Dinis, M. Luzio and P. Montezuma, "On the Design of Frequency-Domain Equalizers for OQPSK Modulations", *33rd IEEE Sarnoff Symposium*, April 2010.

[8] M. Luzio, R. Dinis and P. Montezuma "On the Design of Linear Receivers for SC-FDE Schemes Employing OQPSK Modulation", *72nd IEEE VTC'10 - Fall*, Ottawa, September 2010.

[9] N. Benvenuto and S. Tomasin, "Block Iterative DFE for Single Carrier Modulation", *IEE Elec. Let.*, Vol. 39, No. 19, pp. 1144–1145, Sep. 2002.

[10] R. Dinis, A. Gusmão, and N. Esteves, "On Broadband Block Transmission over Strongly Frequency-Selective Fading Channels",*Proc. Wireless 2003*, Calgary, Canada, July 2003.

[11] R. Dinis, R. Kalbasi, D. Falconer and A. Banihashemi, "Iterative Layered Space-Time Receivers for Single-Carrier Transmission over Severe Time-Dispersive Channels", *IEEE Comm. Letters*, Vol. 8, No. 9, pp. 579–581, Sep. 2004.

[12] A. Gusmão, P. Torres, R. Dinis and N. Esteves, "A Turbo FDE Technique for Reduced-CP SC-Based Block Transmission Systems, *IEEE Trans. on Comm.*, Vol. 55, No. 1, pp. 16-20, Jan. 2007.

[13] R. Dinis, P. Montezuma, N. Souto, and J. Silva, "Iterative Frequency-Domain Equalization for General Constellations", *IEEE Sarnoff Symposium*, Princeton, USA, Apr. 2010.

Bibliography

[1] R. G. Gallager, "Low-density parity-check codes," *Information Theory, IRE Transactions*, vol. 8, pp. 21 – 28, Jan. 1962.

[2] P. Montezuma, V. Astúcia, R. Dinis, and M. Beko, "On the use of multiple grossly nonlinear amplifiers for highly efficient linear amplification of multilevel constellations," *Vehicular Technology Conference (VTC Fall), 2013 IEEE 78th*, Sep. 2013.

[3] A. Gusmão, R. Dinis, J. Conceição, and N. Esteves, "Comparison of two modulation choices for broadband wireless communications," *in IEEE VTC'00 (Spring)*, vol. 2, pp. 1300 – 1305, May 2000.

[4] D. Falconer, S. Ariyavisitakul, A. Benyamin-Seeyar, and B. Eidson, "Frequency domain equalization for single-carrier broadband wireless systems," *Communications Magazine, IEEE*, vol. 40, no. 4, pp. 58 – 66, Apr. 2002.

[5] J. W. Cooley and J. W. Tukey, "An algorithm for the machine calculation of complex Fourier series," *Mathematics of Computation*, vol. 19, no. 90, pp. 297–301, Apr. 1965.

[6] D. J. MacKay and R. M. Neal, "Near shannon limit performance of low density parity check codes," *Electronics Letters*, vol. 33, pp. 457 – 458, Mar. 1997.

[7] D. M. Gruenbacher and A. Serener, "Performance of coded OFDM in a fading environment using high rate low-density parity-check codes," *Proc. GLOBECOM*, vol. 1, pp. 504–508, 2001.

[8] H. Futaki and T. Ohtsuki, "Low-density parity-check (LDPC) coded OFDM systems," *54-th IEEE Vehicular Technology Conference (VTC 2001-Fall)*, vol. 1, pp. 82–86.

[9] B. Lu, G. Yue, and X. Wang, "Performance analysis and design optimization of LDPC-coded MIMO OFDM systems," *IEEE Trans. Signal Processing*, vol. 52, no.2, pp. 348–361, 2004.

[10] H. S. Kim and S. C. Park, "Iteration based performance evaluation of LDPC coded MIMO-OFDM," *Proc. the 8th International Conference Advanced Communication Technology, (ICACT 2006)*, vol. 3, pp. 2103–2105, 2006.

[11] X. Xu and R. Mathar, "Low complexity joint channel estimation and decoding for LDPC coded MIMO-OFDM systems," *IEEE 73rd Vehicular Technology Conference, VTC2011-Spring*, 2011.

[12] G. Ryu and D. Kim, "An efficient decision feedback equalizer combining the LDPC code in cellular relay system," *International Journal of Advanced Science and Technology*, vol. 42, pp. 101–110, May 2012.

[13] M. Gomes, R. Dinis, V. Silva, F. Cercas, and M. Tomlinson, "Iterative FDE design for LDPC-coded magnitude modulation schemes," *Wireless Communication Systems (ISWCS 2013)*, pp. 1–5, 2013.

[14] C. E. Shannon, "A mathematical theory of communication," *Bell System Technical Journal*, vol. 27, pp. 379 – 423, 1948.

[15] J. Proakis, *Digital Communications*. McGraw-Hill, 4th ed., 2001.

[16] R. M. Tanner, "A recursive approach to low complexity codes," *Information Theory, IEEE Transactions*, vol. 27, pp. 533 – 547, Sep. 1981.

[17] S. Freundlich, D. Burshtein, and S. Litsyn, "Approximately lower triangular ensembles of LDPC codes with linear encoding complexity," *IEEE Transactions on Information Theory*, vol. 33, pp. 1484 – 1494, Apr. 2007.

[18] D. Divsalar, H. Jin, and R. McEliece, "Coding theorems for 'turbo-like' codes," *Proceedings of the 1998 Allerton Conference*, pp. 201 – 210, 1998.

[19] S. Benedetto, D. Divsalar, G. Montorsi, and F. Pollara, "A soft-input soft-output APP module for iterative decoding of concatenated codes," *Communications Letters, IEEE*, vol. 1, pp. 22–24, Jan. 1997.

[20] J. Pearl, "Reverend bayes on inference engines: A distributed hierarchical approach," *Proceedings of the second annual conference on Artificial Intelligence*, Aug. 1982.

[21] F. R. Kschischang, B. J. Frey, and H.-A. Loeliger, "Factor graphs and the sum-product algorithm," *IEEE Transactions on Information Theory*, vol. 47, Feb. 2001.

[22] J. Zhao, F. Zarkeshvari, and A. H. Banihashemi, "On implementation of min-sum algorithm and its modifications for decoding low-density parity-check (LDPC) codes," *IEEE Transactions on Communications*, vol. 53, Apr. 2005.

[23] G. D. Forney, "Concatenated codes," *Massachussetts Inst. Technol., Cambridge, MA*, 1966.

[24] S. Benedetto and G. Montorsi, "Design of parallel concatenated convolutional codes," *Communications, IEEE Transactions*, vol. 44, pp. 591 – 600, May 1996.

[25] S. Benedetto, D. Divsalar, G. Montorsi, and F. Pollara, "Serial concatenation of interleaved codes: Performance analysis, design, and iterative decoding," *IEEE Transactions on Information Theory*, vol. 44, pp. 909 – 926, May 1998.

[26] H. Futaki and T. Ohtsuki, "Low-density parity-check (LDPC) coded OFDM systems with M-PSK," *Vehicular Technology Conference, 2002. VTC Spring 2002. IEEE 55th*, vol. 2, pp. 1035 – 1039, 2002.

[27] F. Guo, S. X. Ng, and L. Hanzo, "LDPC assisted block coded modulation for transmission over Rayleigh fading channels," *Vehicular Technology Conference, 2003. VTC 2003-Spring. The 57th IEEE Semiannual*, vol. 3, pp. 1867 – 1871, Apr. 2003.

[28] M. Y. Alias, F. Guo, S. X. Ng, T. H. Liew, and L. Hanzo, "LDPC and turbo coding assisted space-time block coded OFDM," *Vehicular Technology Conference, 2003. VTC 2003-Spring. The 57th IEEE Semiannual*, vol. 4, pp. 2309 – 2313, Apr. 2003.

[29] S. Tseng, Y. Hsu, and Y. Peng, "Iterative multicarrier detector and LDPC decoder for OFDM systems," *Wseas Transactions on Communications*, vol. 11, Mar. 2012.

[30] L. J. Cimini, "Analysis and simulation of a digital mobile channel using orthogonal frequency division multiplexing," *Communications, IEEE Transactions on*, vol. 33, pp. 665 – 675, Jul. 1985.

[31] N. Benvenuto and S. Tomasin, "Block iterative DFE for single carrier modulation," *Electronics Letters*, vol. 38, no. 19, pp. 1144 – 1145, Sep. 2002.

[32] R. Dinis, A. Gusmão, and N. Esteves, "On broadband block transmission over strongly frequency-selective fading channels," *in 15th International Conference on Wireless Communications (Wireless 2003)*, pp. 261 – 269, July 2003.

[33] R. Dinis, R. Kalbasi, D. Falconer, and A. Banihashemi, "Iterative layered space-time receivers for single-carrier transmission over severe time-dispersive channels," *Communications Letters, IEEE*, vol. 8, pp. 579 – 581, sept. 2004.

[34] A. Gusmão, P. Torres, R. Dinis, and N. Esteves, "A turbo FDE technique for reduced-CP SC-based block transmission systems," *Communications, IEEE Transactions on*, vol. 55, no. 1, pp. 16 – 20, Jan. 2007.

[35] R. Dinis, P. Montezuma, N. Souto, and J. Silva, "Iterative frequency-domain equalization for general constellations," *IEEE Sarnoff Symposium, Princeton, USA*, Apr. 2010.

[36] A. Gusmão, V. Gonçalves, and N. Esteves, "A novel approach to modeling of OQPSK-type digital transmission over nonlinear radio channels," *IEEE Journal on Selected Areas in Communications*, vol. 15, no. 4, pp. 647–655, 1997.

[37] P. Montezuma and A. Gusmão, "Design of TC-OQAM schemes using a generalised nonlinear OQPSK-type format," *IEEE Electronics Letters*, vol. 35, no. 11, pp. 860–861, 1999.

[38] F. Amoroso and J. Kivett, "Simplified MSK signaling technique," *IEEE Transactions Communications*, vol. 25, pp. 433–441, Apr. 1977.

[39] S. Pupolin and L. J. Greenstein, "Performance analysis of digital radio links with nonlinear transmit amplifiers," *IEEE Journal of Selected Areas in Communications*, vol. 5, pp. 535–546, 1987.

[40] M. Figueiredo, "A two-stage fully differential inverter-based self-biased CMOS amplifier with high efficiency," *IEEE Trans. Circuits and Systems I*, vol. 58, pp. 1591–1603, Jul. 2011.

[41] P. Montezuma, R. Dinis, and D. Marques, "Low complexity LDPC coded IB-DFE for multilevel modulations and coded OFDM: comparison and complexity trade-offs," *to be presented at 2014 International Conference on Telecommunications and Multimedia (TEMU2014)*, Jul. 2014.

[42] P. Montezuma, D. Marques, V. Astucia, R. Dinis, and M. Beko, "Robust frequency-domain receivers for a transmission technique with directivity at the constellation level," *to be presented at 2014 IEEE 80th Vehicular Technology Conference (VTC2014-Fall)*, Sep. 2014.